THE MIRB FERRISIDEROPHORE TRANSPORTER OF *ASPERGILLUS FUMIGATUS*: STRUCTURAL REQUIREMENTS FOR ACTIVITY

by

Isabelle Raymond-Bouchard
Bachelor of Science, Simon Fraser University, 2007
Associate of Science, Douglas College, 2004

THESIS SUBMITTED IN PARTIAL FULFILLMENT OF
THE REQUIREMENTS FOR THE DEGREE OF

MASTER OF SCIENCE

In the
Department of Biological Sciences

SIMON FRASER UNIVERSITY

Spring 2011

Approval

Name: **Isabelle Raymond-Bouchard**

Degree: **Master of Science**

Title of Thesis: **THE MIRB FERRISIDEROPHORE TRANSPORTER OF *ASPERGILLUS FUMIGATUS*: STRUCTURAL REQUIREMENTS FOR ACTIVITY**

Examining Committee:

Chair: **Dr. Chris J. Kennedy**
Professor, Department of Biological Sciences

_____

Dr. Margo M. Moore
Senior Supervisor
Professor, Department of Biological Sciences

_____

Dr. Michael Silverman
Supervisor
Assistant Professor, Department of Biological Sciences

_____

Dr. Christopher T. Beh
Supervisor
Associate Professor, Department of Molecular Biology and Biochemistry

_____

Dr. Julian Guttman
Internal Examiner
Assistant Professor, Department of Biological Sciences

Date Defended/Approved: April 19 2011

Declaration of
Partial Copyright Licence

Abstract

Siderophores (iron chelators) have been identified as virulence factors in the opportunistic fungal pathogen, *Aspergillus fumigatus (Afu)*. The 14-pass transmembrane protein MirB is postulated to function as a siderophore-transporter, responsible for uptake of the siderophore TAFC. The aim of my research was to identify amino acids in the extracellular loops of *Afu* MirB that are crucial for uptake of Fe-TAFC. Site-directed mutagenesis was used to create MirB mutants and expression of the WT and mutant proteins in *Saccharomyces cerevisiae* strain PHY14 was confirmed by western blotting. TAFC transport assays using ^{55}Fe-labelled TAFC and growth assays with Fe-TAFC as the sole iron source identified alanine 125, tyrosine 577, loop 3 and the second half of loop 7 as crucial for function, since their substitution or deletion abrogated uptake completely. This study has revealed critical residues important for TAFC uptake which could represent potential targets for the development of novel antifungals.

Keywords: Siderophore; Siderophore transporter; Iron transport; *Aspergillus fumigatus*; Aspergillosis; Major Facilitator Superfamily; Unknown Major Facilitator

À ma mère et mon père, pour votre soutien, vos conseils,
votre encouragement, et votre amour.

To my mother and father, for your support, your guidance,
your encouragement and your love.

Acknowledgements

I would like to thank, first and foremost, my senior supervisor Dr. Margo Moore, for all your help, guidance, support, encouragement and endless optimism. This project was fraught with problems and frustration, and your optimism, support, and dedication inspired me to keep going. Thank you.

Thank you also to my committee members, Drs. Michael Silverman and Chris Beh, for your advice and guidance.

A big thank you to all my lab mates, past and present (you know who you are!), for your support and encouragement. Thank you to Cassandra, Nazanin, Juliana, and Janey for your friendship and laughter. It was a blast! A special thank you to Linda Pinto, for all your guidance and expertise. There are a number of undergraduate students who contributed to this work and whom I wish to thank: Cassandra Carroll and Jason Nesbitt for helping to create the MirB mutants; Mina Moinzadeh for helping with immunofluorescence; and Gemma Kieft and Andrew Wong for your help with the MirB-GFP project.

I would also like to thank my family and friends, especially my parents: your love and support has meant the world to me, and without you, I would not be where I am today. A very special thank you to Willow, for being so supportive, loving and understanding, and being the absolute best listener I could ask for.

Lastly, I would like to thank NSERC for their financial support.

Table of Contents

List of Figures

List of Tables

1: Introduction

The aspergilli are a group of ubiquitous, soil dwelling saprophytic fungi that play a fundamental role in the recycling of carbon and nitrogen. The genus *Aspergillus* is composed of over 200 species (Agarwal 2009). *Aspergillus* spp. are important both commercially, in the production of foods and pharmaceuticals, and medically, with several species being important human pathogens. *Aspergillus fumigatus* is the most common causative agent of human infections linked to *Aspergillus* spp., followed by *A. flavus, A. terreus, A. niger*, and *A. nidulans* (Dagenais & Keller 2009).

1.1 Diseases caused by *Aspergillus* spp.

Over the past few decades, as the number of immunosuppressed individuals has increased, so too has the number of individuals worldwide infected by fungal pathogens (Latgé 2001). *Aspergillus* spp. are responsible for a variety of respiratory diseases, which, collectively, are termed aspergillosis. Aspergillosis can be classified as allergic, saprophytic or invasive (Agarwal 2009; Soubani & Chandrasekar 2002). The primary route of infection is through inhalation of fungal spores. The immune status of the host, as well as the virulence of the strain determine which disease is likely to occur. Allergic *Aspergillus* sinusitis, allergic bronchopulmonary aspergillosis [ABPA], and hypersensitivity pneumonias generally occur in asthma and cystic fibrosis patients and are a result of hypersensitivity to inhaled spores/germlings (Thornton 2010; Dagenais & Keller 2009; Agarwal 2009). Saprophytic infections, commonly called aspergillomas,

occur when the fungus invades pre-existing cavities in the lungs, such as those left by a previous tuberculosis infection, and forms masses or balls of mycelia that secrete toxins and allergens (Figure 1-1) (Thornton 2010). Allergic aspergillosis and aspergillomas are not usually life threatening and can be successfully treated with antifungal drugs or surgery. In severely immunocompromised individuals, including leukemia patients, solid-organ and bone marrow transplant patients, individuals with genetic immunodeficiencies (such as chronic granulomatous disease), patients with AIDS, and cancer patients undergoing cytotoxic chemotherapy, the fungus can become invasive (Dagenais & Keller 2009; Brookman & Denning 2000). Invasive aspergillosis (IA) occurs when growing invasive hyphae are able to penetrate and invade the lung tissues and, in some cases, become systemic (Figure 1-1).

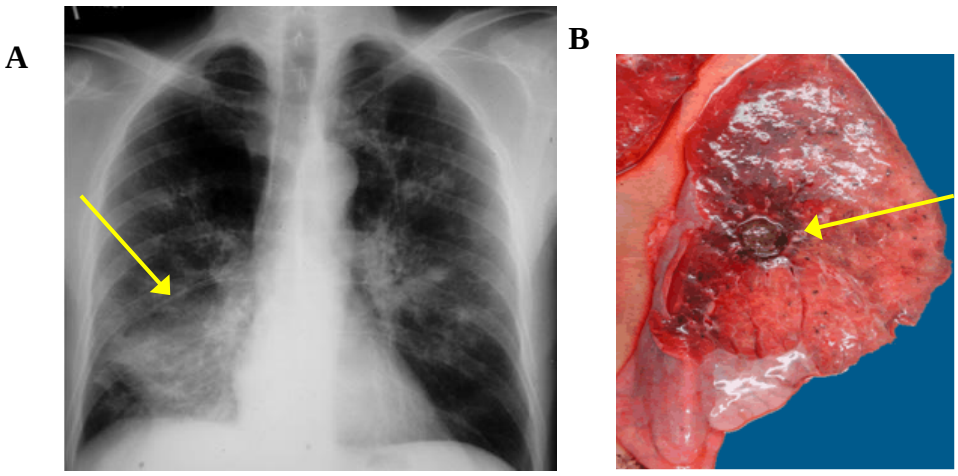

Figure 1-1. **A)** X-ray of patient with invasive pulmonary aspergillosis. **B)** Cross section of a lung following autopsy showing Aspergilloma (fungal ball). Images courtesy of the Fungal Research Trust (The Fungal Research Trust n.d.).

1.2 Invasive Aspergillosis

IA develops as a result of inhalation of fungal conidia (spores) into the lungs. In immunocompromised individuals, the spores may germinate and produce septate hyphae, which can penetrate the epithelial and endothelial barriers and enter the vasculature. In some cases, the fungus may spread to organs such as the heart, kidneys, skin and eyes, or to the central nervous system; this is associated with a poor prognosis.

The first line of defence against conidia is believed to be alveolar macrophages, responsible for phagocytosis and killing of spores (Schaffner et al. 1982; Waldorf et al. 1984). Macrophages are also responsible for inducing an inflammatory response that recruits neutrophils to the site of infection (Dagenais & Keller 2009). Neutrophils are absolutely essential for anticonidial defence and prevention of invasive disease (Mircescu et al. 2009). Unlike macrophages, neutrophils are able to destroy hyphae in addition to conidia, and are crucial for the elimination of germinating spores that have eluded macrophages. Because of the importance played by neutrophils, immunocompromised patients exhibiting neutropenia are the most at risk group for IA (Dagenais & Keller 2009).

Treatment of IA is with antifungal drugs, usually either azoles, such as voriconazole or itraconazole, or polyenes, such as amphotericin B (Walsh et al. 2008). Both of these classes of antifungal drugs target ergosterol, the major fungal sterol present in fungal membranes (Morschhäuser 2010). Polyenes bind directly to ergosterol present in the membrane and cause pore formation, while the azoles inhibit cytochrome P450 14α-demethylase, one of the enzymes required for sterol biosynthesis, leading to ergosterol depletion and accumulation of toxic methylated sterols. Amphotericin B, once

considered the first line of defence against IA, can cause severe side effects such as damage to kidneys and other organs (Flückiger et al. 2006). Recently, the largest randomized clinical trial on treatment of IA revealed that voriconazole is superior to amphotericin B, and as such it is now recommended as the primary treatment for IA (Walsh et al. 2008). However, even with antifungal therapy, the mortality rate for individuals with IA remains fairly high, ranging from 40-90%, depending on the severity of the immunosuppression, the site of infection, and the choice of treatment (Dagenais & Keller 2009).

1.3 *Aspergillus fumigatus*

Aspergillus fumigatus is responsible for >90% of all invasive aspergillosis infections (Latgé 2001). Although a sexual cycle has recently been discovered in the fungus (O'Gorman et al. 2009), *A. fumigatus* usually reproduces mitotically through the formation of specialised reproductive hyphae, called conidiophores, that produce haploid conidiospores (conidia) from stem cells (phialides). Conidia are released into the environment (Figure 1-2). The small size of the conidia (2-3 µm) allows them to remain airborne for extended periods of time. Inhalation of these spores is the primary route of infection in immunocompromised patients. The spores are small enough that they are able to reach deep within the lungs, to the alveoli. That is one of several factors that contribute to making *A. fumigatus* the most efficient pathogen of all the *Aspergillus* spp. Other important features that enhance its virulence include its relatively rapid rate of growth (Latgé 1999), and the fact that mycelia can withstand temperatures of up to 55°C (Brakhage & Langfelder 2002). Conidia can survive at temperatures up to 70°C.

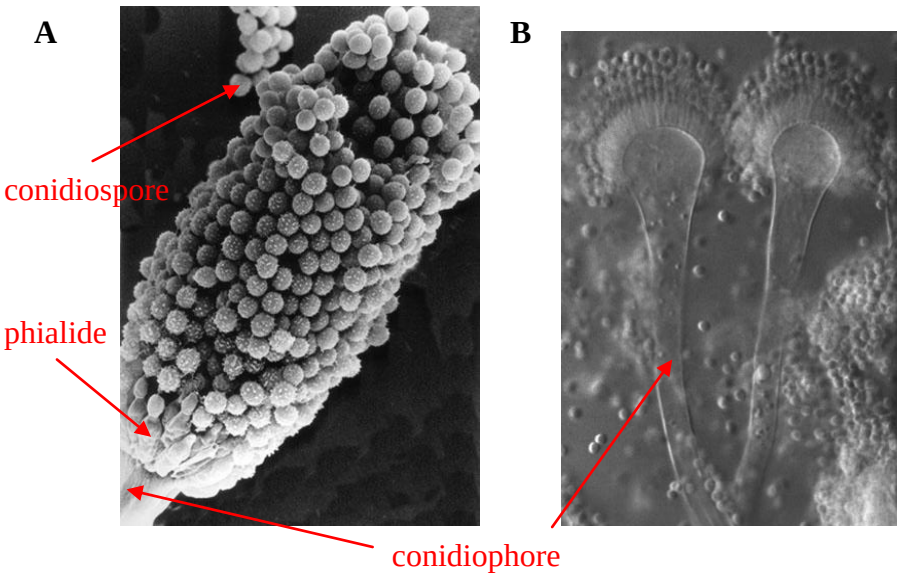

Figure 1-2. **A)** Electron micrograph and **B)** light microscope images of *A. fumigatus* showing conidiophore structure with phialides and conidiospores. Images courtesy of the Fungal Research Trust (The Fungal Research Trust 1998).

Other putative virulence factors have been shown to contribute to the virulence of this fungus in vivo. Much of the evidence gathered to date suggests that the virulence of *A. fumigatus* is multifactorial (Latgé 2001). Components of the cell wall of *A. fumigatus* such as β (1-3)-glucan, galactomannan, and chitins are thought to be important for adhesion and growth of the fungus in lung tissue (Rementeria et al. 2005). Hydrophobic RodA proteins (hydrophobins) present in the cell wall of the conidia form a 'rodlet layer', which helps the conidia bind to collagen and albumin (Thau et al. 1994). Additionally, the presence of these hydrophobin proteins was shown to be important for evasion from the host immune system (Aimanianda et al. 2009). The presence of the 'rodlet layer', which persists until germination, prevents activation of dendritic cells, alveolar macrophages and helper T-cells.

Pigments, such as melanin, also protect *A. fumigatus* against the host innate immune response. Melanin, (formed from 1,8-dihydroxynaphthalene) has been shown to

inhibit reactive oxygen species (ROS) secreted by macrophages and polymorphonuclear phagocytes (Latgé 1999). Enzymes and proteases, such as alkaline serine protease, can degrade the lung matrix proteins, collagen and elastin, and therefore promote growth of mycelia (Rementeria et al. 2005). *A. fumigatus* secretes a number of toxins that are involved in adherence and prevention of phagocytosis. Gliotoxin, for example, inhibits phagocytosis and induces apoptosis in macrophages (Rementeria et al. 2005). Research in these areas is still ongoing, and to date, no completely avirulent *A. fumigatus* mutant strain has been created as a result of the removal of molecules or genes associated with these virulence factors.

In recent years, a number of studies have focused on the role that iron plays in the virulence of *A. fumigatus*. In the human body, the free iron concentration is very low (~10^{-18}M), inhibiting growth of many pathogens. *A. fumigatus* however, is able to grow in human serum, suggesting that it possesses an efficient mechanism of acquiring iron in vivo (Gifford et al. 2002).

1.4 Iron acquisition

With the exception of some lactobacilli and *Borrelia burgdorferi* (Posey & Gherardini 2000; Imbert & Blondeau 1998), virtually all living organisms require iron as a micronutrient. Iron acts as a cofactor in a number of important cellular functions such as respiration, oxygen transport, gene regulation, photosynthesis and DNA synthesis and repair. However, in biological systems, free ferrous iron can form hydroxyl radicals that are highly toxic to cells via the Fenton reaction ($Fe^{2+} + H_2O_2 \rightarrow Fe^{3+} + OH\cdot + OH^-$). As a result, iron is generally sequestered into heme compounds as well as proteins such as ferritin, lactoferrin and transferrin, keeping free iron concentrations several orders of

magnitude too low to allow pathogenic microorganisms to survive solely by using free iron (Krewulak & Vogel 2008). To overcome this nutrient limitation, microorganisms have had to develop specialized mechanisms for procuring iron from their hosts.

In bacteria, there are two general mechanisms for acquiring iron: 1) via the secretion of small molecular weight (< 1000 Da) iron chelators called siderophores; 2) directly from ferrated host proteins, such as transferrin, lactoferrin, or hemoglobin. Siderophores and host heme proteins can be taken up by bacteria as intact molecules using specific receptors/transporters, whereas iron from transferrin and lactoferrin must first be extracted from the host molecule at the bacterial cell surface before it can be transported inside (Krewulak & Vogel 2008).

Fungi can also utilize two major systems for iron assimilation. The first is via secretion of siderophores, much like bacteria. The second is surface reductive iron assimilation characterized by both high and low affinity uptake mechanisms (Johnson 2008). Additionally, a few pathogenic fungi can also utilize heme as an iron source (Johnson 2008). *Aspergillus fumigatus* employs both siderophore secretion and ferric reductase activity for iron assimilation. Survival of A. *fumigatus* in human serum was accompanied by the removal of iron from host iron-binding molecules by siderophores (Hissen et al. 2004). Further studies showed that biosynthesis of siderophores, but not reductive iron assimilation, was required for virulence of *A. fumigatus* in a mouse model of invasive aspergillosis (Hissen et al. 2005; Schrettl et al. 2004). **Therefore, in the mammalian host, siderophore secretion is the main mechanism by which *A. fumigatus* obtains the iron required for its growth and survival.**

1.5 Siderophores

1.5.1 Classes of siderophores

Aspergillus fumigatus is known to synthesize several siderophores including ferricrocin, ferrichrome, ferrichrome C and *N', N'', N'''*-triacetylfusarinine C (TAFC) (Figure 1-3). TAFC constitutes 90% of the dry weight of siderophores produced by *A. fumigatus* grown in serum-containing media (Hissen et al. 2004). All of the siderophores produced by *A. fumigatus* are hydroxamates, one of the three chemical classes of siderophores. The other two classes are carboxylates and catecholates.

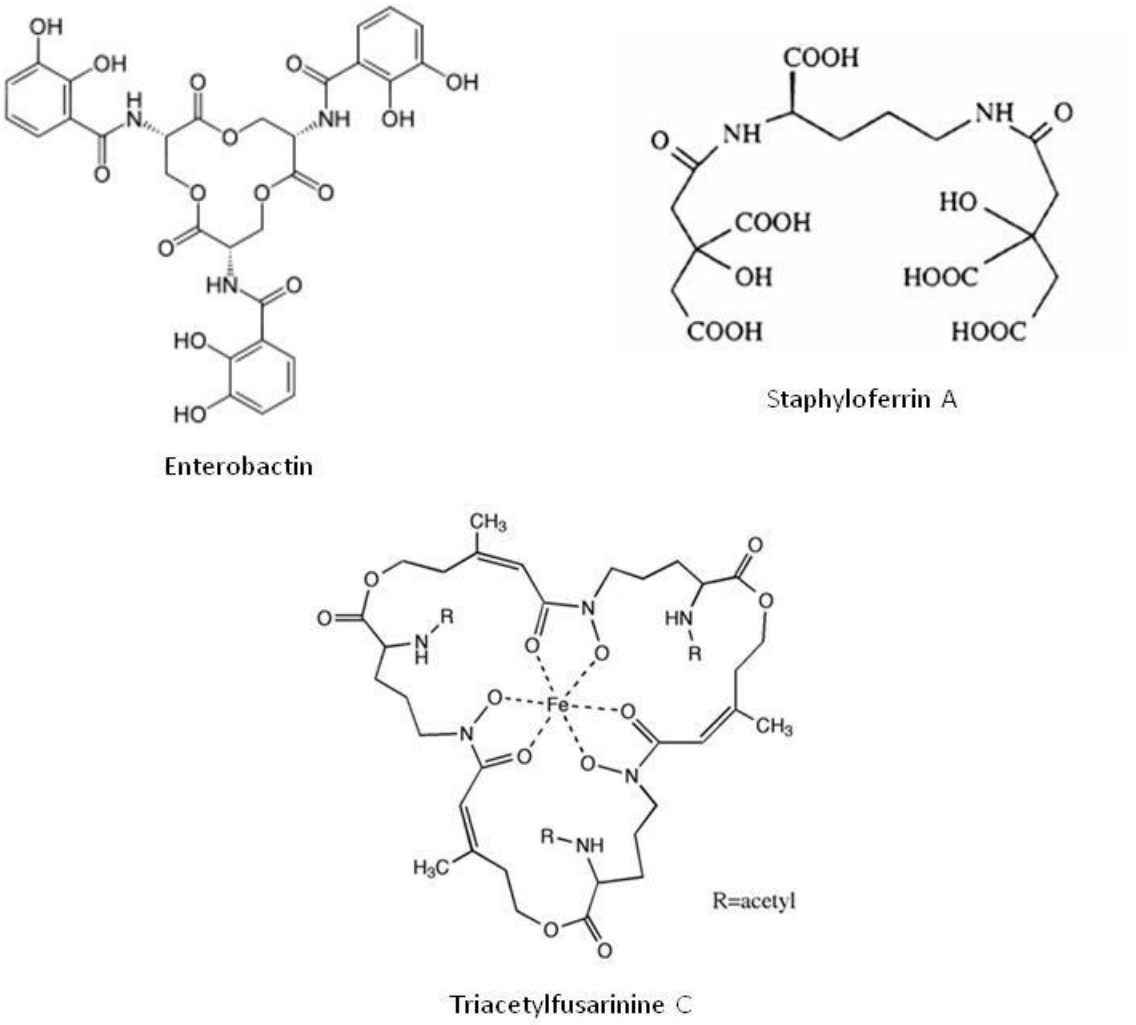

Figure 1-3. Representative siderophores from the three classes: the catecholate enterobactin produced by enteric bacteria such as *Escherichia coli*, staphyloferrin, a carboxylate siderophore made by *Staphylococcus* spp. and *N'*, *N''*, *N'''*-triacetylfusarinine C, a hydroxamate siderophore, the primary siderophore secreted by *Aspergillus fumigatus*.

Classification into each of these groups is dependent on the moiety incorporated into the metal binding site (Krewulak & Vogel 2008). Catecholates contain a catechol group (dihydroxybenzene ring), hydroxamates contain a hydroxylamine bound to carboxylic acid, and carboxylates are made up of carboxylic acids, often in the form of citric acid or a derivative thereof (Drechsel & Jung 1998) (Figure 1-3).

Siderophores are very efficient iron chelators with complex formation constants ranging from $K_f = 10^{52}$ for catecholate siderophores such as enterobactin, 10^{30} for hydroxamates, to 10^{23} for carboxylate siderophores (Drechsel & Jung 1998). To date, more than 500 different siderophores have been discovered and described (Wandersman & Delepelaire 2004). Table 1-1 shows a list of some of the more common siderophores synthesized by bacteria and fungi. Most fungi studied to date make hydroxamate siderophores, with the exception of the Mucorales, which make the carboxylate-type siderophore, rhizoferrin (Carrano et al. 1996). Bacteria make all three kinds of siderophores.

Table 1-1. Common siderophores produced by select bacteria and fungi.

	Hydroxamate	Catecholate	Carboxylate	Other	Reference
Bacteria					
Escherichia coli		Enterobactin			(O'Brien & Gibson, 1970)
Enterobacteriaceae (incl. *Escherichia, Salmonella, Shigella and Klebsiella*)		Enterobactin			(Grass 2006)
Pseudomonas fluorescens group (incl. *Pseudomonas aeruginosa*)		Pyoverdine		Pyochelin	(Cobessi, Celia, & Pattus, 2005; Cox & Adams, 1985; Schalk, Lamont, & Cobessi, 2009)
Streptomyces spp.	Desferrioxamines				(Bickel et al. 1960; Imbert et al. 1995)
Yersinia spp. (& other *Enterobacteriaceae*)				Yersinia-bactin	(Haag et al. 1993; Miller et al. 2006)
Staphylococci spp.			Staphyloferrin A & B		(Meiwes et al. 1990; Drechsel et al. 1993)
Salmonella spp., pathogenic *Escherichia coli*, certain *Klebsiella*		Salmochelin			(Müller et al. 2009)
Fungi					
Ustilago maydis	Ferrichrome Ferrichrome A				(Budde & Leong 1989)
Schizosaccharomyces pombe	Ferrichrome				(Schrettl, et al. 2004)
Penicillium chrysogenum	Ferrichrome Coprogen				(Charlang et al. 1981)

Aspergillus fumigatus	Ferricrocin Fusarinine C TAFC Ferrichrome		(Schrettl et al. 2007; Hissen et al. 2004)
Aspergillus nidulans	Ferricrocin Fusarinine C TAFC		(Charlang et al. 1981)
Neurospora crassa	Ferricrocin Coprogen		(Matzanke et al. 1987)
Fusarium graminearum	Ferricrocin TAFC		(Oide et al. 2006)
Zygomycetes (Mucorales)		Rhizoferrin	(Renshaw et al. 2002)

1.5.2 Siderophore biosynthesis

The synthesis of siderophores is regulated indirectly by free iron levels such that genes encoding biosynthetic enzymes are upregulated only in iron-depleted conditions. There are two main pathways of siderophore biosynthesis (Barry & Challis 2009). The first is dependent on non-ribosomal peptide synthetase (NRPS) modular multienzymes, which are also responsible for biosynthesis of the majority of secondary metabolites produced by microbes. NRPS are large multifunctional enzymes that can synthesize peptides by activating the precursors and incorporating them into the peptide, without the use of the ribosomal machinery. The second is an NRPS-independent siderophore (NIS) biosynthetic pathway, which involves a novel group of synthetase enzymes. Most siderophores, including those from *A. fumigatus*, are biosynthesized via the NRPS pathway.

The general fungal hydroxamate siderophore biosynthetic pathway is illustrated in Figure 1-4**.** Hydroxamate siderophores are derived from the non-proteinogenic amino acid L-ornithine and all share N^5-acyl-N^5-hydroxyornithine as the basic unit (Johnson 2008). Once synthesized, the N^5-acyl-N^5-hydroxyornithine, and sometimes other amino acids, are linked together via the NRPS pathway to complete the siderophore.

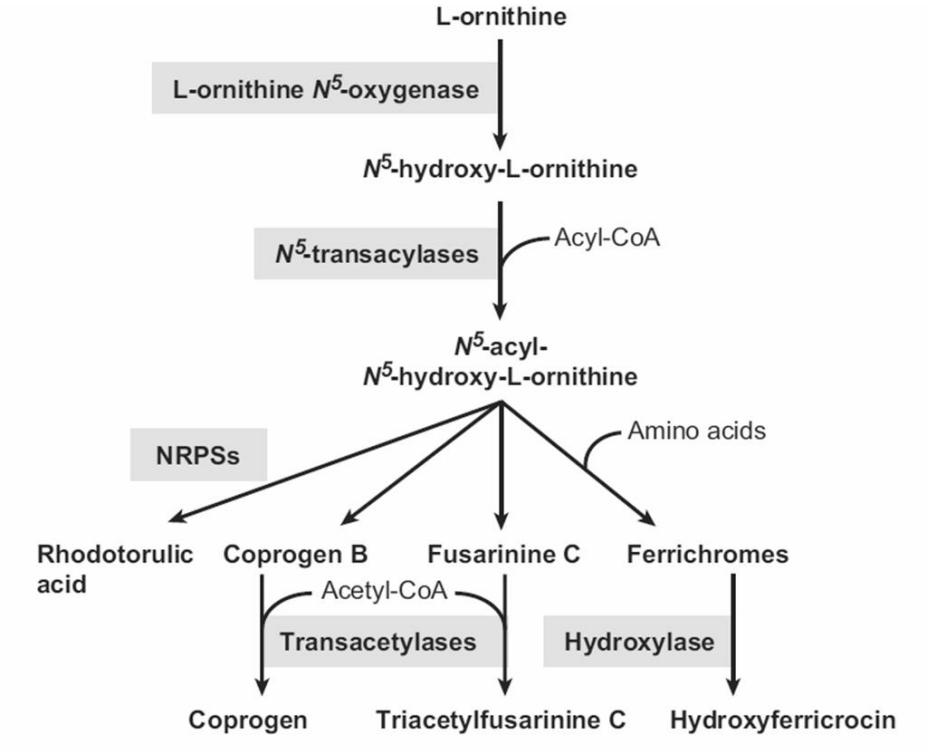

Figure 1-4. Schematic of the general hydroxamate siderophore biosynthesis pathway. Highlighted in grey are the enzymes necessary for biosynthesis of the various siderophores. Reproduced with permission (Haas et al. 2008).

In *Aspergillus fumigatus*, synthesis of hydroxamate siderophores involves five enzymes encoded by the genes *sidA, sidF, sidC, sidD,* and *sidG* (Figure 1-5). L-ornithine N^5-oxygenase, encoded by the gene *sidA,* catalyzes the first step in hydroxamate siderophore biosynthesis, the addition of an N^5-hydroxy group to L-ornithine (Hissen et al. 2005; Schrettl et al. 2004). An N^5-transacylase (*sidF* in the case of TAFC synthesis)

and the non-ribosomal peptide synthetases *sidD* and *sidC*, catalyze the remaining steps for the creation of fusarinine C and ferricrocin (Markus Schrettl et al. 2007). Synthesis of TAFC requires an N^2-transacetylase (*sidG*) to catalyze the addition of N^2-acetyl to fusarinine C. The GATA transcription factor SREA is responsible, at least in part, for regulating expression of these siderophore biosynthesis genes (Schrettl et al. 2008). GATA factors are characterized by their ability to bind to GATA sequence motifs in the regulatory region of target genes. SREA possesses two GATA-type zinc finger motifs, as well as an interjacent cysteine-rich region, which may be involved in iron sensing. SREA is only transcribed in conditions of high iron, where it acts as a repressor of siderophore biosynthesis.

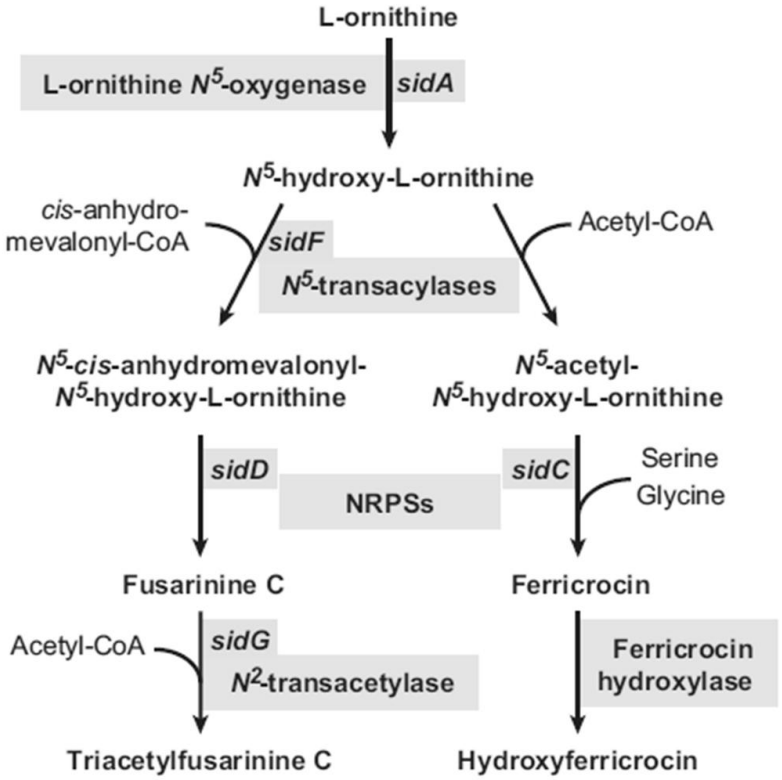

Figure 1-5. Schematic of the hydroxamate siderophores biosynthesis pathway in *Aspergillus fumigatus*. Enzymes and genes required for each biosynthetic step are highlighted in grey. Reproduced with permission (Haas et al. 2008).

The enzyme L-ornithine N^5-oxygenase is absolutely crucial for survival of the fungus in vivo. *sidA* mutants of *A. fumigatus,* unable to synthesize L-ornithine N^5-oxygenase, were found to be lacking in TAFC and ferricrocin, and were unable to grow in low iron media. In addition, the *sidA* mutant strain did not cause invasive aspergillosis in a mouse model of the disease, proving that *sidA* expression is also required for virulence (Schrettl et al. 2004; Hissen et al. 2005). **To date, siderophores biosynthesis is the only true virulence factor that has been identified in *A. fumigatus*.**

Newly synthesized siderophores are secreted outside of cells in an apo-form where they are free to bind ferric iron. Ferrisiderophores are transported back into cells

via membrane proteins called siderophore-transporters/receptors. Many bacteria and fungi also possess mechanisms for uptake of exogenous siderophores ('xenosiderophores') that they themselves do not synthesize. While bacteria and fungi have developed separate and distinct systems for siderophore-iron uptake, much more in known about siderophore transport in bacteria. Therefore, the various transport mechanisms that exist in bacteria will be discussed in detail first, before moving on to a discussion of the uptake systems in fungi and specifically in *A. fumigatus*.

1.6 Siderophore-iron transport in bacteria

Both Gram-negative and Gram-positive bacteria can acquire iron via siderophore-specific receptors/transporters; however, due to the different architecture of their cell envelopes, the mechanism differs for each (Krewulak & Vogel 2008). In Gram-negative bacteria, siderophore-iron uptake pathways involve an outer membrane receptor, a periplasmic binding protein (PBP), and an inner membrane ATP-binding cassette (ABC) transporter (Figure 1-6). In contrast, Gram-positive bacteria recognize extracellular ferrisiderophores via membrane-bound lipoproteins, which bind the siderophore and allow the iron to be transferred to an appropriate ABC transporter for uptake (Figure 1-7).

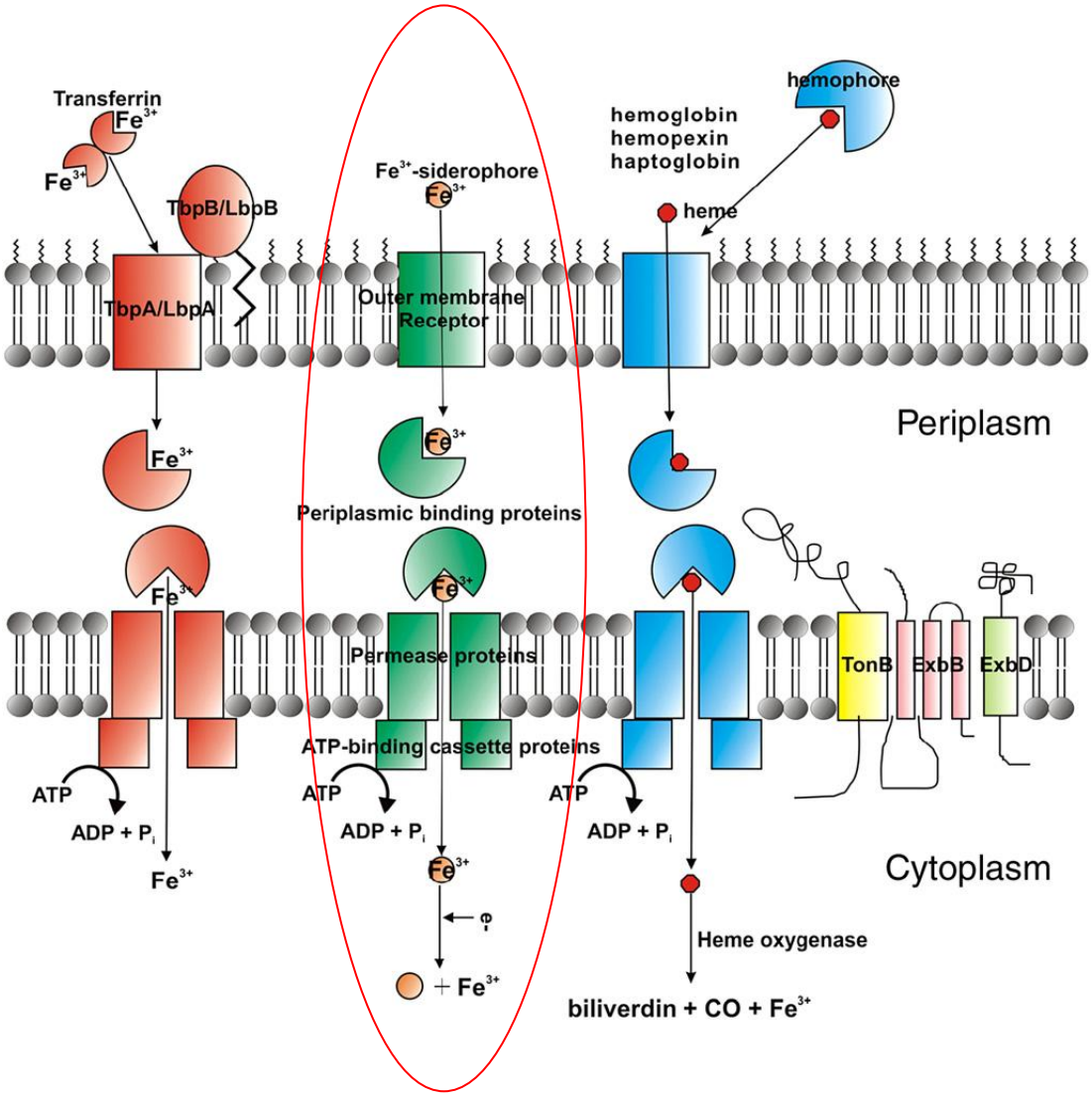

Figure 1-6. Iron uptake pathways in Gram-negative bacteria. The ferri-siderophore pathway is circled red. The entire iron-siderophore complex is transported to the periplasm via an outer membrane receptor. Once in the periplasm, the complex is bound by a periplasmic binding protein, which transfers the siderophore to an ABC permease that then transports the complex into the cytoplasm. Reduction of Fe^{3+} in the cytoplasm leads to dissociation of the iron from the siderophore. The other pathways shown in this figure present the models of iron uptake from transferrin (in red) or heme (in blue). Reproduced with permission (Krewulak & Vogel 2008).

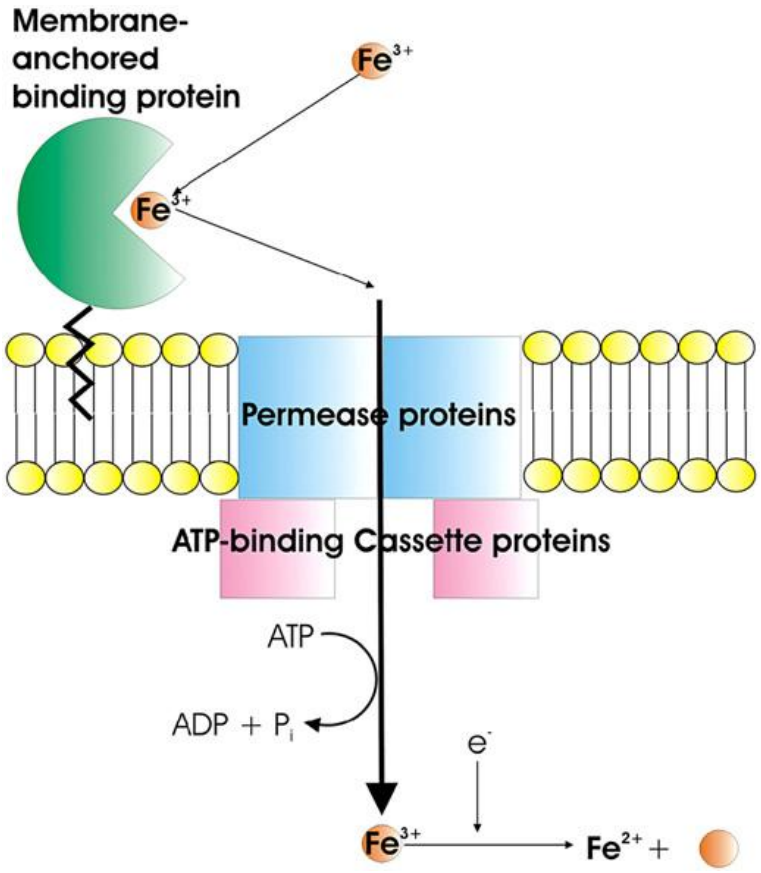

Figure 1-7. The siderophore-iron uptake pathway in Gram-positive bacteria. The siderophore-iron complex is bound by a membrane-anchored binding protein, which transfers the siderophore to an ABC permease that transports the complex into the cytoplasm. Reduction of Fe^{3+} in the cytoplasm leads to dissociation of the iron from the siderophore. Reproduced with permission (Krewulak & Vogel 2008).

1.6.1 Gram-negative bacteria

Outer membrane receptor

The first step in ferrisiderophore uptake is recognition and binding of the ferrisiderophore with its unique receptor at the cell surface. To date, crystal structures have been determined for the *Escherichia coli* enterobactin, ferrichrome, and ferric citrate outer membrane receptors, FepA, FhuA, and FecA, respectively, as well as for the *Pseudomonas aeruginosa* pyoverdin and pyochelin receptors FpvA and FptA,

respectively (Buchanan et al. 1999; Ferguson et al. 1998; Ferguson et al. 2002; Cobessi et al. 2005; Cobessi et al. 2005). Select structures are presented in Figure 1-8. All of the crystallized receptors adopt a typical 22-stranded transmembrane β-barrel structure with an N-terminal globular plug or cork domain. The plug domain sits inside the lumen of the β-barrel blocking access to the periplasm. The β-barrel domain is composed of 10 short periplasmic loops, 22 antiparallel β-strands, and 11 extracellular loops.

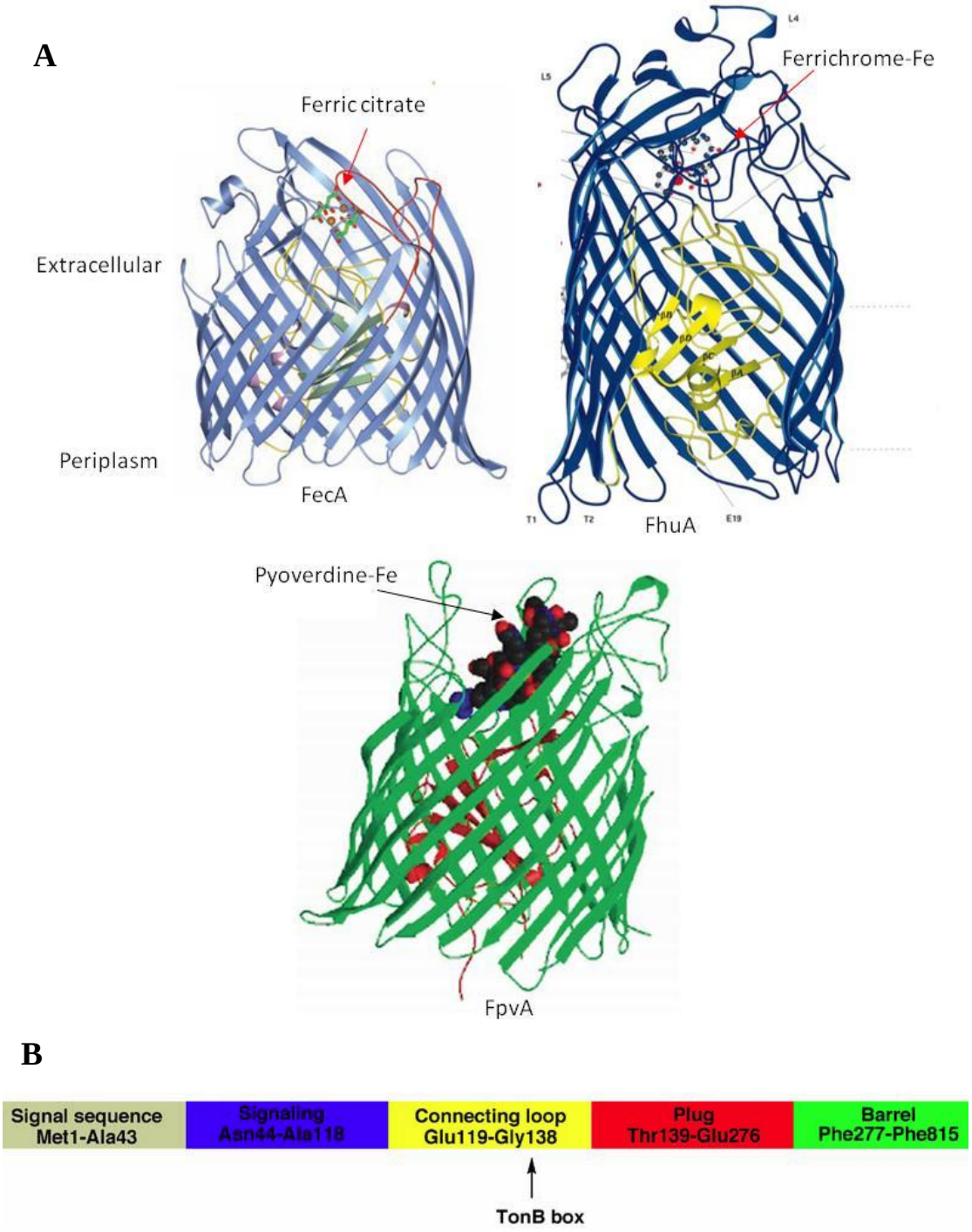

Figure 1-8. **A)** Crystal structures of the *Escherichia coli* ferric citrate and ferrichrome, outer membrane receptors, FecA and FhuA, respectively, and the *Pseudomonas aeruginosa* pyoverdine receptor, FpvA (Ferguson et al. 2002; Ferguson et al. 1998; Cobessi et al. 2005). The plug domain is visible in the lumen of each model. **B)** Schematic representation of the five domains in FpvA (Schalk et al. 2009). Reproduced with permission.

Although crystal structures have only been elucidated for receptors in *E. coli* and *P. aeruginosa,* outer membrane receptors have been characterized in numerous bacteria. Enterobactin receptors have been characterized in *Campylobacter jejuni* (CfrA) and *Bordetella* spp. (BfeA) (Carswell et al. 2008; Anderson & Armstrong 2006). *Yersinia* spp. including *Yersinia pestis*, the causative agent of the plague, along with numerous members of the *Enterobacteriaceae* family, can transport the siderophore yersiniabactin (Ybt) via the FyuA receptor. FyuA is part of the siderophore-dependent yersiniabactin (Ybt) system encoded on pathogenicity islands present in many virulent species (Miller et al. 2006). *Vibrio cholerae* has receptors specific for ferrichrome (FhuA), vibriobactin (ViuA), and enterobactin (IrgA) (Wyckoff et al. 2007). In total, more than 30 protein sequences have been identified as outer membrane receptors responsible for transporting a diverse range of ferrisiderophores (Chakraborty et al. 2007).

Outer membrane receptors are members of the TonB-dependent family of receptors, which utilize energy provided by the periplasmic energy transducer TonB to carry out their function. The N-terminal domain of the outer membrane receptor contains a TonB box that binds to the TonB complex (Figure 1-9). The TonB complex is made up of three proteins: TonB, ExbB and ExbD. TonB consists of three domains, an N-terminal domain that contains a transmembrane helix and a short cytoplasmic region, a central domain located in the periplasm, and the C-terminal domain, also located in the periplasm, which binds to the TonB box of the outer membrane receptor (Figure 1-9) (Krewulak & Vogel 2008). ExbB is a cytoplasmic-membrane protein consisting of three transmembrane domains, while ExbD has, like TonB, a single transmembrane domain and a periplasmic domain (Krewulak & Vogel 2008). TonB, ExbB and ExbD act together

to couple the proton gradient of the cytoplasmic membrane to active transport across the outer membrane (Larsen et al. 1999).

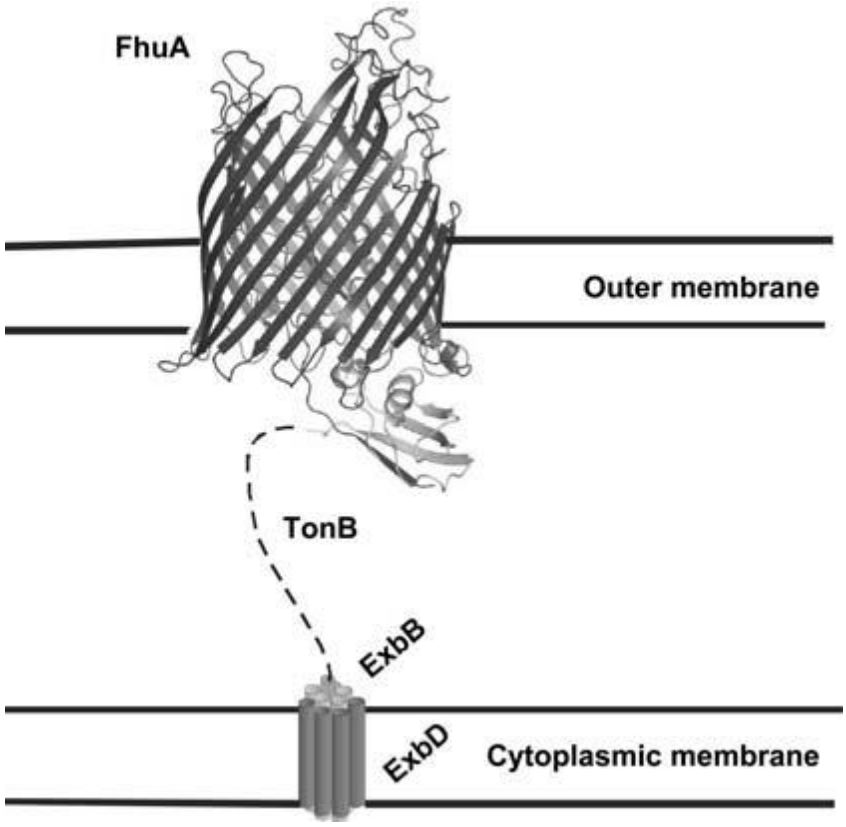

Figure 1-9. Interaction of the outer membrane receptor FhuA from *E. coli* with the TonB complex, TonB, ExbD, and ExbB. The C-terminal domain of TonB, located in the periplasm, makes contact with the TonB box of the OM receptor. Only the transmembrane portions of ExbB and ExbD are shown. Reproduced with permission (Braun & Endriss 2007).

Mechanism of uptake to periplasm

Based on crystallization and mutagenesis data, a "two gating" system has been proposed as the mechanism of siderophore-iron uptake across the outer membrane in *E.coli* and *P. aeruginosa* (Ferguson et al. 2002; Schalk et al. 2009). In this system, binding of the ferri-siderophore to the outer membrane receptor results in electrostatic interactions between the ferri-siderophore and the plug domain, along with numerous

residues found within the extracellular loops, and certain strands of the β-barrel. These interactions cause conformational changes that result in folding of the extracellular loops of the receptor over the binding site forming a 'lid' and essentially trapping the siderophore inside the receptor. This would represent closing of the first gate. In FecA, binding of ferric citrate causes minor (< 0.5 Å) spatial re-arrangement in three of the extracellular loops (4, 5, and 9), while major changes are observed in the seventh (11 Å) and eighth (15 Å) extracellular loops, rendering the binding site inaccessible to solvent, consistent with sequestration of the siderophores (Ferguson et al. 2002). Similarly, fluorescence quenching of fluorescein-labelled FhuA upon binding with Fe^{3+} ferrichrome indicated movement of one or more of the extracellular loops (Bös et al. 1998). There is also evidence for movement of the extracellular loops of FepA during uptake of enterobactin-Fe (Cao et al. 2002; Scott et al. 2002). Current structural information on FpvA does not indicate a conformational change by the extracellular loops. However, fluorescent properties of pyoverdine (Pvd) reveal that the apo- and metal-bound forms of Pvd are in different protein environments when bound to FpvA (Schalk et al. 2009). In addition, when in its binding site, the metal-siderophore complex has been found to be less flexible and solvent-accessible and its environment not as polar as when the siderophore alone is bound, an indication that Pvd-Fe must be sequestered within the transporter.

As described above, in the siderophore-free state, the plug domain of the outer membrane receptor sits in the lumen of the β-barrel, blocking access to the periplasm. This essentially represents the second gate. Upon trapping of the ferri-siderophore and closure of the first gate (the extracellular loop "cap"), conformational changes are

thought to lead to repositioning of the TonB box in the periplasm freeing TonB to interact with the TonB box, thus providing the necessary energy for rearrangement or movement of the plug domain, and thus opening the second gate (Ferguson et al. 2002; Schalk et al. 2009). The siderophore-iron complex would then be free to move into the periplasm. In FhuA and FecA, ligand binding induced changes in the plug domain, including unwinding of a β-helix located just after the TonB box and extension of the N-terminus towards the periplasm (Ferguson et al. 1998; Locher et al. 1998; Ferguson et al. 2002; Van Der Helm et al. 2002). Although a lack of structural and mutagenesis data makes it impossible to identify the mechanism of uptake in other TonB dependent receptors at present, it is likely that a similar mechanism exists there also.

The exact mechanism by which the plug domain is either removed, or perhaps simply rearranged to form an opening, from the lumen of the β-barrel, is unknown at this time, although two models have been proposed. In the first, the energy from the TonB molecule induces allosteric transitions in the plug or barrel domains causing the plug to be ejected from the lumen into the periplasm (Locher et al. 1998). Alternatively, the plug domain would remain inside the barrel, and allosteric transitions would cause rearrangement of the plug inside the lumen to create an opening through which the siderophore could diffuse into the periplasm (Ferguson et al. 1998).

Signalling in outer membrane receptors

FpvA and FecA belong to a subclass of TonB-dependent receptors, called TonB-dependent transducers, because of their role in a signal transduction pathway. In addition to ferri-siderophore uptake, these receptors also function to initiate a signalling cascade. This signalling pathway is responsible for regulating the transcription of the receptor

itself as well as genes involved in siderophore biosynthesis (Koebnik 2005). The N-terminal region of the receptor, located in the periplasm, contains a signalling domain that interacts with the periplasmic portion of a cytoplasmic membrane protein, an anti-sigma factor (Figure 1-10). In *E. coli*, this is FecR (Braun et al. 2003) and in *P. aeruginosa* it is FpvR (Beare et al. 2003). FecR and FpvR activate the sigma factors FecI in *E. Coli* (Braun et al. 2003) and PvdS and FpvI in *P. aeruginosa* (Beare et al. 2003), respectively, leading to transcriptional activation of the target genes.

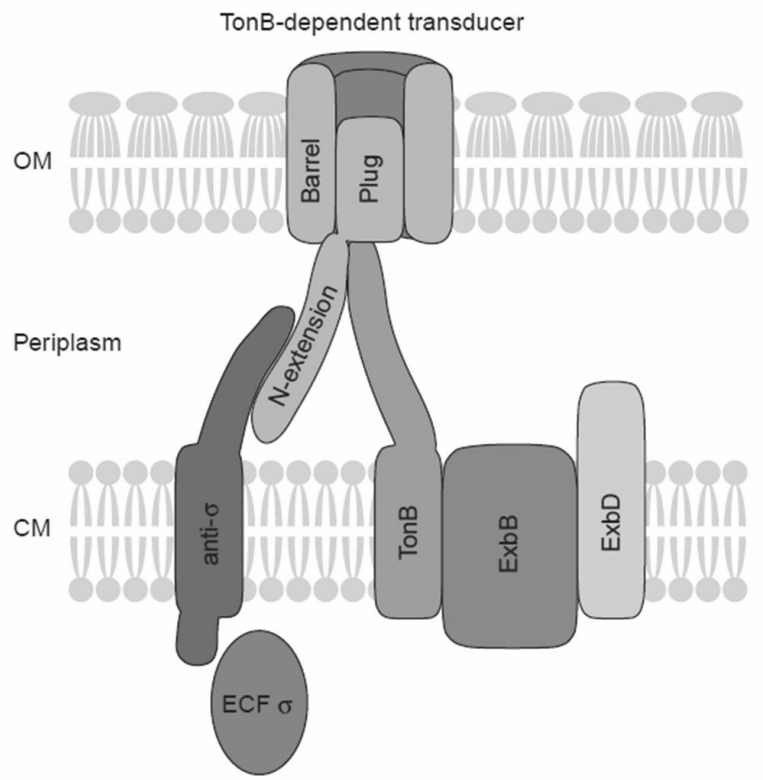

Figure 1-10. Interactions between the TonB-dependent transducer (outer membrane receptor), the TonB complex, including TonB, ExbB and ExbD, and the anti sigma and sigma factors (Extracytoplasmic function subfamily) of the signal transduction pathway. The signalling domain and the TonB box of the transducer are both located on the N-terminal extension. This N-terminal domain is believed to undergo a conformational change upon binding of the siderophore to the receptor, leading to extension into the periplasm, allowing for binding to both the TonB complex and the anti-sigma factor. Binding of the TonB complex induces translocation of the siderophore to the periplasm while activation of anti-sigma factors initiates the signalling cascade. Reproduced with permission (Koebnik 2005).

Uptake and signalling in FpvA appear to be fairly complex processes, and a clear understanding of the relationship between these two distinct, but very closely linked functions, is still lacking. Mutational studies have, however, been able to shed some light. The role of the N-terminal signalling domain in FpvA is purely regulatory; it is required for initiation of the signalling cascade, but is not involved in siderophore uptake (James

et al. 2005). In fact, deletion of the signalling domain had no effect on transport (Shen et al. 2002). Additionally, mutations in the β-barrel domain that were shown to be important for signalling did not appear to have an effect on siderophore uptake (James et al. 2005). In a similar vein, mutations in a number of sites that resulted in abrogation of ferripyoverdin transport did not reduce signalling, an indication that translocation of the siderophore to the periplasm is not required for initiation of the signalling cascade (James et al. 2005).

Binding of ferripyoverdine to FpvA is, however, required for signalling to occur; mutations in the siderophore-binding pocket of FpvA lead to a reduction in signalling (James et al. 2005). While uptake and signalling appear to be quite distinct processes, both can be affected by mutations in certain regions of FpvA. Mutations in the extracellular loops of FpvA, as well as certain regions of the β-barrell and plug domains, had an effect on both uptake and signalling (James et al. 2005).

Using the available mutagenesis data, Schalk et al have attempted to provide some insights into the connection between uptake and signalling (Schalk et al. 2009). Crystal structures of FpvA reveal that in an unloaded state, with no siderophore bound, part of the signalling domain interacts with residues of the TonB box (Schalk et al. 2009). Both of these domains must be freed during uptake and signalling so that they may interact with their respective targets, FpvR and the TonB complex. Additionally, they report that unloaded FpvA is able to interact with TonB in vitro, an indication that TonB may be able to displace the signalling domain and interact with the TonB box (Adams et al. 2006). Thus, Schalk et al. (2009) propose that binding of the siderophore to the receptor reduces the affinity of the TonB box for the signalling domain, allowing the

TonB box to bind with TonB, thus displacing the signalling domain and freeing it to interact with anti-sigma factors and initiate a signalling cascade.

Incorporating this into the two gate system described above, Schalk et al. (2009) proposed the following: Binding of the siderophore to FpvA results in conformational changes in the extracellular loops that effectively trap the siderophore in the receptor binding pocket. This, in turn, would cause a change in conformation of the receptor which would reduce the affinity of the TonB box for the signaling domain, allowing the TonB complex to bind to the TonB box of FpvA, and thus provide the necessary energy for movement of the plug domain out of the lumen of the β-barrel, allowing Pvd-Fe to move into the periplasm. At the same time, the signalling domain, having been displaced by TonB, would now be free to interact with the periplasmic portion of FpvR initiating the cascade that will eventually regulate expression of *fpvA* and siderophore biosynthesis genes.

Periplasmic binding proteins and transport to the cytoplasm

Once the siderophore has been internalized into the periplasm, transport of the siderophore-iron complex, or perhaps only the iron, is carried out by ABC permeases. Periplasmic binding proteins (PBP), a large family of periplasmic proteins that bind and deliver their ligand to cytoplasmic membrane ABC transporters, are responsible for escorting the ferri-siderophore to its respective cytoplasmic membrane transporter. Siderophore binding proteins belong to cluster 8 of the PBP family (Krewulak & Vogel 2008). Siderophore PBPs are less specific than outer membrane receptors for their ligand and are able to bind more than one type of siderophore (Wandersman & Delepelaire 2004); however, each PBP is usually able to shuttle only siderophores from one of the

three classes (Krewulak & Vogel 2008). For example, in *E. coli*, hydroxamates, catecholates and carboxylate type siderophores are bound by the PBPs FhuD, FepB, and FecB, respectively. FhuD and the *C. jejuni* enterobactin PBP CeuE are the only two siderophore PBPs for which a crystal structure has been determined (Müller et al. 2006; Clarke et al. 2002). Both proteins consist of two independently folded domains, the N- and C-terminal domains, connected by a long backbone α-helix (Figure 1-11). Consistent with the types of siderophores that they must bind, the binding domain of FhuD is hydrophobic whereas for CeuE, it is hydrophilic.

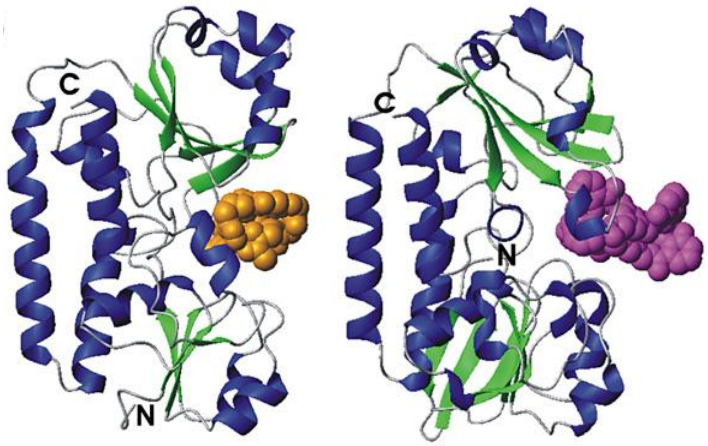

Figure 1-11. Crystal structures of the *E. coli* and *C. jejuni* periplasmic binding proteins FhuD (left) and CeuE (right), respectively. FhuD is in complex with the ferrichrome homolog gallichrome (orange) while CeuE is in complex with ferric-mecam (purple). The PBPs share a similar structure consisting of two independently folded domains connected by a long backbone helix. Reproduced with permission (Krewulak & Vogel 2008).

Proteins that are believed to make up the ABC siderophore transport complex have been discovered in numerous bacteria, although crystal structures have yet to be determined (Krewulak & Vogel 2008). However, the crystal structure of the ABC vitamin B_{12} transporter, BtuCD has been determined and (based on modelling) its

structure is believed to be similar to that of siderophore transporters (Locher et al. 2002). The ABC permease complex is made up of four individual subunits that assemble to form a complete transporter (Figure 1-12). The two α-helical transmembrane BtuC subunits are bound to two cytosolic BtuD subunits that function as ATPases, hydrolysing ATP to provide the necessary energy for the transporter to carry the siderophore, or perhaps only free iron, from the periplasm into the cytosol. Binding of the siderophore-PBP to the periplasmic portion of the transporter signals the ATPases to undergo hydrolysis (Krewulak et al. 2005).

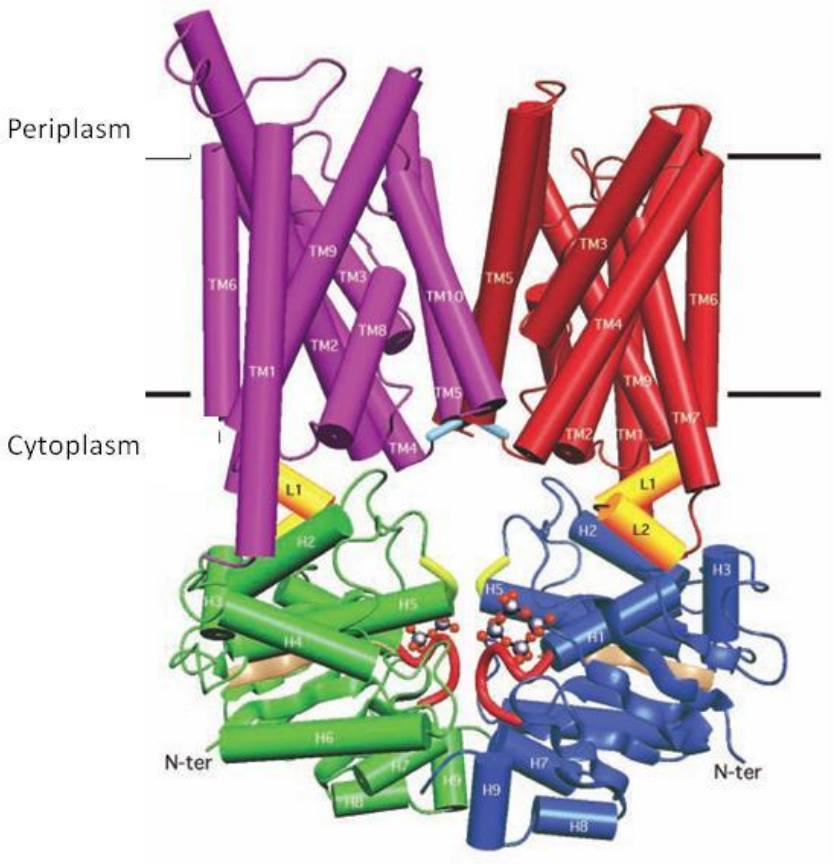

Figure 1-12. Quarternary structure of the vitamin B12 transporter, BtuCD, an ABC transporter made up of four subunits, two transmembrane BtuC subunits and two cytosolic BtuD ATPase subunits that hydrolyze ATP to drive vitamin uptake from the periplasm. Reproduced with permission (Locher et al. 2002).

The interactions between the PBP and the permease that lead to transport are not well understood, although it is believed that ATP hydrolysis, initiated by PBP binding, induces conformational changes in the permease complex (Köster 2001). It is also unclear if the entire siderophore-iron complex is transported into the cytosol or if the iron is first reduced from ferric to ferrous iron in the periplasm leading to dissociation from the siderophore and subsequent uptake by the ABC transporter. *P. aeruginosa* is known to utilize the latter mechanism: dissociation of iron from Pvd-Fe occurs in the periplasm following reduction to ferrous iron (Greenwald et al. 2007). The apo-Pvd molecule is then recycled to the extracellular medium (Schalk et al. 2002) via an ATP-binding cassette efflux transporter, PvdRT-OpmQ (Imperi et al. 2009). In contrast, *E. coli* hydroxamate type Fe-siderophore complexes are transported intact to the cytosol via the FhuBC ATP transporter (Köster 2001).

1.6.2 Gram-positive bacteria

Relatively little is known about iron transport in Gram-positive bacteria compared to Gram-negative bacteria. The Fe-siderophore binding proteins of Gram-positive bacteria are lipoproteins that are tethered to the lipid bilayer of the cytoplasmic membrane (Beasley & Heinrichs 2009). These lipoproteins are members of cluster 8 of the periplasmic binding protein family (named based on their location in Gram-negative bacteria). Once bound to their specific receptor, the ferri-siderophores are brought into the cytoplasm via ABC transporters, which use hydrolysis of ATP to power transport across the membrane (Beasley & Heinrichs 2009; Dale et al. 2004).

In the Gram-positive human pathogen, *Staphylococcus aureus*, the best studied of all the *Staphylococci*, three ABC transporter systems have been demonstrated to be

involved in ferric-siderophore uptake. The first, HtsABC, is involved in transport of staphyloferrin A (Beasley et al. 2009). HtsA is a PBP, while HtsB and HtsC are ATP transporter permeases. The second system, SirABC, is necessary for staphyloferrin B uptake, with SirA acting as the receptor and SirBC as components of the transporter permease (Dale et al. 2004). Finally, in the third system, required for uptake of exogenous ferri-hydroxamate complexes, FhuBG function as the permease, FhuC as the ATP-binding protein, and FhuD1 and FhuD2 are dual receptor lipoproteins that compete for interaction with FhuCBG (Sebulsky et al. 2003; Sebulsky et al. 2004; Sebulsky et al. 2000).

The first crystal structure of a Gram-positive siderophore receptor, from *Bacillus subtilis*, was reported in 2009 (Zawadzka et al. 2009). YclQ, a PBP responsible for recognition of the siderophore petrobactin, adopts a bilobal fold connected by a long α-helix, very much like Gram-negative PBPs (Figure 1-13). The binding pocket contains conserved positively charged and aromatic residues. The other components of this ABC transporter system have also been characterized (Zawadzka et al. 2009); YclN functions as the permease and YclP as the ATPase.

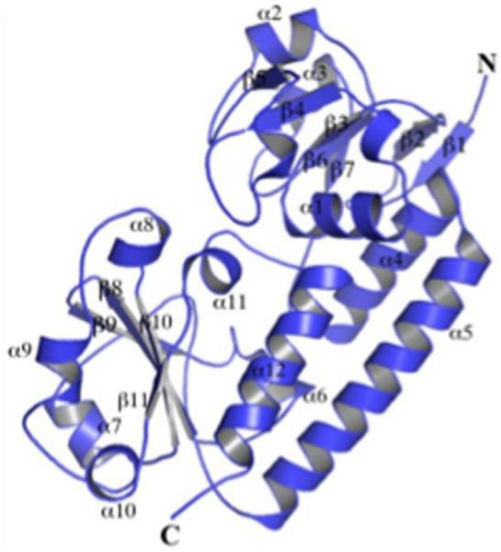

Figure 1-13. Ribbon model of the crystal structure of the siderophore receptor YclQ (a PBP) from *Bacillus subtilis.* Reproduced with permission (Zawadzka et al. 2009).

Members of the *Bacillus cereus* group of organisms, including *Bacillus cereus*, *Bacillus anthracis* and *Bacillus thuringiensis*, possess five putative PBP lipoproteins responsible for binding the siderophores bacillibactin and enterobactin (FeuA), petrobactin (FatB & FpuA), schizokinen (YfiY) and desferrioxamine and ferrichrome (YxeB)(Zawadzka et al. 2009). In the opportunistic pathogen *Listeria monocytogenes*, a putative transporter system for ferrichrome, FhuCDBG, has been discovered (Jin et al. 2006), while in *Mycobacteria* spp. there is evidence for a role of a type VII secretion system, Esx, in proper uptake or utilization of Fe-mycobactin (Siegrist et al. 2009).

These ABC transporters are thought to function in a mechanism similar to the ABC transporters in the cytoplasmic membrane of Gram-negative bacteria (see above).

1.7 Siderophore-iron transport in fungi

Before the siderophore iron complex can be transported across the membrane, it must first cross the fungal cell wall. Although it is possible that specific receptors help bring the siderophore to the membrane surface, due to the relatively small size of the ferrisiderophore (<1000 Da), current theory holds that most siderophores cross the cell wall through non-specific pores (Philpott 2006).

In fungi, siderophores are transported across the membrane via transmembrane transporters belonging to the UMF (unknown major facilitator), recently renamed the SIT (siderophore iron transporter) family, a subgroup within the major facilitator superfamily (MFS) (Haas 2004). MFS permeases transport a wide variety of compounds such as organic anions/cations, simple sugars, oligosaccharides, amino acids, and nucleosides (Pao et al. 1998). MFS members can transport small solutes in response to chemiosmotic ion gradients, and function as: 1) uniporters, which transport only one type of substrate and derive energy from that substrate gradient; 2) antiporters, which transport two or more substrates in opposite directions simultaneously, and utilize the electrochemical gradient of one to transport the other; 3) symporters, which transport two or more substrates like antiporters, but in the same direction across the membrane (Law et al. 2009). SIT members of the MFS family typically have 14 transmembrane α-helices and are believed to function as symporters, coupling translocation of a proton down its electrochemical gradient to transport of the siderophore-iron complex (Winkelmann 2001). While no crystal structures of fungal siderophore transporters exits, several crystal structures have been determined of other MFS transporters, including the *E. coli* lactose symporter LacY (Figure 1-14) and the glycerol-3-phosphate antiporter, amongst others

(Abramson et al. 2003; Huang et al. 2003; Yin et al. 2006; Hirai & Subramaniam 2004; Dang et al. 2010). All of these proteins share a remarkably similar structure regardless of their individual functions as symporters, uniporters, or antiporters (Law et al. 2009).

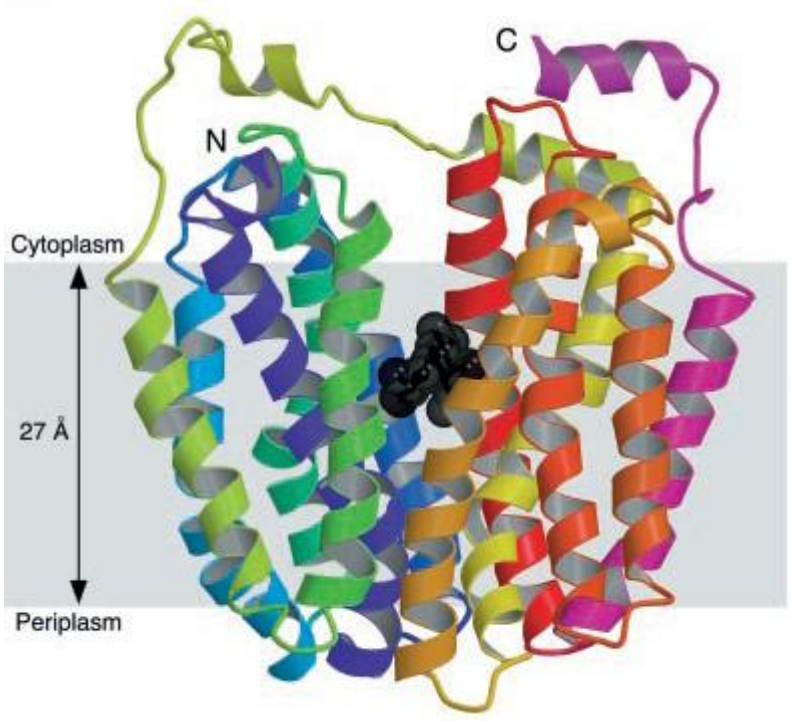

Figure 1-14. Ribbon model of the lactose permease LacY from *E. coli*. The black spheres represent the lactose homolog, β-D-galactopyranosyl-1-thio-β-D-galactopyranoside, situated in the binding pocket of the transporter. Reproduced with permission (Abramson et al. 2003).

1.7.1 Transport in Saccharomyces cerevisiae

Figure 1-15 highlights the siderophore transporters and uptake pathways of the yeast *Saccharomyces cerevisiae*. Most of our knowledge about fungal siderophore-iron transporters comes from work that has been done with *S. cerevisiae*. *S. cerevisiae* does not synthesize siderophores but is able to take up exogenous xenosiderophores through the use of membrane siderophore-iron transporters. Four siderophore-transporters have

been characterized in *S. cerevisiae*, two of which have high substrate specificity (Haas 2004). Enb1p/Arn4p is specific for enterobactin, while Taf1p/Arn2p transports TAFC (Yun et al. 2000). The two other siderophore transporters are the ferrioxamine and ferrichrome transporter Sit1p/Arn3p (Lesuisse et al. 1998), and Arn1p, which transports a number of siderophores (Heymann et al. 2000; Yun et al. 2000).

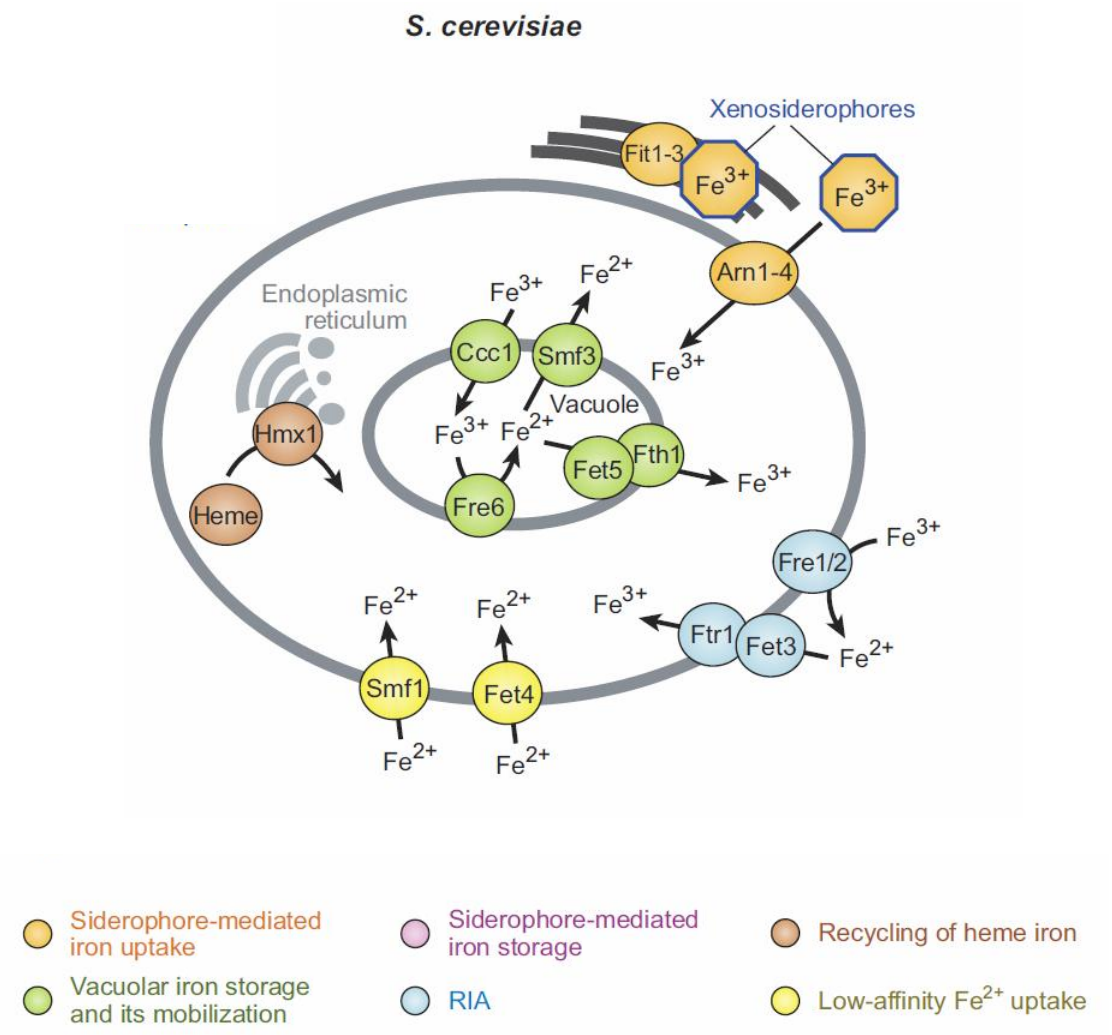

Figure 1-15. Iron transport systems in the yeast *S. cerevisiae*. RIA = reductive iron assimilation. Reproduced with permission (Haas et al. 2008).

The mechanism of siderophore-mediated iron transport across the membrane is well understood in *S. cerevisiae*. Figure 1-16 provides a general overview of the mechanism of siderophore uptake. Transporters for enterobactin and TAFC are not located in the plasma membrane at all times; instead, they are kept in endosome-like vesicles near the plasma membrane and are localized to the plasma membrane when cells are exposed to siderophores (Kim et al. 2002). Furthermore, it is believed that siderophores in *S. cerevisiae* are not simply transported across the plasma membrane but instead are taken up by endocytosis of the transporter after it binds to its specific siderophores (Kim et al. 2002). Once in the endosome, the transporter would shuttle the siderophore-iron complex across the endosomal membrane to the cytosol.

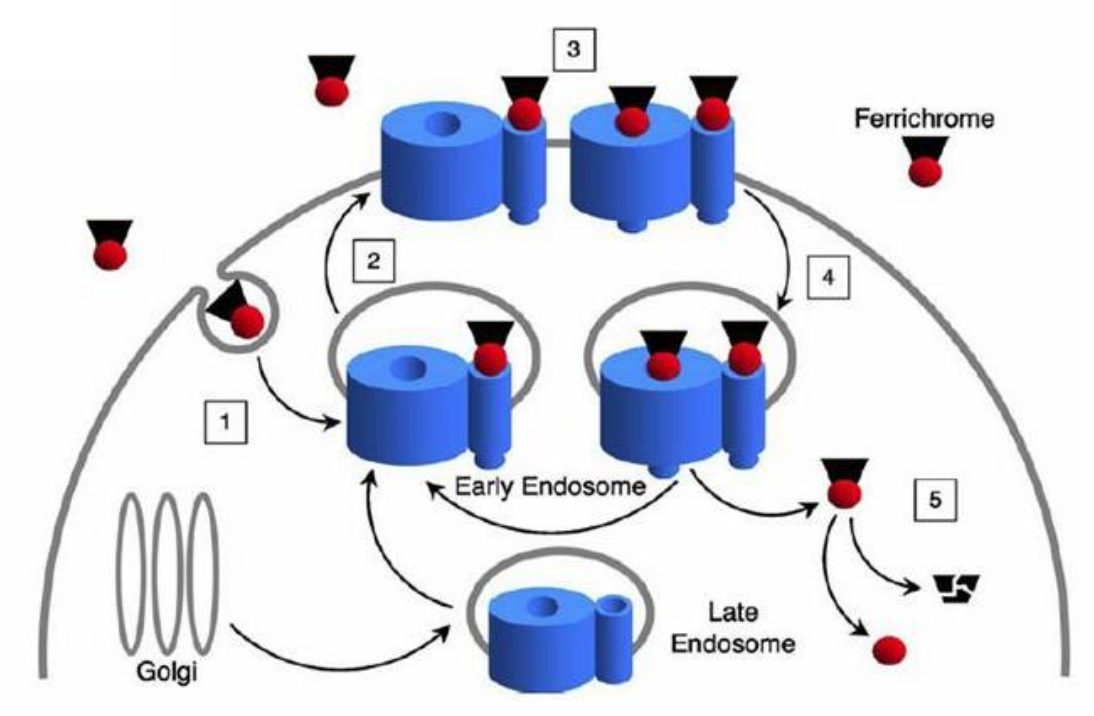

Figure 1-16. Schematic representation of the ferrichrome uptake system and trafficking of the ferrichrome transporter Arn1p in *S. cerevisiae*. Arn1p is sorted from the Golgi directly to endosomal compartments. Ferrichrome present on the surface is internalized by endocytosis (1) and binds to Arn1p in the early endosome. Ferrichrome binding triggers relocalization of Arn1p to the plasma membrane (2), where it is free to bind a second ferrichrome molecule (3). Following binding of the second ferrichrome molecule, Arn1p is ubiquitinated, which signals internalization of the transporter (4). Ferrichrome is released into the cytosol where it is likely degraded to release the iron (5). Reproduced with permission (Philpott 2006).

S. cerevisiae also possesses an alternative mechanism for siderophore-mediated iron uptake that does not involve endocytosis of the siderophore-iron complex (Figure 1-15). Instead, the iron is reduced directly at the cell surface by Fre reductases, leading to release from the siderophore, and subsequently, ferrous iron is taken up by iron permeases through either the high-affinity ferrous iron system (the Fet3p and Ftr1p complex) or through low affinity transporters (Fet4, Smf1) (Yun et al. 2001; Yun et al. 2000).

1.7.2 Transport in other fungi

Although much less is known about transport in other yeasts and filamentous fungi, siderophore-transporters have been characterized in several species. *Candida albicans* possesses only one siderophore transporter, CaArn1p/CaSit1p, a close homologue of the *S. cerevisiae* Sit1p/Arn3p transporter, responsible for the uptake of several siderophores including ferrichrome, TAFC, and ferricrocin (Heymann et al. 2002). In the *Neurospora crassa* genome, several homologs of *S. cerevisiae* siderophore-transporters have been found (Haas 2004). In *Aspergillus nidulans*, MirA, MirB and MirC have been characterized as siderophore transporters (Haas et al. 2003). Expression of MirA, MirB and MirC in a strain of *Saccharomyces cerevisiae* deficient in high affinity iron uptake and lacking endogenous siderophore transporters, followed by Fe^{55}-siderophore uptake assays, revealed that MirA and MirB are enterobactin and TAFC transporters, respectively. Both transporters are highly specific, and functionally similar to the *S. cerevisiae* Enb1p/Arn4p and Taf1p/Arn2p transporters (Haas et al. 2003). Although MirC shows a high degree of conservation with other siderophore transporters, an exact role in siderophore uptake has yet to be found (Haas et al. 2003). In *A. nidulans*, expression of siderophore-transporter encoding genes, as with siderophore biosynthesis, is regulated partly by SREA (Haas et al. 2003; Oberegger et al. 2001).

The mechanism of iron uptake via siderophore-transporters is well understood in *S. cerevisiae* (Refer to the previous section), but less so in other fungi. However, several different mechanisms of have been proposed to occur. In *Ustilago maydis,* a basidiomycete plant pathogen, transport of ferrichrome may occur through a system not unlike that of *S. cerevisiae.* The whole siderophore-iron complex is transported across the

membrane and can be detected inside vesicles (Ardon et al. 1998), suggesting that it may undergo endocytosis. It has been proposed that once inside the endosome, the metal would be removed from the siderophore, which would then be re-excreted intact (Renshaw et al. 2002). In contrast, the siderophore TAFC appears to be transported to the cytosol, where it is then broken down to release the iron (Kragl et al. 2007). Cytosolic TAFC esterases have been characterized in *Mycelia sterilia* (Adjimani & Emery 1988) and *Aspergillus fumigatus* (Kragl et al. 2007), which utilizes primarily TAFC for siderophore-mediated iron acquisition (Hissen et al. 2004). It is also possible the iron is transferred at the membrane from the extracellular siderophore to intracellular ligands (Renshaw et al. 2002), such as may be the case for *Rhodotorula* species (Winkelmann & Huschka 1987).

1.7.3 Iron release in the cytosol

What happens to the siderophore-iron complex in those cases where the complex enters the cell intact, and how the iron is then released to the cytosol, is not clear at this time. However, with endocytosis-mediated uptake of the transporter-siderophore-iron complex, one possibility would be that the decrease in pH in the endosome induces the release of iron from its siderophore. The iron would then be reduced and enter the cytosol via ferrous iron permeases within the endosome membrane. The intact siderophore could then be released from endosomes that recycle to the plasma membrane. Such a mechanism is utilized in mammalian cells to import ferric iron bound to transferrin (Tf) (Kaplan 2002). The extracellular iron-Tf complex binds to Tf receptors (TfR) at the surface of the cell, and the entire iron-Tf-TfR complex is internalized into endosomes. The acidic pH of endosomes dramatically lowers the affinity of Tf for iron allowing the

iron to be released from the receptor-bound Tf. Once the ferric iron is released into the endosome, a ferrireductase present in the endosome reduces ferric iron to ferrous iron permitting its movement into the cytosol through the divalent metal transporter Nramp2 (Gruenheid et al. 1999). The Tf-TfR complex remains in the endosome and is recycled to the plasma membrane.

Another possibility is that the siderophore-iron complex is taken up intact into the cytosol, where the siderophore is then cleaved, consequently releasing the bound ferric iron. Based on the identification of TAFC esterase activity, and the release of hydrolysis products into the culture medium, this mechanism has been suggested for TAFC in *M. sterilia* and *A. fumigatus* (Adjimani & Emery 1988; Kragl et al. 2007). Such a system would also require cytosolic reductases to reduce ferric iron to ferrous iron for use as a cofactor. Movement of the siderophore-iron complex to the cytosol could occur as a result of either direct transport through the transporter across the plasma membrane, or by endocytosis-mediated uptake of the transporter-siderophore-iron complex, as was discussed in the previous sections.

1.8 Siderophore-iron transport in *A. fumigatus*

To date, no studies have examined siderophore transporters in *Aspergillus fumigatus* and very little known about the steps of ferrated siderophore transport in *A. fumigatus.* The genome of *Aspergillus fumigatus* contains seven putative orthologues of siderophore-transporter-encoding genes, including *mirB, mirC, sit1*, and some as yet uncharacterized transporters. Haas et al. (2008) have speculated on the possible siderophore transporters and uptake pathways in *Aspergillus fumigatus* (Figure 1-17), but it should be noted that these are, at this point, purely speculative.

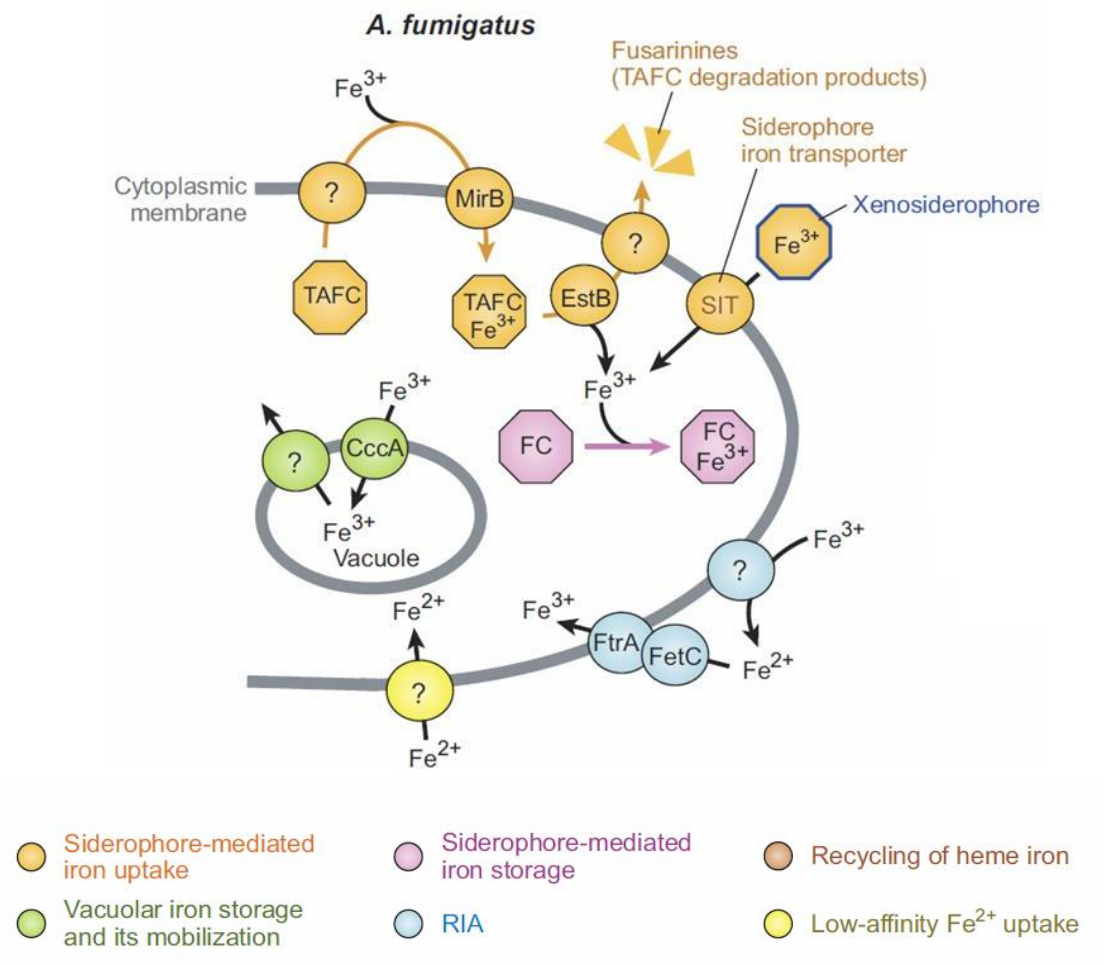

Figure 1-17. Putative iron transport systems in *A. fumigatus*. RIA = reductive iron assimilation. Reproduced with permission (Haas et al. 2008).

1.8.1 Siderophore transporter *MirB*

As the prominent *Aspergillus* pathogen, it is important that we gain more insight into the virulence factors associated with *Aspergillus fumigatus* infections. Considering the importance that siderophores play in its virulence, increasing our understanding of siderophore uptake in *Aspergillus fumigatus* is imperative. Because TAFC is the prominent siderophore produced by *A. fumigatus*, the orthologue of the *A. nidulans* TAFC transporter in *A. fumigatus*, MirB, represents an excellent target to study iron uptake.

A. fumigatus MirB is 612 amino acids long (Figure 2-1) and shares 54% sequence identity, but 67% positive identity, to the MirB protein from *A. nidulans*. Analysis of the *A. fumigatus* MirB sequence using the programs HMMTOP and SOSUI revealed that it is a transmembrane protein with 14 transmembrane α-helices and cytosolic N- and C-termini (see Results). MirB, like all other characterized fungal siderophore transporters, belongs to the siderophore iron transporter family, within the MFS, and is believed to function as a symporter (The Gene Ontology Consortium 2000).

The overall aim of my research is to functionally and structurally characterize siderophore-iron uptake by the transporter MirB in *A. fumigatus*. Specifically, I am interested in identifying amino acids present in the extracellular loops of MirB that are involved in binding and transport of ferrated TAFC. Since these loops form the initial site of contact between the transporter and the ferri-siderophore, we hypothesize that they contain amino acids, most likely conserved among fungal siderophore transporters, which are crucial for binding and transport of ferri-TAFC. We focussed our efforts on the conserved amino acids in these loops as they present the most likely candidates. In *S. cerevisiae*, the transporter for the xenosiderophore ferrichrome, Arn1p, was found to have a high affinity binding site in the last extracellular loop domain (Kim et al. 2005). It is possible that a similar mechanism exists in MirB.

The specific objectives of the project were as follows:

1. to clone the wildtype *mirB* gene into a yeast expression vector and mutate the chosen amino acids using site-directed mutagenesis

2. to transform and express the wildtype and mutated MirB sequences in a strain of the yeast *Saccharomyces cerevisiae* deficient in all endogenous siderophore transporters

3. to perform TAFC transport and growth assays and determine efficiency of TAFC uptake by wildtype and mutated MirB sequences

Multiple sequence alignments of *A. fumigatus* MirB with other fungal siderophore transporters (refer to Materials and Methods), has identified a number of conserved amino acid residues, a select subset of which were chosen for mutagenesis. Site-directed mutagenesis was chosen as the preferable method for mutagenesis because of its ease of use and its ability to specifically target only selected amino acids.

Because *Aspergillus fumigatus* contains a number of other putative siderophore transporters that could potentially play a role in the uptake of TAFC, and because transformation of *A. fumigatus* via homologous recombination can be very challenging (Meyer 2008), the MirB proteins were expressed in a strain of *Saccharomyces cerevisiae* (PHY14) that is deficient in all endogenous siderophore transporters (Heymann et al. 2002). By using PHY14, we can ensure that the only mechanism of siderophore uptake is via MirB.

Elucidating the function of MirB will provide a greater understanding of the mechanisms involved in siderophore function and uptake in *A. fumigatus*. In addition, since synthesis and transport of siderophores are pathways that do not exist in humans, they present possible target areas in the development of new antifungal drugs.

2: Materials and Methods

2.1 MirB bioinformatic analysis

Analysis of the protein and genomic sequences of *mirB* was carried out using a variety of bioinformatics programs and tools. Results from these analyses provided invaluable information about MirB's function, localization, its similarity to other fungal transporters, conserved domains, and expected transmembrane topology. All analyses were conducted using either the genomic sequence from *A. fumigatus* strain Af293 acquired from the Entrez gene database (GeneID: 3505886, Locus: AFUA_3G03640) or the protein sequence, acquired from NCBI Pubmed (PMID: 16372009; Accession: XP_748684). These sequences can be found in Figure 2-2 and Figure 2-1.

```
  1 MLHVLSVGPS HAAFTVEAAM ATMKKFHSIV GEKPAQDAEA PSVDDPNVGQ IRADDKEAAH
 61 APANAETNNE EANPSDGAQA GVKKIEAVTL SWTRGTAIWF LTLVNDFRLS MYTSLNAYAT
121 SSFLGHSLLT VINIVSYVMG GSVYIPMAKA LDLWGRAEGF LLMTFFCILG LILLASSQNL
181 PTYCAGQVFY KVGFGGLSYT WNVLAADVTN LRNRGLAFAF TSSPALISAF AGSKAASDLL
241 AHSTWRWGFG MWAIILPVVA LPIYGLLAYH LRQAEKKGVL VKETRDWSIT PKTVWWAIME
301 FDLPGVLLFA GGFVIFLLPF TLAATAPHGY QTDYIIAMIT LGLALIIAFG FYEMLVAPVP
361 FLNYKFLIDR TVLGACLLDM TYQVSYYCYA SYLPSFLQVV YELDVATAGY VTNTFSVVSF
421 VFLFFAGWLI RWTGRFKWIL WVCVPLYIFG LGLMIHFRQP GGYIGYIVMC EIFFSVAGSV
481 FILCVQLAVL ASVDHQHVAA VLALLFVMGS IGGSIGSAIC GAIWTSTFLS RLERNLPASA
541 MPDLSLIYSS LPTQLSYPVG SATRTAIVEA YGYAQARMLI AGTAFMVLGF IWVGMMRNLN
601 VKNMTQTKGN VV
```

Figure 2-1. 612 amino acid sequence of MirB from *Aspergillus fumigatus* strain Af293.

```
   1 ATGCTTCACG TCTTATCAGT CGGTCCGTCC CATGCAGCGT TTACTGTCGA AGCAGCAATG
  61 GCAACCATGA AGAAATTCCA CTCGATTGTC GGTGAAAAGC CTGCCCAGGA TGCTGAGGCC
 121 CCCTCAGTCG ATGACCCAAA TGTTGGGCAG ATCAGAGCCG ACGACAAGGA GGCTGCTCAT
 181 GCGCCCGCCA ATGCGGAAAC CAATAATGAG GAGGCCAACC CGAGCGACGG AGCTCAGGCT
 241 GGTGTCAAGA AGATAGAGGC TGTGACCCTG AGTTGGACAA GGGGCACAGC GTACGCAATT
 301 CTAGTGCTGT ATGTTTCGCT CCCATTGATT GCTGCATGGG CCAGCCATCC CAAAAGATCA
 361 AACTGCTAAC CTGGTTTTCA TTCTGATAGC ATTTGGTTCC TAACGCTGGT CAACGATTTC
 421 CGACTGTCCA TGTATACAAG CTTGAACGCT TATGCCACAA GTTCTTTCCT CGGCCACTCG
 481 CTGTTGACCG TCATCAACAT TGTGTCCTAC GTCATGGGCG GTTCCGTGTA CATACCGATG
 541 GCCAAGGCGC TGGATCTTTG GGGCCGTGCA GAGGGTTTCC TTCTGATGAC GTTCTTCTGT
 601 ATTCTGGGTT TGATTCTTCT GGCTTCATCC CAGAATCTCC CCACCTATTG CGCCGGACAG
 661 GTAAGACATG ACCACCGCTG ATCTCGTCAT AAGAACTGTC TAACGGCCAG ACGCGCTTTA
 721 GGTCTTCTAC AAGGTCGGGT TCGGTGGGCT TTCATACACC TGGAATGTCC TGGCAGCCGA
 781 TGTGACGAAC CTACGAAACC GAGGGCTGGC GTTTGCTTTC ACCTCGTCCC CTGCTTTGAT
 841 CTCCGCGTTC GCCGGTTCCA AGGCGGCGTC GGATCTCCTG GCCCACTCGA CCTGGCGATG
 901 GGGCTTTGGC ATGTGGGCCA TTATCTTGCC GGTTGTTGCG CTGCCAATTT ATGGCCTTTT
 961 GGCGTACCAC CTACGCCAAG CCGAGAAAAA GGGGGTTCTC GTCAAGGAGA CGAGAGATTG
1021 GAGTATCACC CCGAAGACAG TTTGGTGGGC CATTATGGAA TTTGATCGTA AGTATCAACC
1081 AAGGGCGGTT GTCGCCTCAA AAGGGTTCCT TACCGAAGGC TAATCAATGA TCTTACCACT
1141 CACCTAGTGC CCGGAGTTCT TCTCTTCGCT GGCGGGTTCG TCATATTCCT TCTCCCCTTT
1201 ACTCTGGCGG CGACGGCGCC CCATGGGTAT CAGACCGACT ATATCATTGC GATGATCACT
1261 CTCGGCCTGG CCCTAATCAT CGCTTTTGGC TTCTACGAAA TGCTCGTGGC GCCCGTGCCG
1321 TTCTTGAACT ATAAATTCCT CATTGACCGG ACCGTGCTGG GTGCATGTCT GCTGGATATG
1381 ACATATCAGG TTTCCTACTA CTGCTATGCC AGCTATCTTC CGTCGTTCTT GCAGGTCGTG
1441 TACGAGCTGG ACGTCGCCAC GGCGGGATAT GTCACCAACA CGTTCAGTGT GGTCTCCTTT
1501 GTCTTCCTGT TCTTCGCCGG TTGGCTCATC CGCTGGACCG GTCGTTTCAA GTGGATCCTT
1561 TGGGTGTGCG TTCCGCTCTA CATCTTCGGC CTGGGTCTGA TGATTCACTT CCGTCAACCG
1621 GGCGGATACA TCGGGTACAT CGTTATGTGC GAGATTTTCT TCTCCGTCGC TGGAAGCGTC
1681 TTCATTCTCT GCGTGCAACT GGCGGTGCTT GCGTCCGTTG ATCACCAACA CGTTGCCGCC
1741 GTGCTCGCGT TGCTGTTCGT CATGGGCAGC ATTGGCGGCT CTATCGGCAG CGCAATCTGT
1801 GGAGCAATCT GGACCAGCAC TTTTCTGTCG AGACTGGAGA GGAACTTGCC CGCGTCTGCC
1861 ATGCCTGACT TGAGCTTGAT CTATTCGTCC CTCCCCACCC AGCTCAGCTA CCCCGTCGGA
1921 AGTGCTACCC GGACCGCCAT CGTGGAGGCA TACGGGTATG CCCAAGCAAG GATGCTCATT
1981 GCCGGTACTG CATTCATGGT TCTGGGCTTC ATCTGGGTTG GCATGATGAG GAACCTGAAC
2041 GTGAAAAACA TGACTCAGAC CAAGGGTAAT GTTGTGTAG
```

Figure 2-2. 2079 bp nucleotide sequence of *mirB* from *Aspergillus fumigatus* strain Af293.

2.1.1 Genomic sequence analysis

Basic information about the genomic sequence of *mirB* was obtained from the *mirB* entry in the Entrez gene database (Maglott et al. 2005). To predict the location of introns and exons the web-based program Genewise was used (Birney et al. 2004). To look for possible SREA binding sites in the upstream region of *mirB* a simple perl script was written and run on command line. The script was designed to search the input

sequence for the word 'GATA', the SREA binding site, and report its location in the sequence. The input was a text file containing the sequence immediately upstream of *mirB*, in the promoter region, arbitrarily chosen to be 855bp long.

2.1.2 Protein sequence analysis

The ProtParam tool (Gasteiger et al. 2005) was used to determine the molecular weight and theoretical isoelectric point of MirB. WoLFPsort (Horton et al. 2007) was used to predict the cellular localization of MirB and potentially detect the presence of signal peptides. HMMTOP 2.0 (Tusnády & Simon 1998) and SOSUI 1.11 (Hirokawa et al. 1998) were used to determine the expected membrane topology and 2D structure of MirB.

To look for conserved domains in MirB, the Conserved Domain Database and Search Tool from NCBI was utilized (Marchler-Bauer & Bryant 2004). The sequence was run using default settings (max hit = 100; e-value = 0.01; with low complexity filtering). The search was conducted twice, first using the CDD database, and then second, using the KOG database. Information about the possible function of MirB was obtained from the Gene Ontology website (The Gene Ontology Consortium 2000). This site was accessed by clicking on the links (GO_component, GO_process, and GO_function) provided from the MirB protein sequence page in NCBI (Accession: XP_748684). SWISS-MODEL (Arnold et al. 2006) was used in an attempt to construct a 3D structure of the protein. The 'First Approach mode' was used. The modeling attempt was run using default options: 'e-value 0.00001' and 'select best template'. Selected programs were also used to identify possible glycosylation sites (NetNGlyc, OPAL,

NetOGlyc, and YinOYang) (Gupta & Brunak 2002; Julenius et al. 2005; Frishman & Argos 1996).

2.1.3 Multiple Sequence Alignment

ClustalX 1.83 (Chenna 2003) was used to perform multiple sequence alignments of MirB with various known or putative fungal siderophore transporters. Alignments were carried out to compare *A.f.* MirB against annotated fungal siderophores transporters in *Aspergillus nidulans* (MirB, MirA, MirC), *Schizosaccharomyces pombe* (Str1-3), *Saccharomyces cerevisiae* (Arn1-4), and *Candida albicans* (Arn1), putative TAF transporters in *Aspergillus clavatus*, *Aspergillus terreus*, and *Neosartorya fischeri*, as well as other putative siderophores transporters in *Coccidioides immitis*, *Neosartorya fischeri*, *Aspergillus clavatus*, *Neurospora crassa*, and *Cryptococcus neoformans*. All sequences were obtained from NCBI.

2.2 Growth conditions

Aspergillus fumigatus ATCC 13075 from silica gel stocks was cultured at 37°C on MYPD agar (0.3% malt extract, 0.3% yeast extract, 0.5% peptone, 1% dextrose, pH 6.0, 1.5% agar) until sporulation occurred. Liquid cultures used for RNA extraction were grown in modified Grimm-Allen low iron media (Payne 1994) overnight (O/N) at 37°C.

Saccharomyces cerevisiae strain PHY14 was obtained from Dr. Joachim F. Ernst (Heinrich-Heine-Universität Düsseldorf, Germany), while strain DEY1394 was obtained from Dr. David Eide (University of Wisconsin, Madison, USA). PHY14 and DEY1394 were cultured on YPAD **(**0.0075% adenine hemisulfate, 1% yeast extract, 2% Bacto peptone, 2% dextrose, 2% Bacto agar, dH_20**)** at 30°C. Transformed PHY14 and

DEY1394 strains were cultured on solid agar containing synthetic dextrose (SD) (0.67% yeast nitrogen base without amino acids, 2% dextrose, 1.3g amino acid dropout powder without uracil, 2% Bacto agar, 1L dH_20) at 30°C. Uracil was omitted for selection of transformants. Liquid cultures were grown in synthetic raffinose (SR) (0.67% yeast nitrogen base without amino acids, 2% raffinose, 1.3g amino acid dropout powder without uracil, 2% Bacto agar, 1L dH_20) or SR supplemented with 0.5% galactose (SR + gal) to induce recombinant protein. For a list of *S. cerevisiae* strains used in this study refer to Table 2-1.

Table 2-1. *Saccharomyces cerevisiae* strains and plasmids used in this study.

Strain or Plasmid	Genotype or description	Reference
Strain		
DEY1394	*MATα ade6 can1 his3 leu2 trp1 ura3 fet3-2::HIS3*	(Askwith et al. 1994)
PHY14	Same as with DEY1394 but *arn1Δ::loxP arn2Δ::loxP arn3Δ::loxP enb1Δ::loxP-kanMX-loxP*	(Heymann et al. 2002)
Plasmid		
pESC-URA	Yeast expression vector with Gal10 promoter and FLAG epitope	Stratagene
pESC-mirB	1.8 kb NotI-SpeI *mirB* cDNA fragment in pESC-URA	This study
pESC-mirB/R570A	Same as pESC-mirB but with Arginine to Alanine substitution at position 570, loop 7	This study
pESC-mirB/Y577A	Tyrosine to Alanine substitution at position 577, loop 7	This study
pESC-mirB/A125D	Alanine to Aspartic acid substitution at position 125, loop 1	This study
pESC-mirB/Y398A	Tyrosine to Alanine substitution at position 398, loop 5	This study
pESC-mirB/W251/253A	Tryptophan to Alanine double substitution at positions 251 and 253, loop 3	This study
pESC-mirB/N-termDel	N-terminal deletion of first 12 amino acids (following Met)	This study
pESC-mirB/C-termDel	C-terminal deletion of last 5 amino acids	This study
pESC-mirB/F129D	Phenylalanine to Aspartic acid at position 129, loop 1	This study
pESC-mirB/Loop3Del	Loop 3 deletion of amino acids 247-256	This study
pESC-mirB/Loop6Del	Loop 6 deletion of amino acids 467-474	This study
pESC-mirB/Loop7Del1	Loop 7 deletion 1 of amino acids 533-544	This study
pESC-mirB/Loop7Del2	Loop 7 deletion 2 of amino acids 566-580	This study

2.3 Creation of expression vectors

2.3.1 Construction of pESC-*mirB*

mirB was PCR amplified from cDNA from wildtype *A. fumigatus* (strain 13073) using primers NotIp-ESCmirBfor and SpeIp-ESCmirBrev (Table 2-2) containing *NotI* and *SpeI* cut sites and subsequently cloned into the multiple cloning site of the yeast expression vector pESC-URA (Agilent Technologies), under the control of the GAL10 promoter (Figure 2-3). pESC-URA contains the FLAG epitope (Sigma), which results in C-terminal tagging of the gene of interest. The resulting pESC-*mirB* vector was transformed into competent *Escherichia coli* cells and positive colonies selected for on agar plates containing 200 µg/ml ampicillin. The presence of the *mirB* insert was confirmed by colony PCR using vector specific Gal10 forward and reverse primers (Agilent Technologies), as well as by restriction digest, using *NotI* and *SpeI* following miniprep (Qiagen QIAprep Spin MiniPrep Kit) of select transformant colonies. Sequencing was performed to ensure no errors were present in the sequence.

Table 2-2. Primers used for the creation of pESC-*mirB* and mutant plasmids.

Primer name	Primer sequence (5' to 3')
NotIp-ESCmirBfor	ATTGCGGCCGCATGCTTCACGTCTTATCAGTCG
SpeIp-ESCmirBrev	CCGACTAGTGCCACAACATTACCCTTGGT
mirB-R570AFor	GTCGGAAGTGCTACCGCTACCGCCATCGTGGAG
mirB-R570ARev	CTCCACGATGGCGGTAGCGGTAGCACTTCCGAC
mirB-Y577AFor	CCGCCATCGTGGAGGCAGCCGGGTATGCCC
mirB-Y577ARev	GGGCATACCCGGCTGCCTCCACGATGGCGG
mirB-A125DFor	CAAGCTTGAACGCTTATGACACAAGTTCTTTCCTCGG
mirB-A125DRev	CCGAGGAAAGAACTTGTGTCATAAGCGTTCAAGCTTG
mirB-Y398AFor	CTACTACTGCTATGCCAGCGCTCTTCCGTCGTTCTTGACG
mirB-Y398ARev	CTGCAAGAACGACGGAAGAGCGCTGGCATAGCAGTAGTAG
mirB-W251AFor	TCCTGGCCCACTCGACCGCCCGAGCCGGCTTTGGCATGTGGGC
mirB-W251ARev	GCCCACATGCCAAAGCCGGCTCGGGCGGTCGAGTGGGCCAGGA
mirB-NtermdelF	GGGCGGCCGCATGGCGTTTACTGTCG
mirB-NtermdelR	CGACAGTAAACGCCATGCGGCCGCCC
mirB-CtermdelF	GTGAAAAACATGACTCAGACCGCACTAGTATCGATGGATTAC
mirB-CtermdelR	GTAATCCATCGATACTAGTGCGGTCTGAGTCATGTTTTTCAC
MirB-F129D-F	ACGCTTATGCCACAAGTTCTGATCTCGGCCACTCGCTGTTG
MirB-F129D-R	CAACAGCGAGTGGCCGAGATCAGAACTTGTGGCATAAGCGT
MirB-loop3del-F	GGCGTCGGATCTCCTGATGTGGGCCATTATCT
MirB-loop3del-R	AGATAATGGCCCACATCAGGAGATCCGACGCC
MirB-loop6del-F	GATTCACTTCCGTCAACCGATGTGAGAGATTTTCTTCT
MirB-loop6del-R	AGAAGAAAATCTCGCACATCGGTTGACGGAAGTGAATC
MirB-loop7-1597del-F	GCAATCTGGACCAGCTCTGCCATGCCTGAC
MirB-loop7-1597del-R	GTCAGGCATGGCAGAGCTGGTCCAGATTGC
MirB-loop7-1696del-F	CTCAGCTACCCCGTCCAAGCAAGGATGCTC
MirB-loop7-1696del-R	GAGCATCCTTGCTTGGACGGGGTAGCTGAG

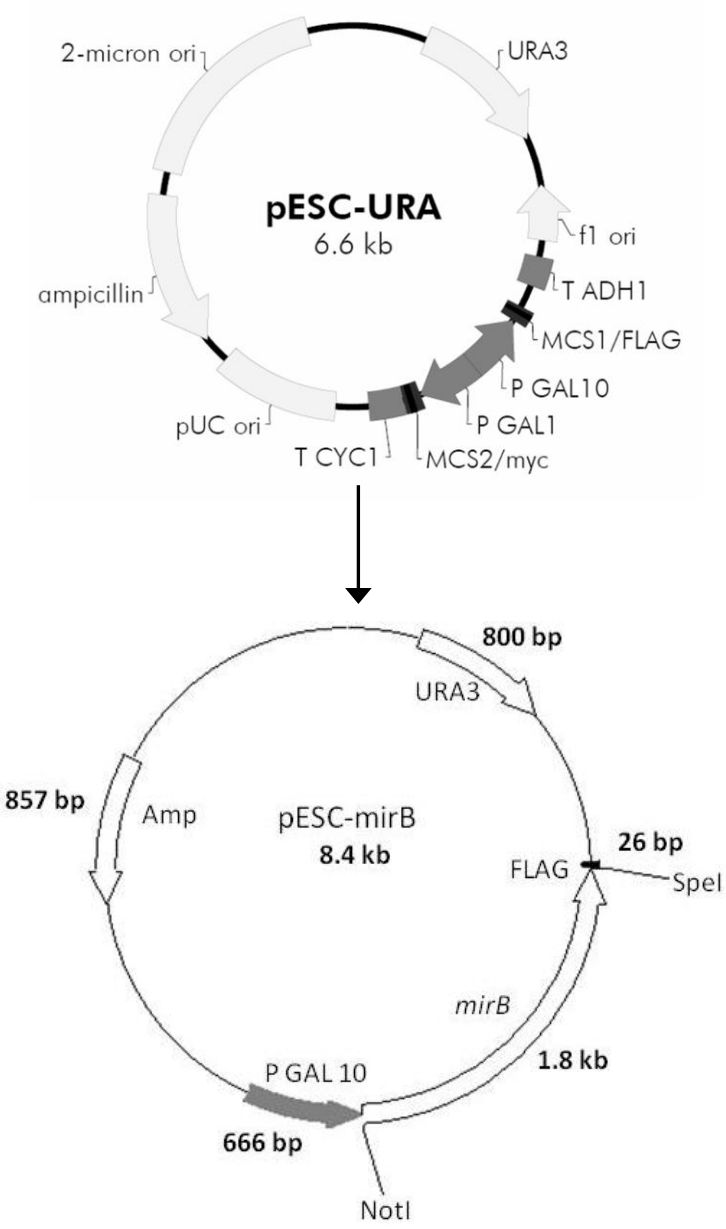

Figure 2-3. Diagram of yeast expression vector pESC-URA and the recombinant plasmid pESC-*mirB*. The *mirB* gene was inserted between the NotI and SpeI cut sites in the multiple cloning site of pESC-URA and is C-terminal tagged with the FLAG epitope.

2.3.2 Creation of MirB mutants

MirB has seven extracellular loops that contain several conserved amino acids (refer to Results). Since these may potentially have a role in recognition and binding of

ferrated TAF, we targeted seven of those amino acids for mutation (Table 2-1 & Figure 2-4). To study the importance of the loops themselves in uptake, we also created deletion mutants, targeting 7-14 amino acids, of loops 3, 6 and 7 (Table 2-1 & Figure 2-4). Due to the length of the seventh loop, two different deletions mutants were created, targeting opposite ends of the loop. For all of the loop deletion mutants, care was taken to leave a few amino acids in the loop so as to, in theory, allow for proper looping and re-insertion in the membrane. Additionally, we also created N- and C-terminal deletion mutants to identify potential sorting signals.

The technique of site-directed mutagenesis, using Agilent Technologies' QuikChange Lightning mutagenesis kit, was used to introduce mutations in the wildtype *mirB* gene located on the pESC-*mirB* vector. Primers were designed using Agilent Technologies' QuikChange Primer Design Program (Agilent Technologies n.d.) and contained the appropriate base changes. Codon usage bias was taken in to account when selecting the appropriate codons. A list of all primers used can be found in Table 2-2. The mutated plasmids were transformed and selected for in *E. coli*, as with wildtype. All resulting mutant plasmids were confirmed by sequencing.

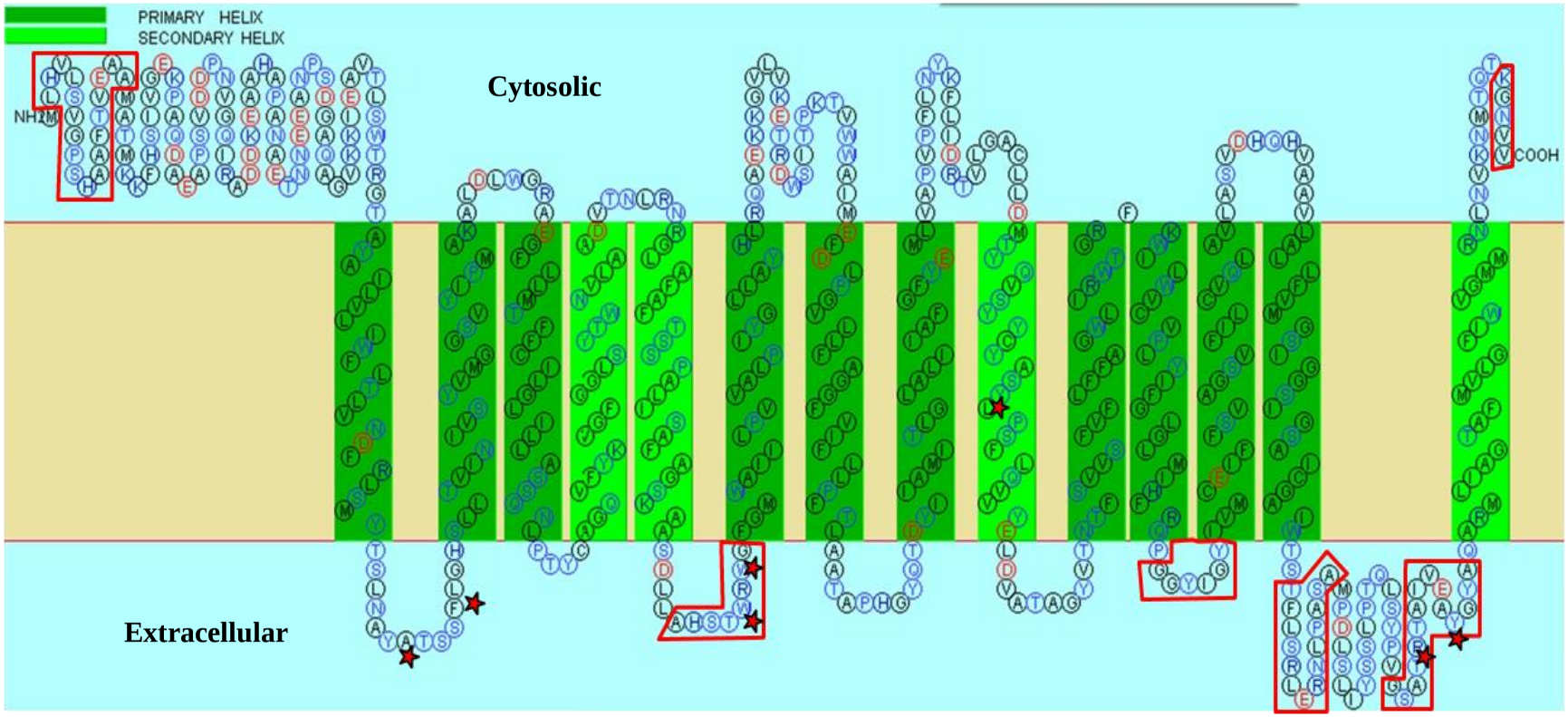

Figure 2-4. Schematic of the 2D membrane topology of MirB as predicted by SOSUI 1.1 (Hirokawa et al. 1998). Residues highlighted with red stars were targetted for mutagenesis, while boxed residues were targeted for deletion.

2.3.3 Transformation of *Saccharomyces cerevisiae*

Since *Aspergillus fumigatus* contains a number of other putative siderophore transporters that could potentially play a role in the uptake of TAFC, all wildtype and mutant pESC-*mirB* vectors were transformed into PHY14, a strain of *Saccharomyces cerevisiae* deficient in all endogenous siderophore transporters (Heymann et al. 2002). Transformations were carried out using the lithium acetate method as outlined in the pESC-URA manual (Stratagene). Colony PCR, performed on putative transformant colonies using Gal10 forward and reverse primers, confirmed the presence of the wildtype or mutant *mirB* plasmid in each individual transformant strain.

2.4 Immunoblotting

Since all MirB proteins are tagged with the FLAG epitope, to test for the presence of the MirB proteins, western blotting using monoclonal anti-FLAG antibodies (Sigma) was attempted with protein extracted from all of the wildtype and mutant strains.

2.4.1 Protein isolation using subcellular fractionation

Initially, subcellular fractionation by differential centrifugation was used to isolate the plasma membrane fraction from the total cell lysates of PHY14 strains as outlined previously (Sun-Wada et al. 1998). For these experiments, expression of *mirB* was induced by growing the yeast in synthetic galactose media (SG; 0.67% yeast nitrogen base without amino acids, 2% galactose, 1.3g amino acid dropout powder, 2% Bacto agar, 1L dH_20).

2.4.2 Protein isolation using trichloroacetic acid (TCA) precipitation

To improve protein yields, TCA precipitation of proteins from total cell lysates was performed. Expression of the MirB proteins was induced by growing the strains in SR media supplemented with 0.5% glucose. SR with 0.5% galactose was used instead of SG media in order to increase biomass. The TCA precipitations were conducted as outlined in Keogh et al. (2006).

2.4.3 Immunoblotting

Protein from each strain (40 µg) was loaded on 8 M Urea-SDS-PAGE gels. 2 M urea was added to the loading buffer (2X; 5.2 ml dH_20, 0.6 ml 0.5 M Tris pH 6.8, 0.95 ml glycerol, 0.5 ml 20% SDS, 0.25 ml β-mercaptoethanol, and 0.5 ml 1% bromophenol blue) to encourage denaturation of membrane proteins and samples were heated at 40°C for 45 min. Proteins were transferred onto a nitrocellulose membrane (Amersham Hybond-ECL) and blocked overnight in 3% BSA diluted in Tris-buffered saline with Tween-20 (TBST) (12.1 g Tris base, 8.8 g NaCl, pH 7.5, 0.1 % Tween 20, 1 L H_20). Membranes were then incubated for two hours at room temperature with mouse monoclonal anti-FLAG antibody conjugated to HRP (Sigma), diluted to 1.1 µg/ml (1:1000) in TBST with BSA. Membranes were washed three times, 5 min each, in TBST before the addition of the chemiluminescence substrate (Thermo Scientific SuperSignal West Pico), and then exposed to film (Kodak BioMax Light Film). In some experiments, the anti-FLAG antibody was pre-sorbed to PHY14-URA cell lysate spoted onto a nitrocellulose membrane; a pencil was used to draw a grid on the membrane and approximately 20 µg of PHY14-URA cell lysate was spoted onto the middle of each grid. The membrane was allowed to dry, and then blocked for 1 hour at room temperature in

3% BSA in TBST. The membrane was then incubated O/N at room temperature with the anti-FLAG antibody (1.1 µg/ml) to remove any non-specific binding, and the antibody solution was subsequently used for the westerns.

2.5 Growth assays

To test the ability of the various strains to grow on media with Fe-TAFC as the sole source of iron, a viability assay was developed. In this assay, only those strains expressing a functional MirB should be able to grow.

2.5.1 Growth assays using liquid cultures

Growth assays using liquid cultures were done in 96-well plates containing SR with 0.2% galactose were inoculated with *S. cerevisiae* expressing wild type MirB (MirBWT), PHY14-URA, and DEY1394-URA to an OD of 0.1 and a total volume of 200 µl. Wells contained either cells and media only, cells and media with 500µM of bathophenanthroline sulfonate (BPS), a free iron chelator (Cowart et al. 1993) or cells and media with 500 µM BPS and 50 µM of Fe-TAFC as the sole source of iron. Attempts were made to optimize the experiment by varying a number of factors including the initial inoculum size (OD_{620} 0.1-0.35), the amount of galactose in the media (0.2-0.5 %), the amount of BPS used (250-1000 µM), the amount of Fe-TAF added (10-50 µM), and by using a different free iron chelator, 2,2'-dipyridyl (250 µM). All plates were incubated in a humidified chamber at 30 °C and growth was monitored over several days by measuring OD_{620}.

2.5.2 Growth assays on solid agar

Two different methods were performed to determine growth on solid medium. For the first method, 5 µl of O/N SD cultures at an OD_{600} of 0.5 was transferred onto plates containing SR + gal with 500 µM of BPS and 50 µM of Fe-TAFC. Control plates with SR + gal only and SR + gal with 500 µM BPS were also included. This assay was first attempted with SG media instead of SR + gal but was eventually replaced with SR + gal to encourage better growth of cultures. Plates were incubated at 30 °C for 5-7 days. For the second method cultures were grown O/N in SD and the concentration of each culture determined by cell counting using a haemacytometer. Cultures were subsequently diluted to 10^8, 10^7, 10^6 and 10^5 cells/ml in 96-well plates, and then transferred using a 48-pin transfer tool to appropriate plates. Plates were prepared as described for the first method with the exception that a 5 ml overlay of 150 µM Fe-TAFC was used instead of adding 50 µM TAFC directly to the media.

2.6 ^{55}Fe-TAF uptake assays

To determine the rate and extent of iron uptake from Fe-TAFC for each of the yeast strains expressing a wildtype or a mutant MirB protein, TAFC transport assays were performed using TAFC labelled with radioactive iron, ^{55}Fe. Desferri-TAFC was purified from liquid cultures of *Aspergillus fumigatus* by Linda Pinto (Moore laboratory, Simon Fraser University) according to procedures developed in our laboratory. Briefly, Amberlite XAD16 (Supelco) resin was added to culture supernatants of *Aspergillus fumigatus* and incubated 2 hours at 37°C with shaking. Siderophores were eluted from the resin using 100% methanol. The eluate was evaporated to dryness and the siderophores were separated by flash chromatography on a silica gel column packed in

dichloromethane. The desferri-TAFC was eluted with methanol:water:acetic acid (80:19.9:0.1) and freeze dried. Purity of the TAFC was checked using thin layer chromatography (TLC) and mass spectrometry. To make ^{55}Fe-TAFC, 41 nmoles of radioactive $^{55}FeCl_3$ was added to 50 nmoles desferri-TAFC in solution and left to react at room temperature for two hours. Formation of ^{55}Fe-TAF was confirmed by TLC (mobile phase: 80% methanol in dH_2O).

For the ^{55}Fe uptake assay, 2 µM of ^{55}iron-labelled TAFC was added to galactose-induced yeast cells, and cells were incubated at 30°C for 60 min in SR in the presence of 100 µM BPS. After various incubation periods, cells were collected by filtration onto glass microfiber filters (Ahlstrom) and washed 4 times with assay buffer 1 (2% raffinose, 50 mM sodium citrate, 10 µM cold Fe-TAF) and 2 (2% raffinose, 50 mM sodium citrate, 200 µM BPS, 5% BSA), and the bound radioactivity determined by liquid scintillation counting. Statistical analysis was conducted using GraphPad Prism 5.

2.7 Immunofluorescence

To determine the cellular localization of the MirB-FLAG construct in yeast cells, immunocytochemistry was performed with the wildtype MirB strain and the A125D mutant. Slides were prepared as previously described with some modifications (Silver 2009). Slides of PHY14-URA and MirBWT without 1° antibody were included as negative controls. O/N cultures grown in SR were diluted and transferred to induction media at an OD of 0.5. Induced yeast cells were incubated at room temperature (RT) with 5 µg/ml of the plasma membrane and endosomal marker, FM4-64FX (Invitrogen) for 20 min, centrifuged at 800*g*, washed with media, and then resuspended in media and fixed with 4 % formaldehyde for 15 min. Fixed cells were washed first with 0.1 M potassium

phosphate pH 6.5, then with P solution (0.1 M potassium phosphate pH 6.5, 1.2 M sorbitol), and subsequently spheroplasts were made by adding 15 µl of 10 mg/ml zymolyase (US Biological) in P solution. Spheroplast formation was observed microscopically by looking for the appearance of less refractile cells, indicative of spheroplast formation. After 25 min, spheroplasts were centrifuged, resuspended in P solution, and applied to grease-pencil wells on 0.1 % poly-l-lysine coated slides. Adherent yeast spheroplasts were then permeabilized by immersion in ice-cold methanol for 5 min followed by 30 s in ice-cold acetone. Slides were washed once with PBS-BSA and then exposed to mouse anti-FLAG antibodies (Sigma), diluted 1:300 in PBS-BSA (3.67 µg/ml), for 2 hours. Wells were washed four times with PBS-BSA before the addition of the Alexa Fluor 488 conjugated anti-mouse antibodies (Invitrogen), diluted 1:300 in PBS-BSA to 6.67 µg/ml. Following a 2-hour incubation, wells were washed three times in PBS-BSA and once with PBS. DNA was stained with the addition of 1 µg/ml of DAPI in PBS to the wells and incubated for 5 min. Slides were washed with PBS, and sealed with a cover slip after the addition of a drop of ProLong Gold antifade reagent (Invitrogen). Images were collected using a WaveFX Spinning Disc Confocal System (Quorum Technologies) and Zeiss Axio observer inverted microscope. Image acquisition and processing was performed using the Velocity software (PerkinElmer).

2.8 Localization of a MirB-GFP construct in *A. fumigatus*

To determine the subcellular localization of MirB in *Aspergillus fumigatus* under iron limited conditions, a *mirB-gfp* fusion construct was created to replace endogenous *mirB,* via homologous recombination, resulting in a MirB-GFP expressing strain of *A. fumigatus,* which could be used for immunofluorescence studies (Refer to Appendix 3).

3: Results

3.1 MirB bioinformatics analysis

The Entrez gene database entry for *A. fumigatus mirB* reports that the gene is 2079bp, is located on chromosome 3, and contains 3 introns and 4 exons (Figure 3-1). The program Genewise (Birney et al. 2004) confirmed the presence and locations of these introns and exons. Introns are located from 291-389bp (99bp), 661-721bp (61bp), and 1068-1147bp (80bp). The program did not find any untranslated regions at either the 3' or 5' end. Using a perl script, two possible SREA binding sites (GATA sites) were found in the promoter region of *mirB* (855bp). The perl script result indicates that they are located at -845 bp and -34 bp, respectively, from the start codon (Figure 3-2).

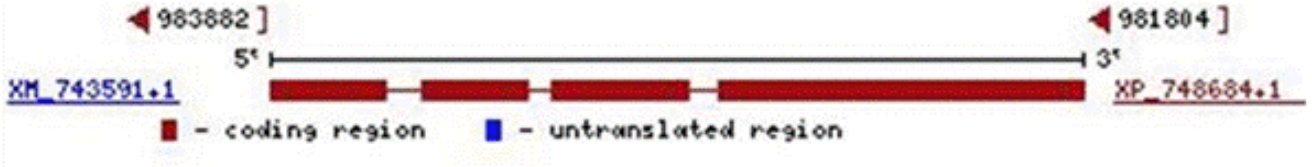

Figure 3-1. Schematic of the Af *mirB* gene (2079 bp) with introns (red line) and exons (red rectangles) from the Entrez gene database (Maglott et al. 2005). Introns are located from 291-389, 661-721, and 1068-1147 bp from the start. *mirB* is located from 981804-983882 bp on chromosom 3. NCBI Pubmed MirB Accesssion number: XP_748684.

```
   1 CAACAAGTAC GATACTCCAC CGCCAGGCAT TGAGGAGGGA GAGGTACGGT ATTCGATCAC
  61 TAGGGAGGAA TGGTTGCGGA TGCAAAAGCC CAGCATGACT CGAAGTCGCT GGTTTCCGGC
 121 TTTCGCCAGC TGGCTGCCCC GATTGCTCCT GTCCAGGCTC TGGTCCTATA TTTTCCAAGG
 181 GCGTAGGCTC GCAGCTGGGG CGGCCAGCCC CTGAACACAA TAAAGAGACC TTGTTCTAGG
 241 AACTATGGAA ATTGTCTCTC CGTTTCTAAG TCATGCATTA AAGTGTTTGC AGTGAGAGAT
 301 CTGTTGAAAC GTAGTTCGAG ACTACTGCCT GGCATCACCC AACATCCTCT ATAGCGCCAG
 361 GCGCGCCATA CGCGCCATGC ATAATCTCTC GTTGGGCTTT AGGGCTGTAA TGGTTTGACC
 421 TTATCAATCT TCGGCCGTGG AATAGTTCCG CGTCGCAGTG GCGCCAACTA ACGGTGGTTT
 481 AGACAGAGGT CGGACCATGG CCGCCTCGTG AGCAAGTGAT GTGTCAGTGA CTGAATGTAT
 541 GTTTTTGCTA CGAACGGCTT GGCACGCTTA TTTTGCATGT GCTATTGGCG CGAAAACGAG
 601 GCCATGAACC CCCCCCCCCC CCCCGGTCAG TCTATCCTTG TTAGGCCCGT ACAAGTGTGG
 661 GACGGCTAGG CGTATGGGCA CTGGTATCAC GCGGTAACAA TGCGTGTGGG AACCCTCTTG
 721 GGCTGCAGCG TCGGTTGCGT AAGACCCGAC ATTATCTGAT CAAAATACAG GGCATATCGG
 781 TGCCACACGG CGTAGGCACT GAGACTTACG TAAAGAATGT AGATAACCTG TGCCGGAAGC
 841 CGGTATTTAA CATTCATGCT
```

Figure 3-2. Location of putative SREA binding sites (GATA) upstream of *mirB*. The two GATA sites (bold) are located at -34 bp and -845 bp from the ATG start codon (bold).

Using the program ProtParam, (Gasteiger et al. 2005) the molecular weight of MirB (612 amino acids) and the theoretical pI were calculated to be 66.85 kDa and 7.14, respectively. The program WoLFPsort (Horton et al. 2007) predicted the localization of MirB to be in the plasma membrane. No known localization signals were found using WoLFPsort, although the C-terminal does contain a KKXX-like motif (TKGNV), a possible ER membrane retention signal (Vincent et al. 1998).

Membrane topology analysis carried out by HMMTOP (Tusnády & Simon 1998) and SOSUI (Hirokawa et al. 1998) confirmed the plasma membrane prediction of WoLFPsort. They determined MirB to be a transmembrane protein with 14 transmembrane α-helices connected by loops, with cytosolic N- and C-termini. MirB is not predicted to contain any β–strands. Figure 2-4, without the conserved amino acids,

was created by SOSUI, and shows the 2D structure and predicted 2D membrane topology of *A. fumigatus* MirB. A schematic of this arrangement is shown in Figure 3-6.

Four different conserved domains were found using NCBI Conserved Domain search (Marchler-Bauer & Bryant 2004): TRI12, MFS-1, KOG0254 and KOG0255 (Figure 3-3). All four domains correspond to transporters that are members of the Major Facilitator Superfamily (MFS). The function of MirB as suggested by Gene Ontology (The Gene Ontology Consortium 2000) is that of a membrane-bound siderochrome-iron (ferrioxamine) uptake transporter. Such proteins operate as symporters, catalyzing the transfer of a solute from one side of a membrane to the other using a proton gradient. Multiple sequence alignment of MirB with various characterized or putative fungal siderophore transporters found numerous conserved amino acids (Figure 3-4). Using information about conserved amino acid residues obtained from these alignments, a select number of conserved, identical or similar, amino acids present in the extracellular loops were chosen for mutation (Figure 2-4).

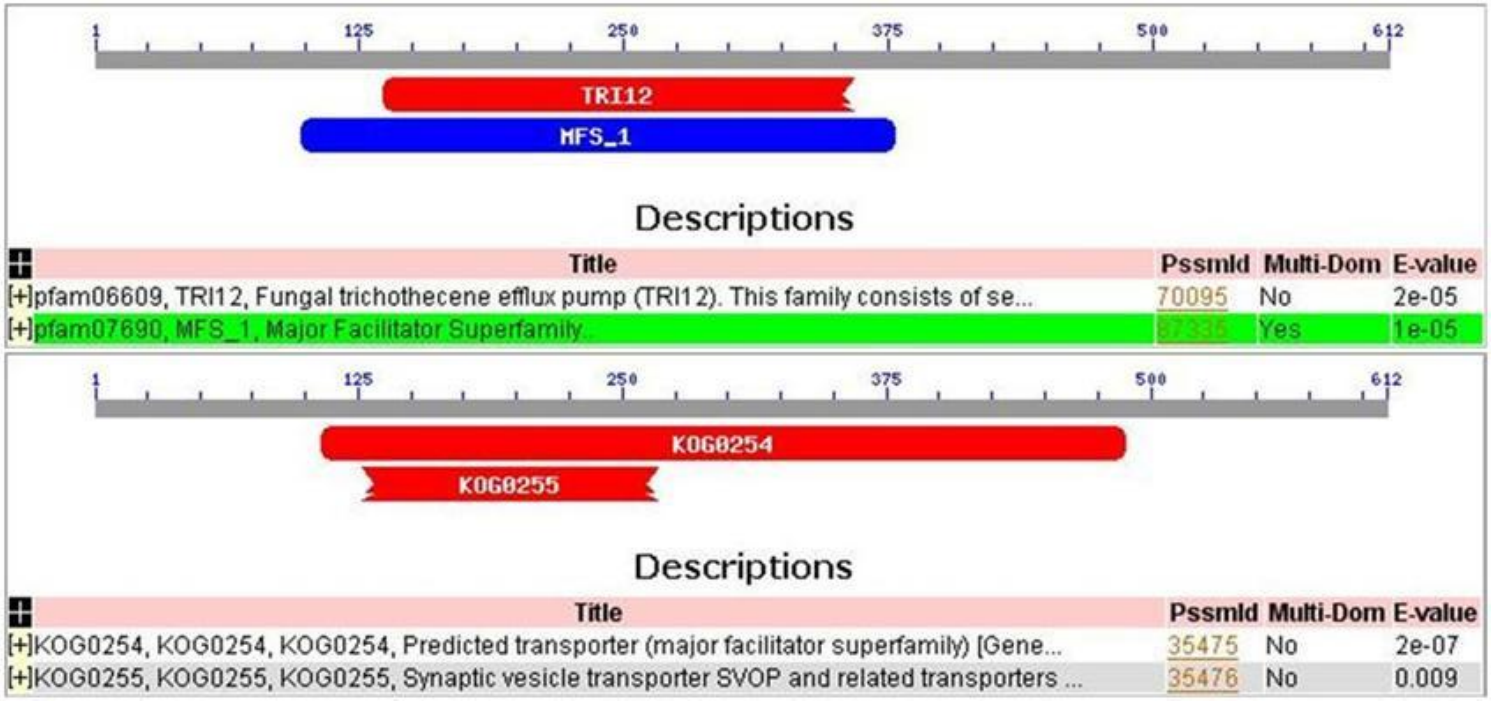

Figure 3-3. MirB conserved domains as predicted by NCBI Conserved Domain. The domains correspond to four membrane permeases all of whom are members of MFS.

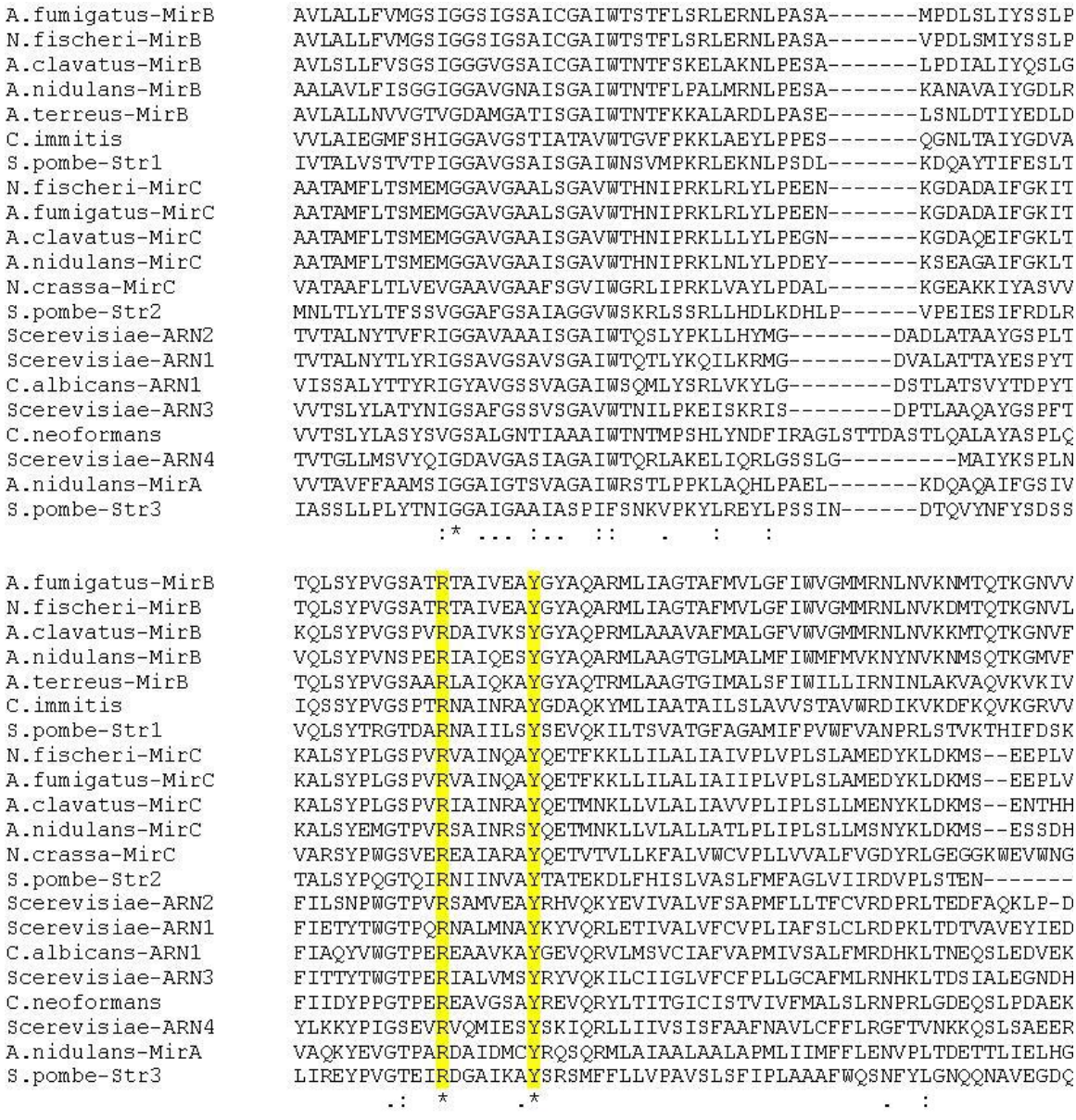

Figure 3-4. Partial multiple sequence alignment of *A. fumigatus* MirB with 20 characterized or putative fungal siderophore transporters. This alignment covers amino acids 506-618 of AfMirB. Included are the two amino acids in the seventh extracellular loop, arginine and tyrosine (highlighted), chosen for mutagenesis (refer to Figure 2-4).

Analysis of MirB by SWISS-MODEL (Arnold et al. 2006) was able to render a partial 3D model of MirB (Figure 3-7). The glycerol-3-phosphate (GlpT) transporter from *Escherichia coli*, another member of the MFS, was used for structural comparisons (pdb#

1pw4A). However, the sequence identity was only 7.843%, and the E value was 5.7E-12; therefore, this model may not be very representative of the actual structure of MirB. The MirB model (Figure 3-7) includes amino acids 144 to 444 which, according to SOSUI and HMMTOP, should include transmembrane hydrophobic domains (TMDs) 3 to 10 (of 14), cytosolic loops (CL) 2-6 (of 8), and extracellular loops (EL) 2-5 (of 7). A 2-D schematic of these TMDs and loops, based on the SOSUI model, can be seen in Figure 3-6. The original SOSUI model is shown in Figure 3-5. However, the 3D model only includes TMDs 3-6 and 9-10 (along with part of TMD 11), CL 3, 4 and 6 and EL 2, 3 and 5. The absence of TMDs 7-8, EL 4, and CL 5 in the 3D model is a result of SWISS-MODEL predicting a very long 100 a.a. CL 4 domain, the sequence of which, SOSUI and HMMTOP predict forms a short CL 4 domain and subsequently TMD 7, EL 4, TMD 8 and CL 5. The discrepancy between the models is most likely a result of SWISS-MODEL attempting to fit the 14 TMD MirB sequence to that of the 12 TMD GlpT transporter in order to construct an acceptable 3D model. It is worthwhile to note that the residues presented in the model form what appears to be a helical channel and that the overall structure resembles that of LacY in *E. coli* (Figure 1-14).

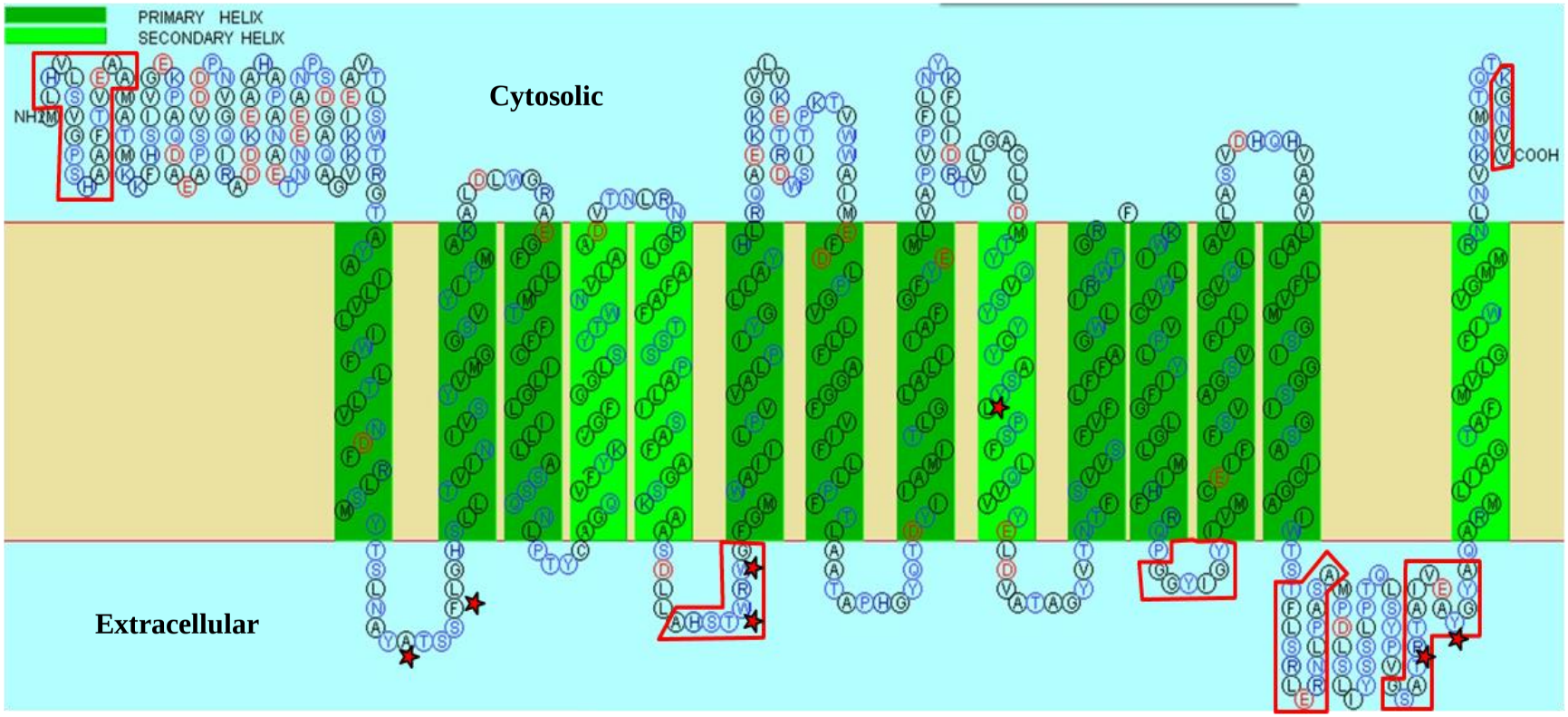

Figure 3-5. The 2D membrane topology of MirB, as predicted by SOSUI, showing the seven extracellular loops and fourteen transmembrane domains. Residues highlighted with red stars were targetted for mutagenesis in this study, while boxed residues were targeted for deletion.

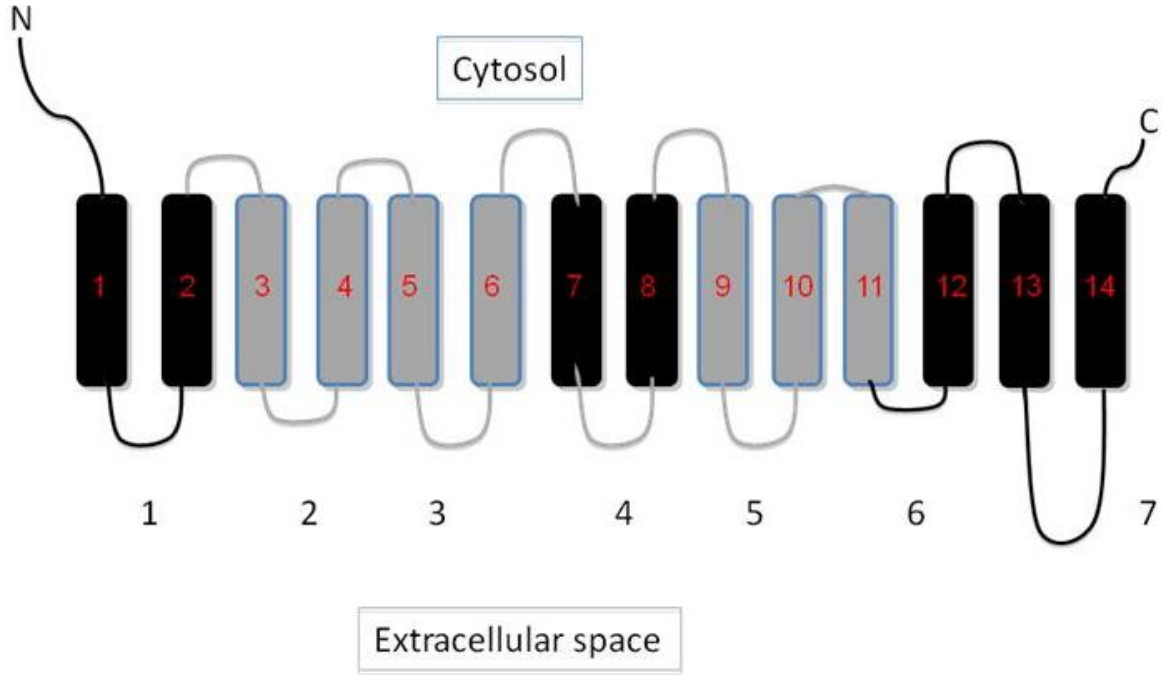

Figure 3-6. 2-D schematic of MirB (adapted from SOSUI model) from *A. fumigatus*. The cylinders represent the 14 transmembrane domains and the extracellular loops are numbered 1-7. TMDs 3-6 and 9-11 (grey), along with extracellular loops 2, 3 and 5 are included in the SWISS-MODEL shown in Figure 3-7.

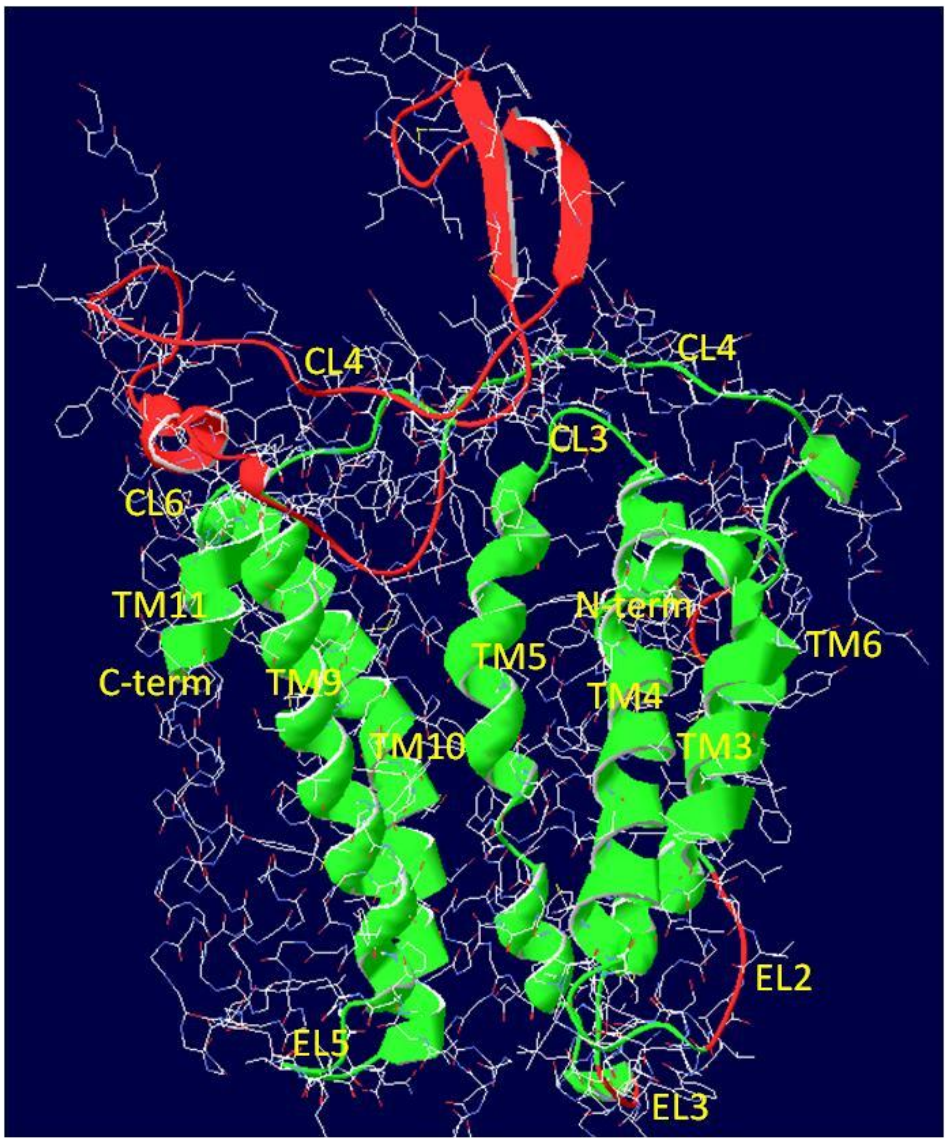

Figure 3-7. Ribbon model of amino acids 144-444 of MirB predicted by SWISS-MODEL. Represented in the model are, according to SOSUI, hydrophobic domains (TM) 3-6 and 9-11 (of 14), cytosolic loops (CL) 3, 4 and 6 (of 8) and extracellular loops (EL) 2, 3 and 5 (of 7). While SWISS-MODEL predicts a very long 100 a.a. cytosolic loop 4 (CL4) domain, according to SOSUI and HMMTOP, these amino acids form a short cytosolic loop 4 as well as the TM domains 7-8, extracellular loop 4 and cytosolic loop 5. This explains the absence of TM domains 7-8, EL4, and CL5 in the model above. Protein pdb# 1pw4A was used as the template.

Two possible N-glycosylation sites, with the tripeptide sequence Asn-X-Ser or Asn-X-Thr, were found. The first, Asn-Pro-Ser (amino acids 73-75), contains a proline

residue in the middle, and so is unlikely to be an actual N-glycosylation site. The second, an Asn-Met-Thr tripeptide is located at the N-terminus (609-611); however, this may also not be real, as N-glycans are generally not found in the cytosolic domains of transmembrane proteins (Wheatley & Hawtin 1999). Eleven potential O-N-acetylglucosamine (O-GlcNAc) sites were found. These are serines at amino acid position 6, 127, 228, 239, 532, 562, and threonines at 125, 215, 227, 290, and 418. No potential O-N-acetylgalactosamine (O-GalNAc) sites were identified in MirB. It should be noted that the programs used to predict possible O-glycosylation sites are designed for human/mammalian proteins and their accuracy in fungi is unknown.

Based on the data gathered from the bioinformatics analysis of MirB, including the predicted membrane localization with 14 transmembrane domains, the presence of conserved domains belonging to members of the MFS, and the similarity to *A. nidulans* MirB, we hypothesized that *A. fumigatus* MirB functions as a siderophore transporter. Because of its close relation to MirB from *A. nidulans*, it is also likely that *A. fumigatus* MirB is responsible for uptake of the ferrated siderophore TAFC.

3.2 Creation of pESC-*mirB* vector and MirB mutants

mirB (1.8 kb) amplified from *A. fumigatus* cDNA was successfully cloned into the multiple cloning site of pESC-URA and subsequently transformed into *Escherichia coli*. Both colony PCR on select colonies (data not shown) and restriction digest following miniprep of transformant colonies (Figure 3-8) confirmed the presence of an insert of the expected size.

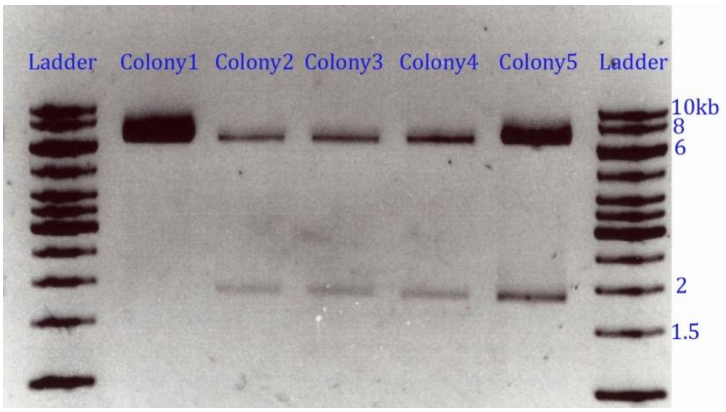

Figure 3-8. Restriction digest of pESC-mirB isolated from five *E.coli* colonies transformed with the plasmid. Expected size of *mirB* is 1.8kb and cut vector is 6.6kb.

Sequencing of the *mirB* insert in these plasmids showed differences in the amplified cDNA sequence (from ATCC 13073) compared to the published putative mRNA sequence from the Af293 strain. Plasmids isolated from several colonies were sequenced, and in each case, *mirB* was found to contain an additional 18 bases (GTACGCAATTCTAGTGCT) starting at position 291 (Figure 3-9). In the current annotated putative mRNA sequence, these bases are predicted to be part of the first intron. However, based on the sequencing results, these bases appear to be a part of the mRNA sequence of *mirB*, and result in an extra 6 amino acids in the protein sequence (YAILVL). Figure 3-10 lists the new amino acid sequence with the additional 6 amino acids. Sequencing was repeated with newly synthesized cDNA to ensure that this was not the result of an error during the original RT-PCR. The same result was obtained so it was concluded that at least in strain ATCC 13073, MirB is 618 amino acids, not 612.

```
   1 ATGCTTCACG TCTTATCAGT CGGTCCGTCC CATGCAGCGT TTACTGTCGA AGCAGCAATG
  61 GCAACCATGA AGAAATTCCA CTCGATTGTC GGTGAAAAGC CTGCCCAGGA TGCTGAGGCC
 121 CCCTCAGTCG ATGACCCAAA TGTTGGGCAG ATCAGAGCCG ACGACAAGGA GGCTGCTCAT
 181 GCGCCCGCCA ATGCGGAAAC CAATAATGAG GAGGCCAACC CGAGCGACGG AGCTCAGGCT
 241 GGTGTCAAGA AGATAGAGGC TGTGACCCTG AGTTGGACCA GGGGCACAGC GTACGCAATT
 301 CTAGTGCTCA TTTGGTTCCT AACGCTGGTC AACGATTTCC GACTGTCCAT GTATACAAGC
 361 TTGAACGCTT ATGCCACAAG TTCTTTCCTC GGCCACTCGC TGTTGACCGT CATCAACATT
 421 GTGTCCTACG TTATGGGCGG TTCCGTGTAC ATACCGATGG CCAAGGCGCT GGATCTTTGG
 481 GGCCGTGCAG AGGGTTTCCT TCTGATGACT TTCTTCTGTA TTCTGGGTTT GATTCTTCTG
 541 GCTTCATCCC AGAATCTCCC CACCTATTGC GCCGGACAGG TCTTCTACAA GGTCGGGTTC
 601 GGTGGGCTTT CATACACCTG GAATGTCCTG GCAGCCGATG TGACGAATCT ACGAAACCGA
 661 GGGCTGGCGT TTGCTTTCAC CTCGTCCCCT GCTTTGATCT CCGCGTTCGC CGGTTCCAAG
 721 GCGGCGTCGG ATCTCCTGGC CCACTCGACC TGGCGATGGG GCTTTGGCAT GTGGGCCATT
 781 ATCTTGCCGG TTGTTGCGCT GCCAATTTAT GGCCTTTTGG CGTACCACCT ACGCCAAGCC
 841 GAGAAAAAGG GGGTTCTCGT CAAGGAGACG AGAGATTGGA GTATCACCCC GAAGACAGTT
 901 TGGTGGGCCA TTATGGAATT TGATCTGCCC GGAGTTCTTC TCTTCGCTGG CGGGTTCGTC
 961 ATATTCCTTC TCCCCTTTAC TCTGGCGGCG ACGGCGCCCC ATGGGTATCA GACCGACTAT
1021 ATCATTGCGA TGATCACTCT CGGCCTGGCC CTAATCATCG CTTTTGGCTT CTACGAAATG
1081 CTCGTGGCGC CCGTGCCGTT CTTGAACTAT AAATTCCTCA TTGACCGGAC CGTGCTGGGT
1141 GCATGTCTGC TGGATATGAC ATATCAGGTT TCCTACTACT GCTATGCCAG CTATCTTCCG
1201 TCGTTCTTGC AGGTCGTGTA CGAGCTGGAC GTCGCCACGG CGGGATATGT CACCAACACG
1261 TTCAGTGTGG TCTCCTTTGT CTTCCTGTTC TTCGCCGGTT GGCTCATCCG CTGGACCGGT
1321 CGTTTCAAGT GGATCCTTTG GGTGTGCGTT CCGCTCTACA TCTTCGGCCT GGGTCTGATG
1381 ATTCACTTCC GTCAACCGGG CGGATACATC GGGTACATCG TTATGTGCGA GATTTTCTTC
1441 TCCGTCGCTG GAAGCGTCTT CATTCTCTGC GTGCAACTGG CGGTGCTTGC GTCCGTTGAT
1501 CACCAACACG TTGCCGCCGT GCTCGCGTTG CTGTTCGTCA TGGGCAGCAT TGGCGGCTCT
1561 ATCGGCAGCG CAATCTGTGG AGCAATCTGG ACCAGCACTT TTCTGTCGAG ACTGGAGAGG
1621 AACTTGCCCG CGTCTGCCAT GCCTGACTTG AGCTTGATCT ATTCGTCCCT CCCCACCCAG
1681 CTCAGCTACC CCGTCGGAAG TGCTACCCGG ACCGCCATCG TGGAGGCATA CGGGTATGCC
1741 CAAGCAAGGA TGCTCATTGC CGGTACTGCA TTCATGGTTC TGGGCTTCAT CTGGGTTGGC
1801 ATGATGAGGA ACCTGAACGT GAAAAACATG ACTCAGACCA AGGGTAATGT TGTGTAG
```

Figure 3-9. Nucleotide sequence of Af*mirB* obtained from amplified cDNA. The bases highlighted in bold represent nucleotides previously believed to be part of the first intron.

```
  1 MLHVLSVGPS HAAFTVEAAM ATMKKFHSIV GEKPAQDAEA PSVDDPNVGQ IRADDKEAAH
 61 APANAETNNE EANPSDGAQA GVKKIEAVTL SWTRGTAYAI LVLIWFLTLV NDFRLSMYTS
121 LNAYATSSFL GHSLLTVINI VSYVMGGSVY IPMAKALDLW GRAEGFLLMT FFCILGLILL
181 ASSQNLPTYC AGQVFYKVGF GGLSYTWNVL AADVTNLRNR GLAFAFTSSP ALISAFAGSK
241 AASDLLAHST WRWGFGMWAI ILPVVALPIY GLLAYHLRQA EKKGVLVKET RDWSITPKTV
301 WWAIMEFDLP GVLLFAGGFV IFLLPFTLAA TAPHGYQTDY IIAMITLGLA LIIAFGFYEM
361 LVAPVPFLNY KFLIDRTVLG ACLLDMTYQV SYYCYASYLP SFLQVVYELD VATAGYVTNT
421 FSVVSFVFLF FAGWLIRWTG RFKWILWVCV PLYIFGLGLM IHFRQPGGYI GYIVMCEIFF
481 SVAGSVFILC VQLAVLASVD HQHVAAVLAL LFVMGSIGGS IGSAICGAIW TSTFLSRLER
541 NLPASAMPDL SLIYSSLPTQ LSYPVGSATR TAIVEAYGYA QARMLIAGTA FMVLGFIWVG
601 MMRNLNVKNM TQTKGNVV
```

Figure 3-10. Amino acid sequence of MirB with the additional 6 amino acids (bold) not present in the published putative mRNA sequence from strain Af293.

In addition, the *mirB* gene from *A. fumigatus* strain 13073 contains five strain-specific base changes from that of the published sequence, obtained from strain Af293. These are highlighted in Figure 3-11. These base changes do not result in any amino acid changes.

```
   1 ATGCTTCACG TCTTATCAGT CGGTCCGTCC CATGCAGCGT TTACTGTCGA AGCAGCAATG
  61 GCAACCATGA AGAAATTCCA CTCGATTGTC GGTGAAAAGC CTGCCCAGGA TGCTGAGGCC
 121 CCCTCAGTCG ATGACCCAAA TGTTGGGCAG ATCAGAGCCG ACGACAAGGA GGCTGCTCAT
 181 GCGCCCGCCA ATGCGGAAAC CAATAATGAG GAGGCCAACC CGAGCGACGG AGCTCAGGCT
 241 GGTGTCAAGA AGATAGAGGC TGTGACCCTG AGTTGGACCA GGGGCACAGC GTACGCAATT
 301 CTAGTGCTGT ATGTTTCGCT CCCATTGATT GCTGCATGTG CCAGCCATCC CAAAAGATCA
 361 AACTGCTAAC CTGGTTTTCA TTCTGATAGC ATTTGGTTCC TAACGCTGGT CAACGATTTC
 421 CGACTGTCCA TGTATACAAG CTTGAACGCT TATGCCACAA GTTCTTTCCT CGGCCACTCG
 481 CTGTTGACCG TCATCAACAT TGTGTCCTAC GTTATGGGCG GTTCCGTGTA CATACCGATG
 541 GCCAAGGCGC TGGATCTTTG GGGCCGTGCA GAGGGTTTCC TTCTGATGAC TTTCTTCTGT
 601 ATTCTGGGTT TGATTCTTCT GGCTTCATCC CAGAATCTCC CCACCTATTG CGCCGGACAG
 661 GTAAGACATG ACCACCGCTG ATCTCGTCAT AAGAACTGTC TAACGGCCAG ACGCGCTTTA
 721 GGTCTTCTAC AAGGTCGGGT TCGGTGGGCT TTCATACACC TGGAATGTCC TGGCAGCCGA
 781 TGTGACGAAT CTACGAAACC GAGGGCTGGC GTTTGCTTTC ACCTCGTCCC CTGCTTTGAT
 841 CTCCGCGTTC GCCGGTTCCA AGGCGGCGTC GGATCTCCTG GCCCACTCGA CCTGGCGATG
 901 GGGCTTTGGC ATGTGGGCCA TTATCTTGCC GGTTGTTGCG CTGCCAATTT ATGGCCTTTT
 961 GGCGTACCAC CTACGCCAAG CCGAGAAAAA GGGGGTTCTC GTCAAGGAGA CGAGAGATTG
1021 GAGTATCACC CCGAAGACAG TTTGGTGGGC CATTATGGAA TTTGATCGTA AGTATCAACC
1081 AAGGGCGGTT GTCGCCTCAA AAGGGTTCCT TACCGAAGGC TAATCAATGA TCTTACCACT
1141 CACCTAGTGC CCGGAGTTCT TCTCTTCGCT GGCGGGTTCG TCATATTCCT TCTCCCCTTT
1201 ACTCTGGCGG CGACGGCGCC CCATGGGTAT CAGACCGACT ATATCATTGC GATGATCACT
1261 CTCGGCCTGG CCCTAATCAT CGCTTTTGGC TTCTACGAAA TGCTCGTGGC GCCCGTGCCG
1321 TTCTTGAACT ATAAATTCCT CATTGACCGG ACCGTGCTGG GTGCATGTCT GCTGGATATG
1381 ACATATCAGG TTTCCTACTA CTGCTATGCC AGCTATCTTC CGTCGTTCTT GCAGGTCGTG
1441 TACGAGCTGG ACGTCGCCAC GGCGGGATAT GTCACCAACA CGTTCAGTGT GGTCTCCTTT
1501 GTCTTCCTGT TCTTCGCCGG TTGGCTCATC CGCTGGACCG GTCGTTTCAA GTGGATCCTT
1561 TGGGTGTGCG TTCCGCTCTA CATCTTCGGC CTGGGTCTGA TGATTCACTT CCGTCAACCG
1621 GGCGGATACA TCGGGTACAT CGTTATGTGC GAGATTTTCT TCTCCGTCGC TGGAAGCGTC
1681 TTCATTCTCT GCGTGCAACT GGCGGTGCTT GCGTCCGTTG ATCACCAACA CGTTGCCGCC
1741 GTGCTCGCGT TGCTGTTCGT CATGGGCAGC ATTGGCGGCT CTATCGGCAG CGCAATCTGT
1801 GGAGCAATCT GGACCAGCAC TTTTCTGTCG AGACTGGAGA GGAACTTGCC CGCGTCTGCC
1861 ATGCCTGACT TGAGCTTGAT CTATTCGTCC CTCCCCACCC AGCTCAGCTA CCCCGTCGGA
1921 AGTGCTACCC GGACCGCCAT CGTGGAGGCA TACGGGTATG CCCAAGCAAG GATGCTCATT
1981 GCCGGTACTG CATTCATGGT TCTGGGCTTC ATCTGGGTTG GCATGATGAG GAACCTGAAC
2041 GTGAAAAACA TGACTCAGAC CAAGGGTAAT GTTGTGTAG
```

Figure 3-11. *mirB* gene from strain 13073. Highlighted are five base changes in this sequence when compared to the published sequence from strain Af293. The nucleotides in the original Af293 sequence are, in order, A (+279), G (+339), C (+513), G (+591), and C (+790). None of these base changes result in an amino acid change in MirB.

Other than the aforementioned changes, the pESC-mirB plasmid isolated from colony 2 (Figure 3-8) did not contain any errors, and it was therefore chosen for mutagenesis and transformation into *S. cerevisiae*.

All mutant plasmids were successfully created (Refer to Table 1-1 for the list of mutants created). Sequencing confirmed the presence of the mutation in each case. All mutant and wildtype *mirB* plasmids were transformed into *S. cerevisiae*. Colony PCR performed on transformant colonies confirmed the presence of the wildtype *mirB* plasmid (Figure 3-12) and the plasmid in each mutant strain (data not shown). Colony Y2 was chosen as the wildtype MirB (MirBWT) strain for all subsequent experiments.

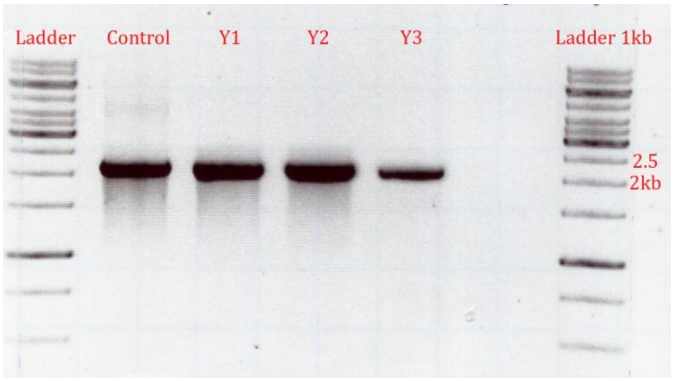

Figure 3-12. Colony PCR of three yeast colonies (Y1-Y3) transformed with wildtype pESC-mirB (expected size 2.1 kb). Control represents *mirB* (also 2.1 kb) amplified directly from pESC-mirB vector using the same primers.

3.3 Immunoblotting

To test for the presence of the MirB-FLAG proteins, western blotting of membrane proteins using anti-FLAG antibodies (Sigma) was attempted on all of the wildtype and mutant transformants. Initially, subcellular fractionation by differential centrifugation was used to isolate the plasma membrane fraction from total cell lysates of the MirBWT strain in order to determine the subcellular localization of the MirB-FLAG

protein. Isolation of adequate amounts of such fractions from yeast spheroplasts proved to be difficult and western blots of the fractions yielded either very faint or no bands (data not shown).

To improve protein yields, subcellular fractionation was forgone in favour of TCA precipitation of protein from total cell lysates. A first set of western blots performed using extracted protein are provided in Figure 3-13. The expected molecular size of the MirB-FLAG protein is 69 kDa. All strains showed a band in the 70 kDa range, including the negative control, PHY14-URA, transformed with empty pESC-URA vector. PHY14 not transformed with pESC-URA also appeared to show a band, but it was very faint compared to PHY14-URA (Figure 3-14). To rule out contamination as a reason for the presence of the band in the PHY14-URA sample, stock cultures of PHY14 were re-transformed with pESC-URA, but western data still showed the presence of the band at 70 kDa (data not shown). Colony PCR of PHY14-URA using primers specific for mirB confirmed that the gene was not erroneously transformed into this strain (data not shown). Since PHY14-URA has been transformed with pESC-URA, it is possible that exposure to galactose would lead to induction of the FLAG epitope, even in the absence of a recombinant protein. However, this does not explain why the PHY14-URA band is ~70 kDa considering the small size of the FLAG tag (1 kDa), unless there is random binding of the epitope to PHY14 proteins of a size similar to MirB. It is also possible, given the faint band seen in the PHY14 sample, that there is non-specific binding of the anti-FLAG antibody to an unknown PHY14-URA protein.

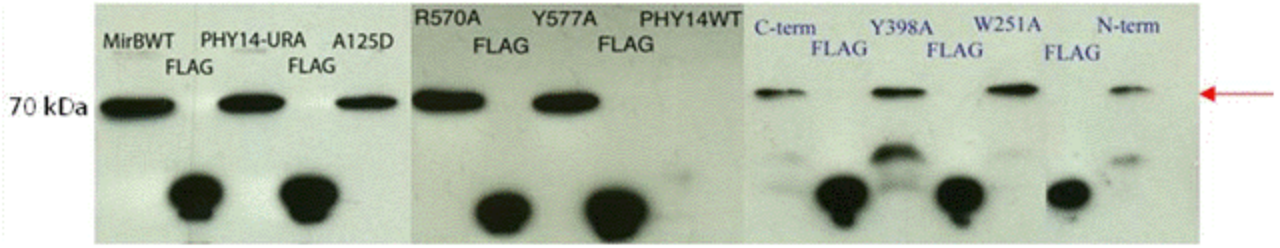

Figure 3-13. Western blot of MirBWT and mutants. Expected size of MirB-FLAG is 69 kDa (red arrow). "FLAG" refers to the commercial FLAG-BAP control protein (Sigma), with an expected size of 49 kDa. The mutant strains are listed in Table 2-1.

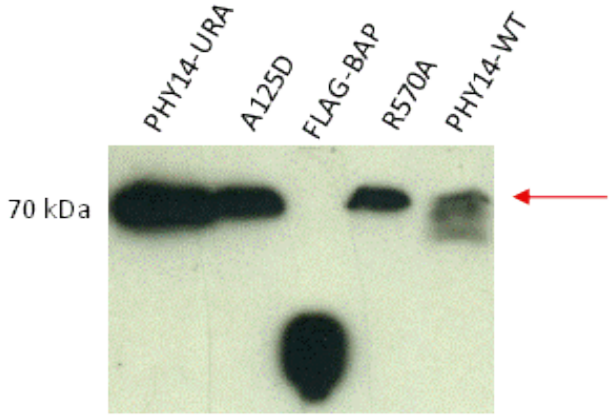

Figure 3-14. Western blot showing the band in PHY14 not transformed with pESC-URA, labelled PHY14-WT. Expected size of MirB-FLAG proteins is 69 kDa (red arrow). FLAG-BAPis a control protein (Sigma), with an expected size of 49 kDa.

In an attempt to remove this non-specific binding, the antibody solution was first exposed O/N to a dot blot containing PHY14-URA protein (Refer to Appendix 1). This solution was then used for incubation with the western blot membrane. This technique proved to be successful and subsequent westerns showed presence of a band only in lysates from MirBWT and mutant strains but not from PHY14-URA (Figure 3-15). Bands were of the correct size: ~69 kDa. From the results, it is clear that the MirB-FLAG protein is expressed in each strain. MirBWT, A125D, Y398A, W251/253A, R570A, Y577A, and the C-term and N-term deletion mutants all have comparable expression levels, whereas expression of F129D and the remaining deletion mutants were lower.

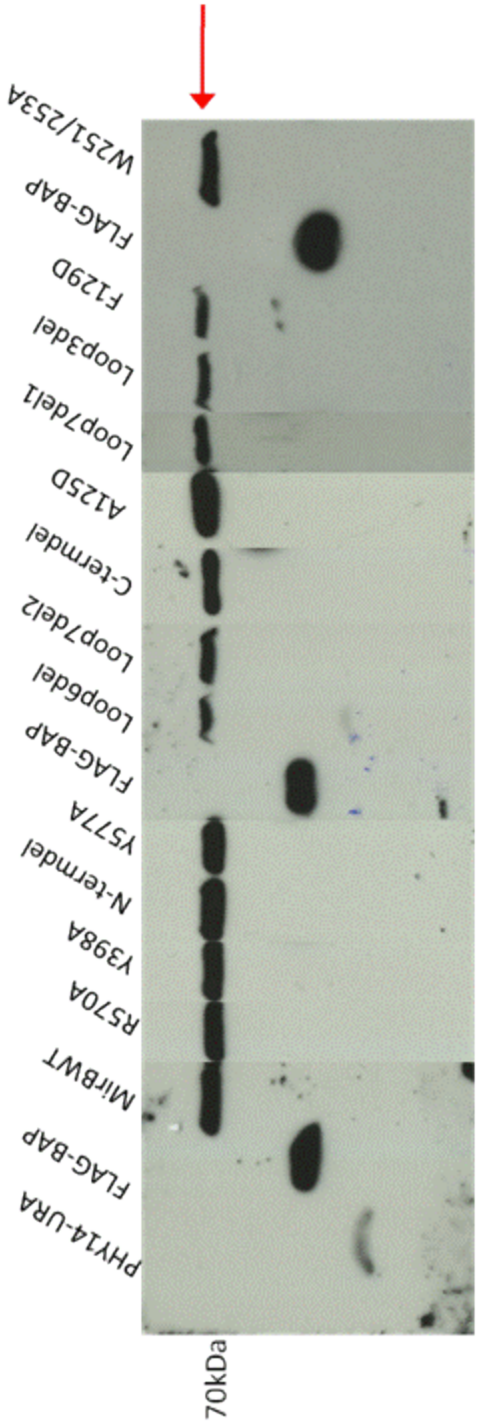

Figure 3-15. Western results for all MirB strains and PHY14-URA using anti-FLAG antibodies previously pre-adsorbed to PHY14-URA lysate on dot blots. MirB-FLAG is 69 kDa (red arrow). FLAG-BAP is 49 kDa. For each yeast TCA precipitate, the same amount of protein was loaded on the SDS-PAGE gel (40 µg).

3.4 Growth assays

3.4.1 Growth assays using liquid cultures

Since only functional MirB proteins should be able to transport TAFC and use it as a source of iron for growth, liquid assays using 96-well plates were perfomed to determine the viability of the strains on media supplemented with Fe-TAFC as the sole source of iron. Unfortunately, it was not possible to obtain conclusive results from this assay. Growth of MirBWT and PHY14-URA was comparable in SR + gal media supplemented with iron chelators BPS or dipyridyl plus Fe-TAFC. Galactose was added to the media to induce expression of the MirB proteins. The growth observed was unexpected as PHY14-URA does not possess any siderophore transporters. The most likely reason for this result is the fact that compared to MirBWT, PHY14-URA has a much faster growth rate in SR + gal media. Because MirBWT showed a significant lag phase in this media, by the time it entered exponential phase in SR + gal media with BPS/dipyridyl and Fe-TAFC, PHY14-URA would have been able to overcome the iron limitation in the media, likely through breakdown of Fe-TAFC (via esterases) or via acquisition of what little iron remained in media using its low affinity iron uptake mechanisms (Dix et al. 1994).

3.4.2 Growth assays on solid agar

Because of problems with the liquid culture assay, the focus was shifted to performing growth assays on solid media. Results from inoculation of plates with 5 µl of cells (OD_{600} = 0.5) can be found in Figure 3-16. All strains showed approximately equal growth on SR + gal only plates and, as expected, no growth on iron-limited plates

containing SR + gal with 500 µM BPS. On SR + gal/BPS supplemented with 50 µM Fe-TAFC, growth was observed for the parent strain, DEY1394-URA, MirBWT and all MirB mutants, except for A125D. Although F129D was able to grow on this media, growth was minimal. None of the deletion mutants showed any growth, nor did PHY14-URA, as expected. It is unlikely that the initial inoculum size led to the observed variation in growth because care was taken to sample all liquid cultures at the same OD and use the same inoculum size.

A SR + gal with 500 µM BPS and 50 µM Fe-TAF

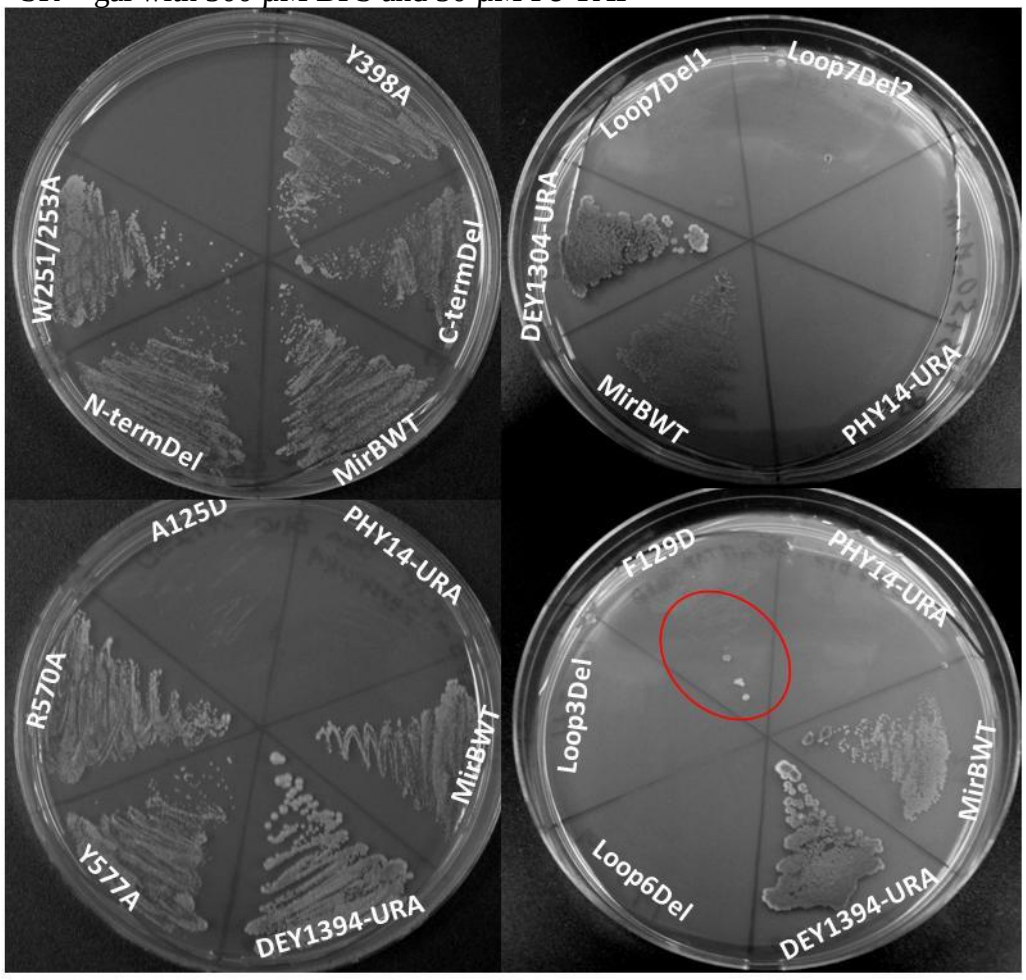

B SR + gal with 500 µM BPS SR + gal

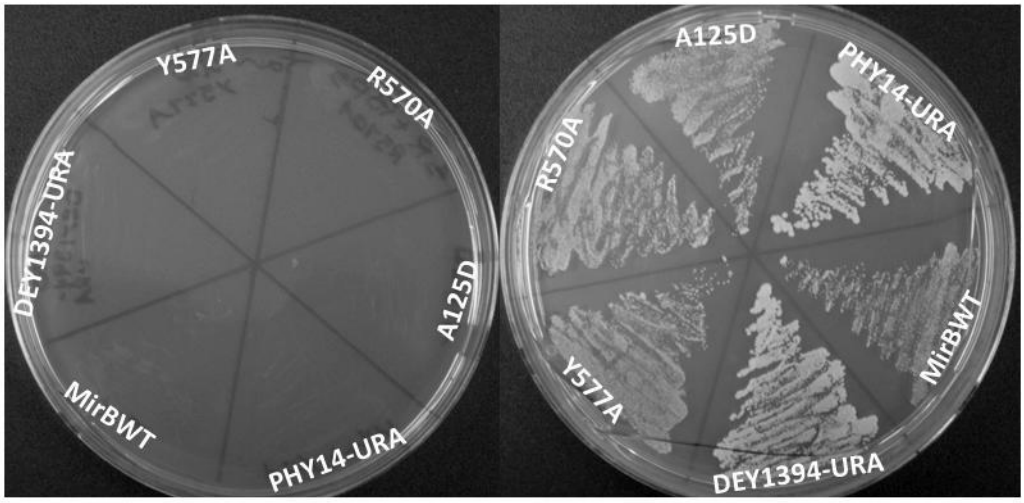

Figure 3-16. **A)** Growth of all MirB strains, DEY1394-URA, and PHY14-URA, on SR + gal plates with 500µM BPS and 50µM Fe-TAF. The red circle highlights the regions of F129D growth. **B)** Representative plates of SR + gal with 500 µM BPS (left panel), and SR + gal only (right panel). The same level of growth was observed by all other strains on these plates.

The growth assays were also done on solid medium using a semi-quantitative analysis comparing colony formation from serially diluted cultures of the different strains (pin method). These results can be found in Figure 3-17. Most of the results corroborated those from the previous assay, with a few exceptions. As seen with the plate assay, this assay showed that on SR + gal with BPS and Fe-TAFC, the C-termDel, F129D, Y398A, N-termDel, and R570A mutants showed growth comparable to MirBWT, whereas the A125D, Loop7Del2, and Loop3Del mutants were detected only at the highest concentration 10^7, indicating growh comparable to PHY14-URA, the negative control. Unlike the previous assay, Loop7Del1 grew as well as MirBWT, while Y577A did not show growth above that of PHY14-URA. Also different was the growth of the W251/253A and Loop6Del mutants. W251/253A and Loop6Del, which had growth

equivalent to MirBWT and PHY14-URA, respectively, in the previous assay, appear to have intermediate growth defects in this assay. These strains grew at the middle concentration, unlike PHY14-URA, but growth was less pronounced than that of MirBWT. All of the strains grew at the three concentrations, 10^5, 10^6, and 10^7 cells/ml on iron replete media (SR + gal, positive control), while only very light growth was observed at 10^7 cells/ml on iron limited media (SR + gal with 500 µM BPS, negative control) (Figure 3-18).

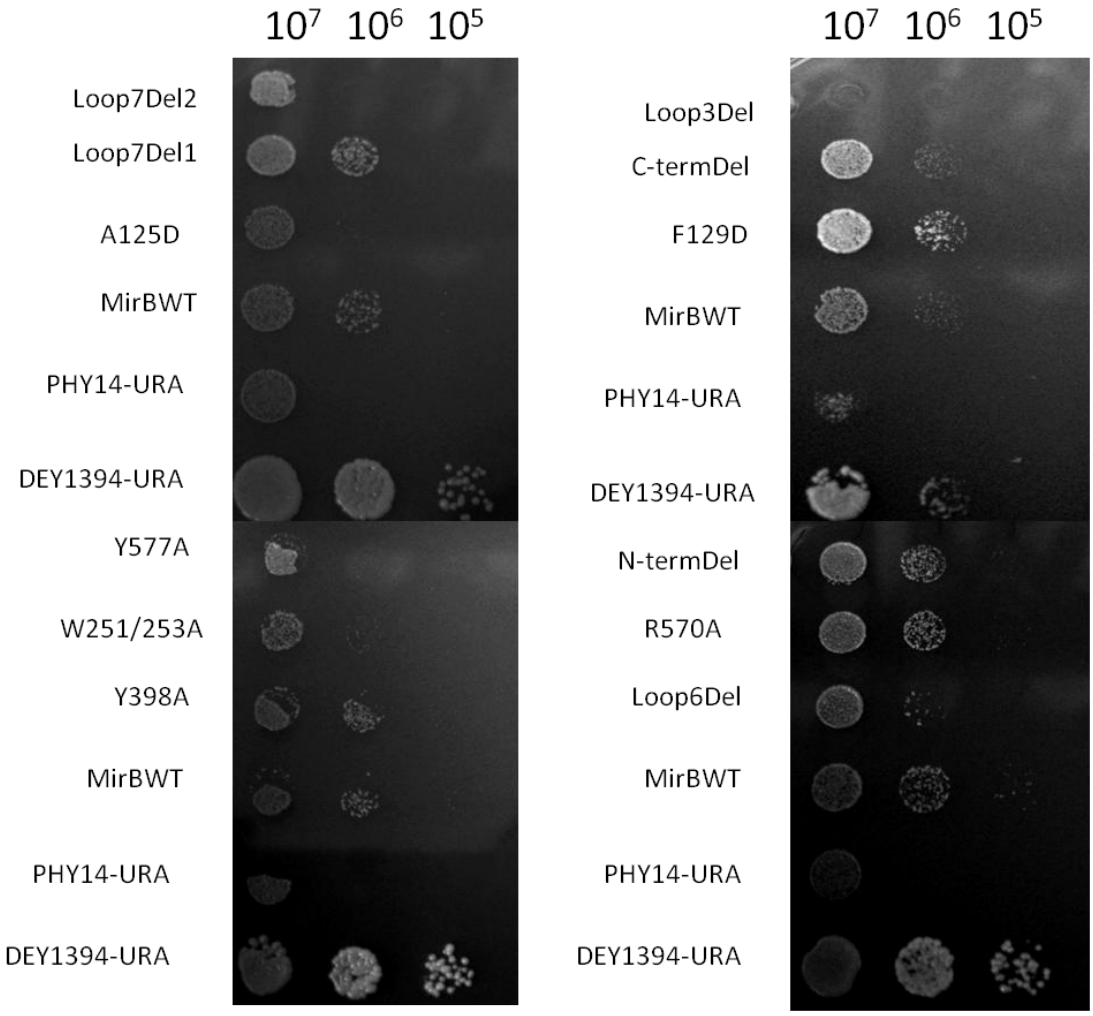

Figure 3-17. Growth of all strains on SR+ gal media with 500 µM BPS and 150 µM TAFC. Plates were incubated at 30 °C for one week.

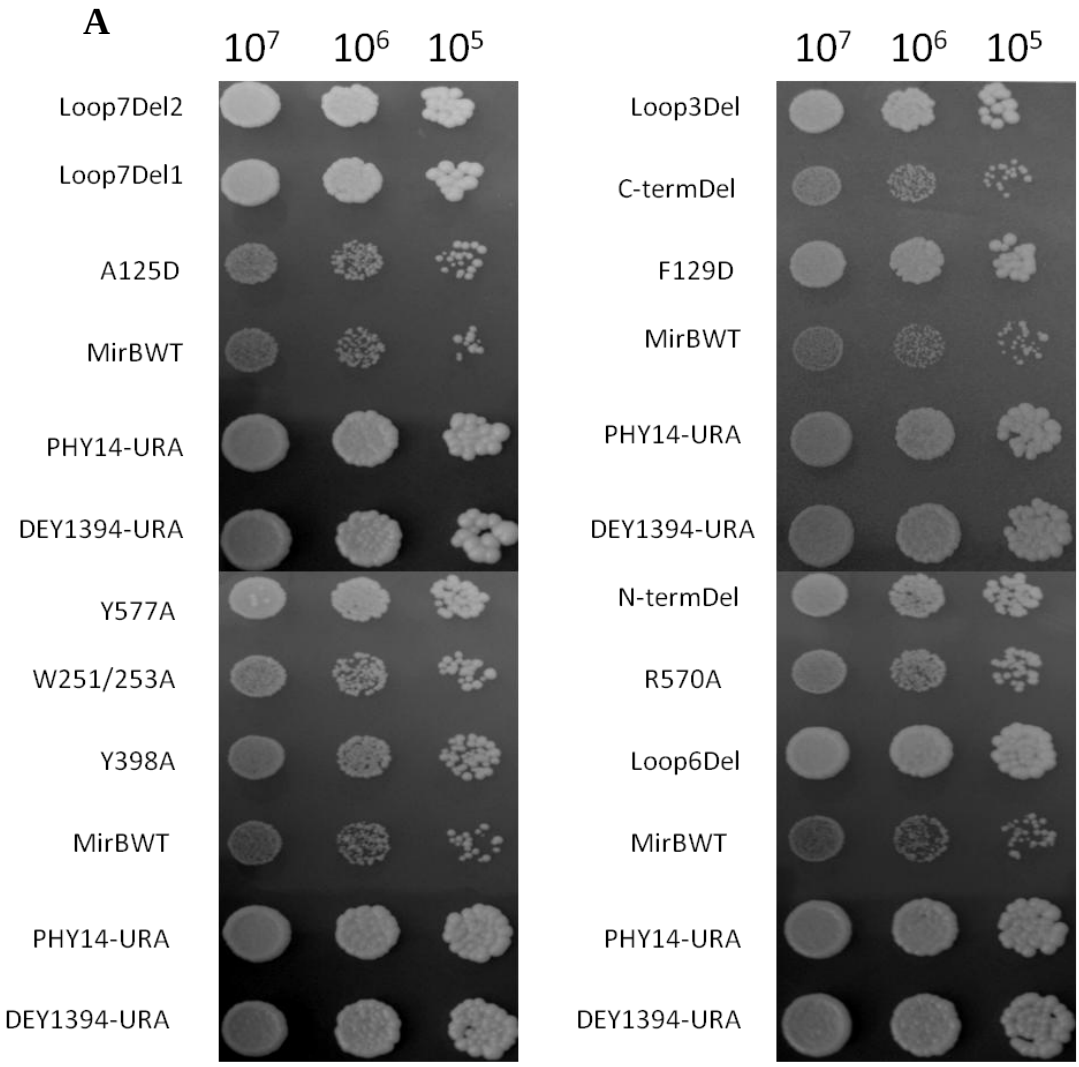
A
10^7
10^6
10^5
Loop7Del2
Loop7Del1
A125D
MirBWT
PHY14-URA
DEY1394-URA
Y577A
W251/253A
Y398A
MirBWT
PHY14-URA
DEY1394-URA
10^7
10^6
10^5
Loop3Del
C-termDel
F129D
MirBWT
PHY14-URA
DEY1394-URA
N-termDel
R570A
Loop6Del
MirBWT
PHY14-URA
DEY1394-URA

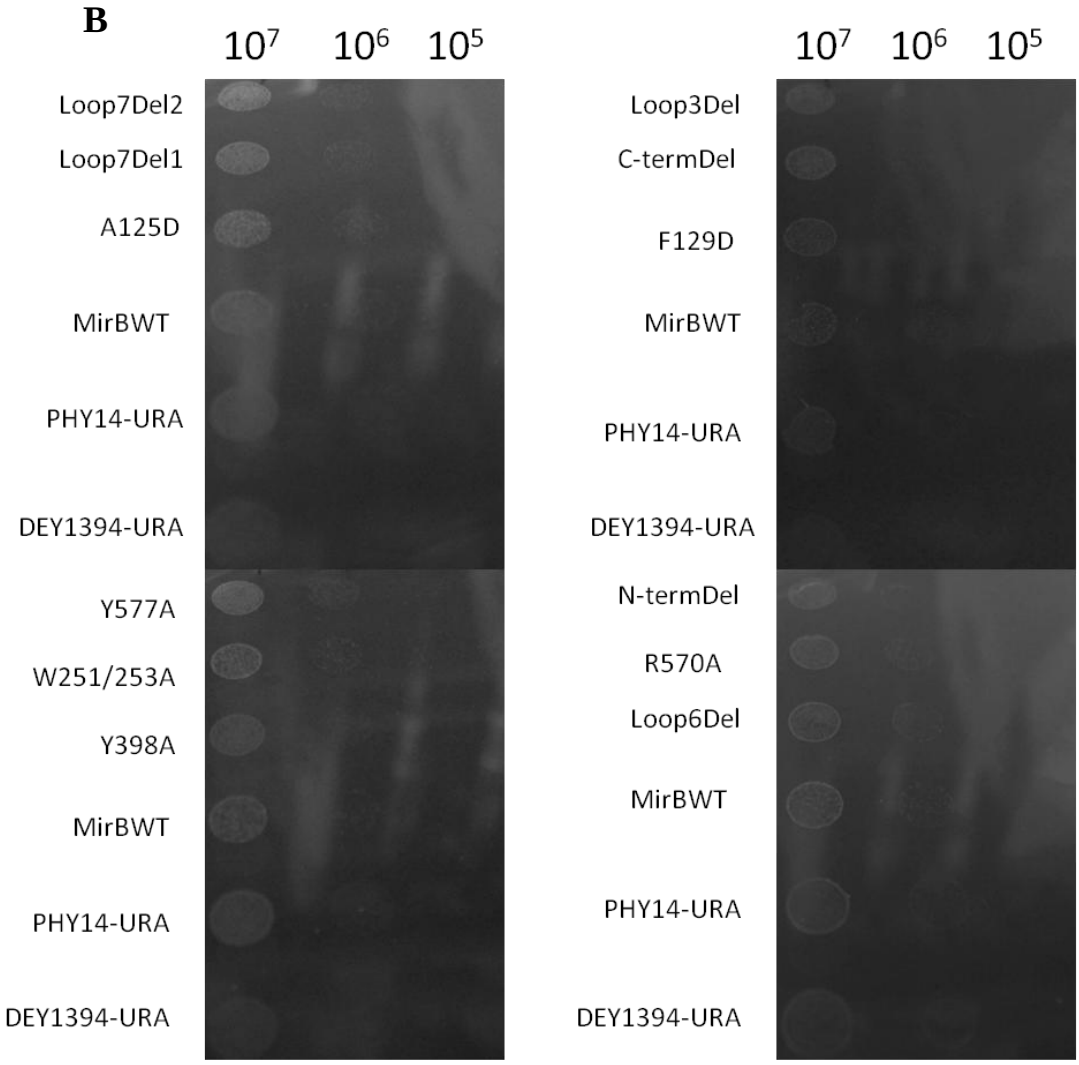

Figure 3-18. **A)** Growth of all strains on SR + gal only media (positive control). **B)** Growth on SR + gal media with 500 μM BPS (negative control).

The differences in growth observed between the two assays are most likely due to changes in concentration, since at a high enough inoculum (10^7), all strains, including PHY14-URA, show the ability to grow on SR + gal with BPS and Fe-TAFC. Observation of growth over several dilutions provides more complete information with regards to the ability of these strains to grow on this media, and allows us to eliminate those concentrations at which the strains can overcome iron limitation, regardless of whether or

not they possess a siderophore transporter. Additionally, since this semi-quantitative assay requires the use of titre via cell counting, as opposed to OD, it is therefore a more accurate representation of actual cell concentration. As such, the results obtained from this assay (summarized in Table 3-1) are believed to be more accurate.

Table 3-1. Growth of all strains on SR + gal with 500 µM BPS and 150 µM TAFC.

+++ = growth comparable to DEY1394-URA (all transporters);
++ = growth above PHY14-URA background, but below DEY1394-URA;
+ = growth comparable to PHY14-URA (negative control)

Strains	Growth on SR+BPS+TAFC
DEY1394-URA	+++
MirBWT	+++
C-termDel	+++
N-termDel	+++
F129D	+++
Y398A	+++
R570A	+++
Loop7Del1	+++
W251/253A	++
Loop6Del	++
Y577A	+
A125D	+
Loop3Del	+
Loop7Del2	+
PHY14-URA	+

Based on the results obtained from both growth assays, it is clear that the addition of Fe-TAFC as the sole source of iron was able to provide MirBWT with the iron necessary for growth, and since MirB is the only TAFC transporter present in this strain,

these results show that MirB is being expressed and functioning properly. The negative control, PHY14-URA (empty vector) was unable to grow on SR + gal media supplemented with BPS and Fe-TAFC, except at the highest concentration, proving that growth of transformed strains at lesser densities was due to the presence of the transporter. The loop 1 mutant A125D, the loop 7 mutant Y577A, and the loop 3 and the second loop 7 deletion mutants were the only mutants for which growth was completely reduced to background levels on this media indicating that the mutation has abrogated binding or transport of FE-TAF. Alternatively, it is possible that the protein is not being targeted properly to the plasma membrane.

3.5 Iron uptake assays

To establish that TAFC-bound iron was being transported by MirB, ^{55}Fe-TAFC uptake assays were performed for MirBWT, all MirB mutant strains, as well as for PHY14-URA. The results are presented in Figure 3-19A. Uptake assays were originally measured on strains following 30 min of incubation with ^{55}Fe-TAFC (Figure 3-16B). The incubation time was subsequently increased to 60 min to determine if this would result in higher uptake rates for the MirBWT and mutant strains (Figure 3-16A). Uptake rates for MirBWT were significantly higher than that of the mock transformed control, PHY14-URA. A one way analysis of variance (one-way ANOVA) conducted using rates from all MirB strains and PHY14-URA found the means to be significantly different ($p < 0.05$). Using Dunnett's Multiple Comparison Test ($p < 0.05$), statistically significant differences between groups were determined. On Figure 3-19, uptake rates were compared to MirBWT and PHY14-URA. Only the C-termDel mutant was found to have uptake rates similar to MirBWT. Uptake rates for Y398A were significantly different from both

PHY14-URA and MirBWT. Because of the high variation observed in N-termDel and F129D counts, these strains were not included in the statistical analysis. However, it is clear from the graph (Figure 3-19) that uptake rates in these strains were not lower than the wild type MirB uptake rate. None of the other strains differed significantly from the negative control, PHY14-URA.

A

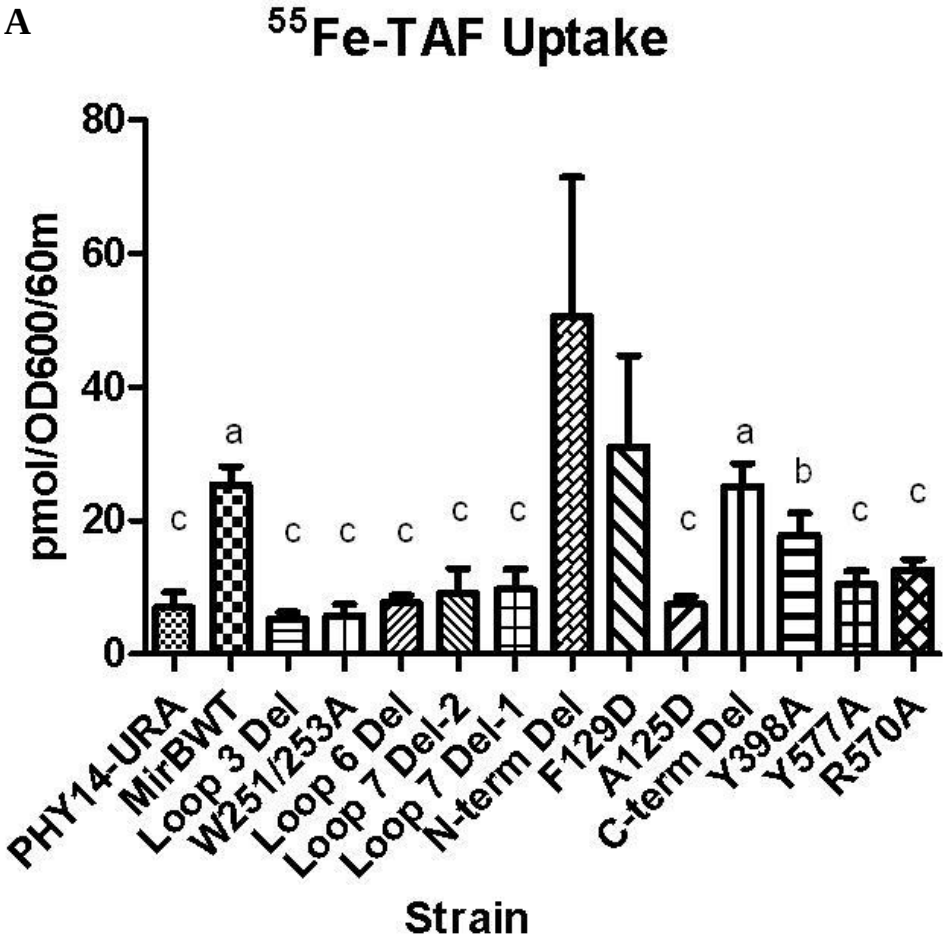
55Fe-TAF Uptake
pmol/OD600/60m
80
60
40
20
0
a
c
c
c
c
c
c
a
b
c
c
PHY14-URA
MirBWT
Loop 3 Del
W251/253A
Loop 6 Del
Loop 7 Del-2
Loop 7 Del-1
N-term Del
F129D
A125D
C-term Del
Y398A
Y577A
R570A
Strain

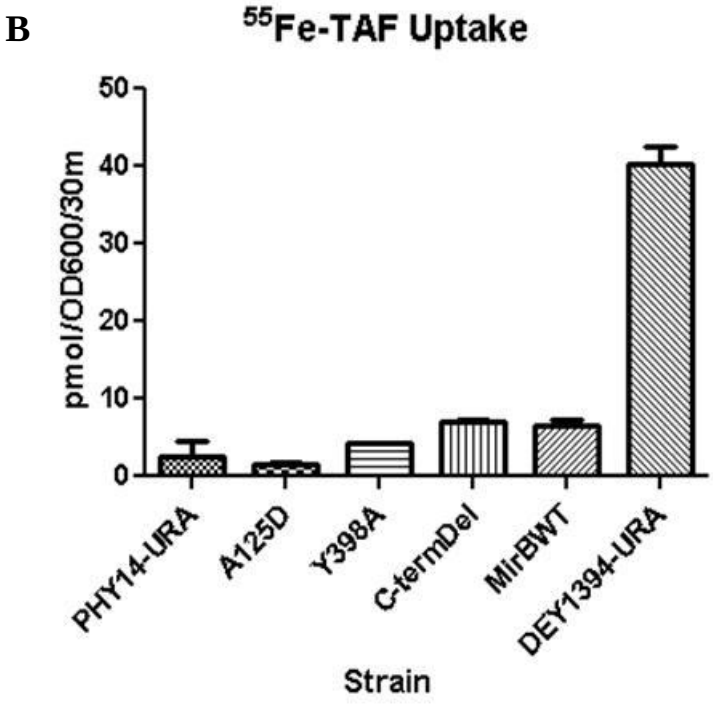

Figure 3-19. **A)** ^{55}Fe-TAF uptake rates for all MirB strains and PHY14-URA. Bars with the same letter are not significantly different (Dunnett's Multiple Comparison Test, $P < 0.05$). **B)** Uptake rates for PHY14-URA, its parental strain, DEY1394 (contains all endogenous siderophore transporters) and select MirB mutant strains after 30 min. Rate of uptake of MirBWT is about 1/5 that of DEY1394-URA after 30 min. The background radioactivity of the negative control (PHY1-URA) is likely attributable to surface binding of Fe-TAFC.

Together with the results from the growth assays, these iron uptake data show conclusively that MirBWT transports Fe-TAFC. Furthermore, it would appear that neither the N-term or C-term deletions, nor the F129D mutation, had any impact on uptake of Fe-TAFC. While uptake by the Y398A mutant was less then MirBWT, the mutation did not eliminate uptake completely. However, all other mutations had a significant impact on the ability of MirB to take up Fe-TAFC, reducing uptake levels to background levels.

3.6 Immunofluorescence localization in yeast

To localize MirB within *S. cerevisiae*, immunofluorescence microscopy was attempted several times using the negative control, PHY14-URA and the Y2 strain expressing the wildtype MirB. While these have been somewhat successful (Figure 3-20), two significant issues arose. First, a high level of background fluorescence from the mouse monoclonal anti-FLAG antibody (bound to 2° anti-mouse Alexa fluor-488 conjugated antibody) was observed in the PHY14-URA slides. This is most likely due to non-specific binding of this antibody to proteins in PHY14-URA, which was observed on the western blots (Figure 3-13). Pre-adsorption of the antibody to PHY14-URA cell lysates removed most of the background allowing us to confidently assign signal to the presence of MirB. Secondly, successful staining with the FM4-64FX dye has been difficult. Problems were encountered with retention of the dye during slide preparation. Additionally, the dye is unstable, resulting in a rapid loss of signal. Nevertheless, the slides with the wild type MirB expressed in yeast revealed punctate staining throughout the cytoplasm suggesting that the protein may be localized in vesicles as well as in the plasma membrane. Optimization of fluorescence microscopy is currently underway to reduce background fluorescence and to improve uptake and retention of FM4-64FX in yeast cells. When this is completed, we will be able to determine whether the decrease in iron uptake and growth of certain MirB mutant strains is attributable to mis-localization or to a true lack of transporter activity.

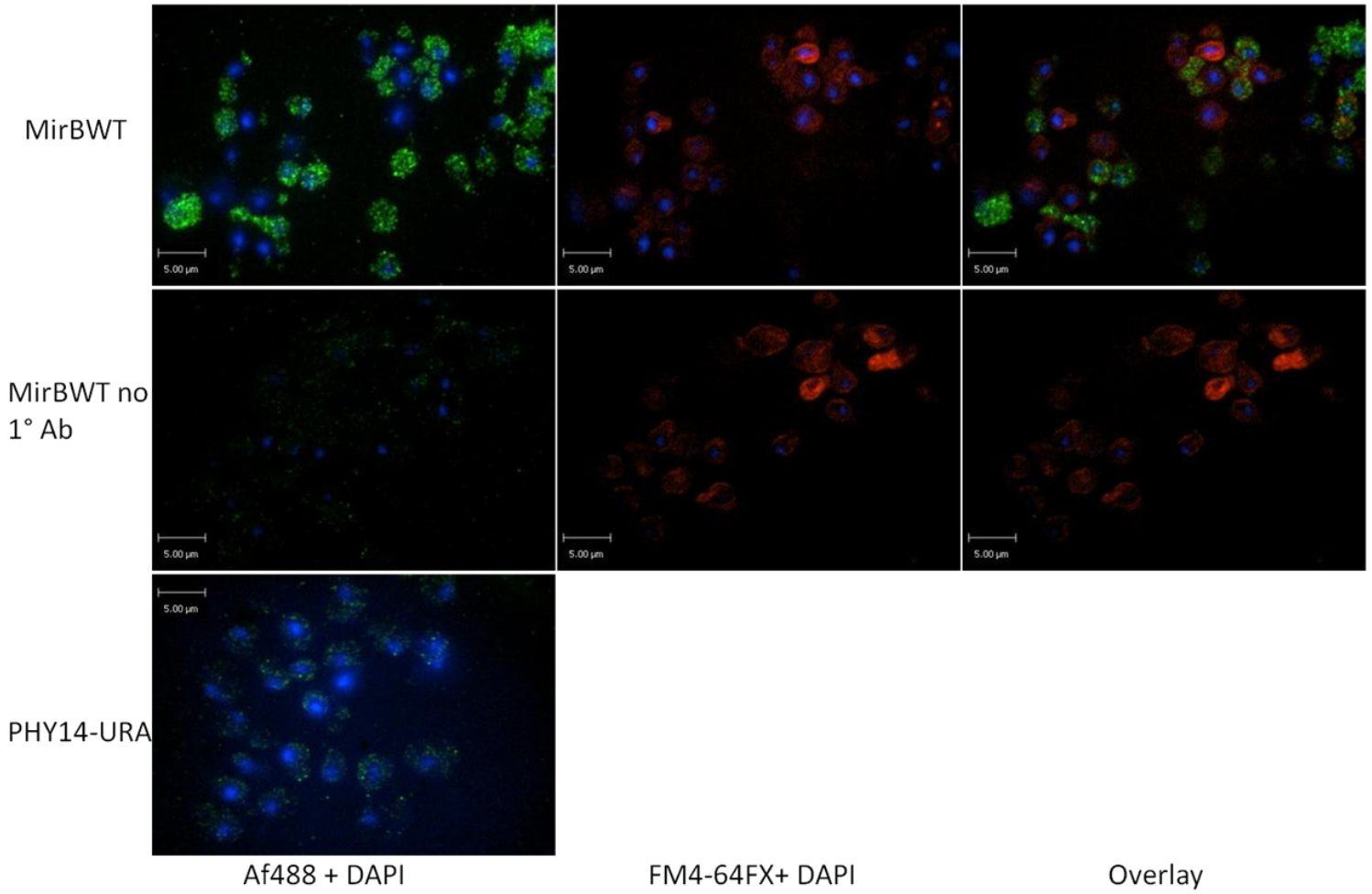

Figure 3-20. Fluorescent microscopy on MirBWT and PHY14-URA. MirB-FLAG was detected using mouse anti-FLAG primary antibodies, followed by anti-mouse Af488-conjugated secondary antibodies. FM4-64FX was used to stain plasma membrane and endosomes, while DAPI was used to stain DNA. PHY14-URA samples did not stain properly with FM4-64FX.

4: Discussion

Based on the results of the growth and ^{55}Fe-TAFC transport assays (Figure 3-17 and Figure 3-19), I can conclude that MirBWT functions as a siderophore transporter and that it is capable of transporting Fe-TAFC. Growth of MirBWT in media supplemented with Fe-TAFC was comparable to DEY1394, which possesses not only the endogenous *S. cerevisiae* TAFC transporter Arn2p, but all other *S. cerevisiae* iron uptake permeases and xenosiderophore transporters including Arn1p (various siderophores), Arn3p (ferrioxamine and ferrichrome), and Arn4p (enterobactin) (Yun et al. 2000; Lesuisse et al. 1998; Heymann et al. 2000). While the ^{55}Fe-TAFC uptake rates observed in MirBWT were lower than those of DEY1394-URA, they were significantly higher than those for the negative control strain, PHY14-URA and were similar to published rates for *A. nidulans* MirB (Haas et al. 2003). It remains to be determined if *Afu* MirB is capable of transporting other siderophores besides TAFC. However, since the two previously characterized TAFC transporters, *A. nidulans* MirB and *S. cerevisiae* Arn2p (Haas et al. 2003; Yun et al. 2000), are very specific for TAFC and do not appear to transport other hydroxamate siderophores, it is likely that *Afu* MirB is predominantly, if not solely, a TAFC transporter. As noted in the Introduction, fungal siderophore-transporters belong to the SIT family of permeases and are believed to function as symporters. Results from the bioinformatics analysis indicate that the same is true for *Afu* MirB.

It is not known at this time if the GATA sites found in the promoter region of *mirB* are true binding sites for transcription factors. However since siderophore-

biosynthesis and siderophore-transporter-encoding genes, including *mirB* in *Aspergillus nidulans* and *sidA* in both *A. nidulans* and *Aspergillus fumigatus,* are all regulated by SREA (Schrettl et al. 2008; Oberegger et al. 2001; Haas et al. 2003), it is probable that SREA is also a regulator of *mirB.* It is important to note however that, in an *A. nidulans* SREA mutant, *mirB* was found to only be partially derepressed (Haas et al., 2003), an indication that there is some other, as yet uncharacterized mechanism for regulating expression of *mirB.*

To better compare the various *Afu* MirB mutants, an overall score was assigned to each strain based on its ability to transport ^{55}Fe-TAFC and/or use Fe-TAFC as a source of iron for growth (Table 4-1). The substitutions of alanine 125 and tyrosine 577, and deletions of loop 3 and the second half of loop 7 had the most severe impact, abrogating function completely. Indeed, the inability of these mutants to both transport ^{55}Fe-TAFC, and use Fe-TAFC as a source of iron, suggests that these amino acids and loops are crucial for proper functioning of the transporter. Whether the lack of uptake seen in the Loop7Del2 mutant is due solely to the absence of tyrosine 577, one of the deleted amino acids, or if there are other functionally crucial amino acids in this region of loop 7 is unknown. It would be worthwhile to investigate this further.

Table 4-1. Fe-TAFC uptake scores for *Afu* MirB strains as determined based on their ability to transport Fe-TAFC and use it as a source of iron for growth. Stars indicate mutants who were not included in the statistical analysis for ^{55}Fe-TAFC uptake, but who were assigned the same letter as MirBWT because uptake rates were not any lower then MirBWT.

1 = good growth/uptake comparable to MirBWT;
2 = good growth/no uptake;
3 = no growth/no uptake comparable to PHY14-URA

Strains	**Viability on SR+BPS+TAF plates**	**^{55}Fe-TAF uptake**	**Score**
MirBWT	+++	a	1
C-termDel	+++	a	1
N-termDel	+++	a*	1
F129D	+++	a*	1
Y398A	+++	b	1
R570A	+++	c	2
Loop7Del1	+++	c	2
W251/253A	++	c	2
Loop6Del	++	c	2
Y577A	+	c	3
A125D	+	c	3
Loop3Del	+	c	3
Loop7Del2	+	c	3
PHY14-URA	+	c	3

It is possible that the complete loss-of-function seen in the absence of loop 3 and the second half of loop 7 is due to misfolding of the protein. Nevertheless, the fact that the other two loop deletion mutants (loop 6 and the first half of loop 7) retained some functionality indicates that they must be properly folded and that deletion of an entire loop, or large sections of a loop, are not necessarily enough to cause misfolding. Of course, this does not completely rule out the possibility that deletions in loop 3 or the second half of loop 7 could affect interactions between amino acids necessary for proper folding. Immunofluorescence is underway to test this and ensure proper localization of these mutants.

In Arn1p, the *S. cerevisiae* ferrichrome transporter, and the only other fungal siderophore transporter for which any structural data is available, mutations of numerous amino acids in the seventh loop, including four tyrosine residues, resulted in significant or complete loss of transport and binding of the siderophore by the transporter (Kim et al. 2005). One of these Arn1p mutants, QRYR-A, contained mutations in several amino acids in the seventh loop, including the conserved tyrosine (577) and arginine (570) residues mutated in this study and highlighted in Figure 3-4. It would be interesting to see if individual mutation of this conserved tyrosine residue in *S. cerevisiae* (a.a. 558) would result in the same phenotype as seen in my study. The mutagenesis data from Arn1p, combined with our data from *Afu* MirB, point to the seventh loop as having a fundamental and conserved role in fungal siderophore uptake. More specifically, the loss-of-function observed in the seventh loop tyrosine mutants, both in this study (tyrosine 577 in MirB) and by Kim et al. (2005) (tyrosine 534 and 538 in Arn1p), suggests that tyrosine may be a key amino acid in uptake of fungal siderophores. While the structures

of the two siderophores, TAFC and FC, are different, they are both nevertheless hydroxamate siderophores and share the same basic core structure, N^5-acyl-N^5-hydroxyornithine.

With the exception of a family of drug efflux pumps and a family of sialate symporters (Pao et al. 1998), MFS transporters are usually composed of 12, not 14 (as in MirB), transmembrane domains and therefore do not possess a sixth or seventh extracellular loop. The presence of these extra loops does not appear to be directly related to symport activity. If this were the case, we might expect those families whose transporters function as symporters to also have 14 transmembrane domains, and this is not the case (Pao et al. 1998). These loops may instead be important for substrate specificity.

Concerning the first loop of Arn1p, Kim et al. (2005) found that mutations in that loop, while able to dramatically reduce uptake, were not enough to prevent binding of the siderophore or growth of those mutant strains on FC. Unlike Kim et al, this study identified a crucial amino acid in the first loop, A125D, which had one of the most pronounced loss-of-function phenotypes. The other first loop mutant however, F129D, did not appear to be important.

While the tryptophan 251 & 253, arginine 570, loop 7 deletion 1, and loop 6 deletion mutants did not appear to be able to transport ^{55}Fe-TAF (Figure 3-19), they retained the ability to use ^{55}Fe-TAF for growth (Figure 3-17), an indication that the transporter in these strains must retain some activity. This is especially true for the arginine substitution and the loop 7 deletion 1 since these strains exhibited growth almost comparable to MirBWT. In the case of the two tryptophan and the loop 6 mutants,

growth was only barely above background, and would suggest a very important, if not crucial, role in uptake. It is possible that deletion of the first half of loop 7and loop 6, and substitutions of the tryptophan and arginine residues, lead to a reduction of affinity of the transporter for the siderophore, and thus slowed down uptake to undetectable levels after 1 hour of exposure to ^{55}Fe-TAF. Although not directly involved in binding and transport of Fe-TAFC, these residues, perhaps especially loop 6 and the two tryptophans in loop 3, may be involved in stabilizing interactions between the transporter and the siderophore, or retention of the siderophore in the binding site.

The lack of a characterized TAFC transporter in bacteria, combined with the structural and functional differences between fungal and bacterial transporters, makes direct comparisons of *Afu* MirB with bacterial siderophore transporters difficult. However, there exist some important similarities between these transporters with regards to the types of amino acids involved in binding of hydroxamate siderophores. The binding pockets of the *E. coli* ferrichrome outer membrane transporter FhuA (Ferguson et al. 1998) and the PBP FhuD (Clarke et al. 2000) contain numerous amino acids involved in extraction of ferrichrome from the environment and binding in the pocket. Almost all of these are aromatic residues. Given the relative hydrophobicity of hydroxamate siderophores, it is not surprising that these residues would be involved in binding of TAFC in MirB and FC in Arn1p, FhuA and FhuD.

The solved 3D structure of TAFC is presented in Figure 4-1 (Hossain et al. 1980). TAFC is made up of three identical molecules of N^2-acetyl-N^5-cis-anhydromevalonyl-N^5-hydroxy-L-ornithine bound together via ester bonds. The iron-chelating center is made up of three five-membered rings formed by the hydroxamate groups of the N^2-acetyl-N^5-

hydroxy-L-ornithines. The three ester and acetyl groups (highlighted in Figure 4-1) extend out towards the outside of the molecule and are likely to be involved in hydrogen bonding with more polar amino acids. However, with the exception of these groups, the remainder of the molecule is hydrophobic. Association of the receptor with these regions of the molecule would involve primarily hydrophobic and van der Waals interactions.

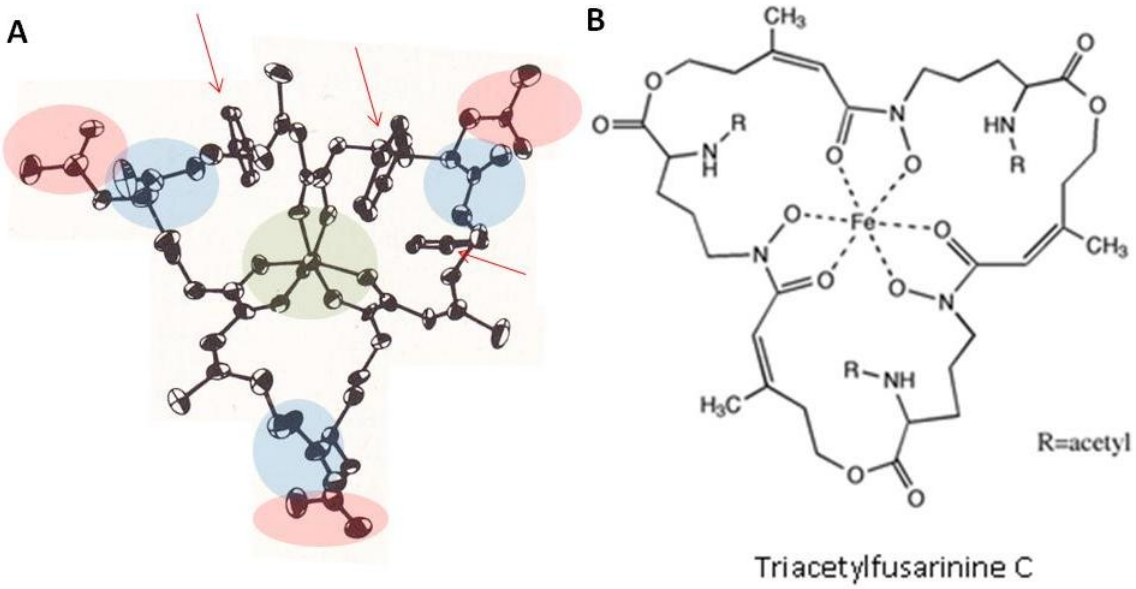

Figure 4-1. **A**) 3-D structure of TAFC bound to three benzene molecules (arrows). Highlighted are the N-acetyl groups (pink), the ester bonds (blue) and the iron molecule with its six coordinating oxygens (green). **B**) Schematic representation of TAFC (which shows the N-acetyl groups facing inwards). 3-D structure of TAFC reproduced with permission (Hossain et al. 1980).

The reduction in uptake seen in all the loop deletion mutants (Figure 3-19) cannot be explained solely by the observed reduced expression levels (Figure 3-15). The F129D mutant, whose expression was comparable to the deletion mutants, exhibited transport rates that were similar to MirBWT (Figure 3-19) and was able to utilize Fe-TAFC

efficiently for growth (Figure 3-17). These data suggest that even with a lower level of expression, uptake of Fe-TAFC by F129D was not compromised, and is therefore unlikely to compromise uptake in the loop deletion mutants.

The three remaining mutants, C-termDel, N-termDel and Y398A, did not show any appreciable defect in growth on Fe-TAFC compared to MirBWT. Transport of ^{55}Fe-TAFC in Y398A was reduced but still significantly above background, whereas no reduction in ^{55}Fe uptake was observed in the N- or C-terminal deletions. In fact, deletion of the five N-terminal amino acids increased ^{55}Fe-TAF uptake (Figure 3-19). While fluctuations in the rate of uptake observed in the N-termDel mutant make conclusions somewhat tentative, it is possible that deletion of these amino acids may have had an impact on localization, leading to increased levels of MirB protein in the plasma membrane, which could explain the higher rate of uptake. Yeast proteins Kex2p and DPAP A, an α factor processing enzyme and a dipeptidyl aminopeptidase, respectively, both of which are targeted to the endosomal pathway, contain signals for retention in the late Golgi (Bowers & Stevens 2005; Bryant & Stevens 1997; Brickner & Fuller 1997). Removal of these signal sequences which, in the case of DPAP A, is contained in the N-terminal region, lead to accelerated relocation to the late endosome. While such a mechanism could help explain the increased uptake seen in the N-termDel mutant, the presence of a signal at the N-terminus of MirB is still purely speculative.

The crystal structures of the bacterial MFS transporters LacY, GlpT, EmrD, OxlT and FucP reveal that these transporters fold into two distinct domains, N- and C-terminal domains, each with 6 TM helices that adopt a 2-fold pseudo symmetry and form a central pore in the membrane (Figure 1-14) (Radestock & Forrest 2011). They have been

crystallized in both an inward-facing (cytoplasmic) conformation (Figure 1-14) (Huang et al. 2003; Abramson et al. 2003), and an outward-facing (extracellular) conformation (Dang et al. 2010), as well as in an intermediary state, closed off to both sides (Hirai & Subramaniam 2004; Yin et al. 2006). Translocation of the substrate requires movement from one conformation to the other. These crystal structures are remarkably similar between the transporters, regardless of function, substrate specificity, or sequence identity. Therefore, it is possible that *Afu* MirB adopts an overall structure that is not unlike the one presented in Figure 1-14 and Figure 3-7. That is, *Afu* MirB would form a helical channel with 14 TM domains folded into two distinct halves, each with 7 TM helices, creating a central pore in the membrane. As with the other transporters, movement of the substrates (proton and siderophore) across the membrane would require conformational changes from an outward-facing conformation to the inward-facing conformation. However, it is important to note that the 3D model of *Afu* MirB should be viewed as quite speculative given that the % identity between MirB and the template was very low (7.843%).

There are other important differences between fungal siderophore transporters and most other MFS permeases that could very well impact overall 3D structure. One, as previously mentioned, is the presence of two extra TM domains. A second is the fact that all of the MFS crystal structures determined to date are from bacteria, and we have yet to discover if eukaryotic MFS permeases adopt a similar structure. Furthermore, evidence would suggest that fungal siderophore transporters are taken up along with their substrate through endocytosis of the entire complex (see Figure 1-16 and further discussion below). This is in contrast to other MFS permeases, which act to shuttle their substrate

across the membrane through the transporter to the cytoplasm (Law et al. 2009). Another key difference between MFS transporters and Arn1p, and possibly other fungal siderophore transporters as well, is the presence of two substrate binding sites in Arn1p (Moore et al. 2003), instead of one, as is the case in other MFS members. It appears that development of this second binding site was possible in part because of the presence of the two additional TM domains 13-14 (Kim et al. 2005).

Although the exact mechanism of siderophore uptake in *A. fumigatus* is still unknown, one could speculate that uptake follows a mechanism similar to that of *S. cerevisiae*; that is, that uptake is mediated by endocytosis of the entire transporter-siderophore-iron complex. The proposed model of uptake for *S. cerevisiae* begins with internalization of ferrichrome by fluid-phase endocytosis to the early endosome, where it is free to bind to one of the two binding sites on Arn1p, the receptor site, formed largely by the seventh loop (Kim et al. 2005; Moore et al. 2003). This would cause a change in the conformation of the transporter to the outward-open form (typical of MFS transporters), opening the second binding site and causing re-localization to the plasma membrane (Kim et al. 2005). Binding of the second ferrichrome molecule to the second site, the transporter site, would cause endocytosis of the complex and, subsequently, a change in conformation to the inward-open form of the transporter leading to release of the siderophore to the cytosol.

In this model, the siderophore is transported intact into the cytosol from the lumen of the endosome via translocation across the endosomal membrane through the transporter. The existence of a cytosolic TAFC esterase in *A. fumigatus* (Kragl et al. 2007) is an indication that Fe-TAFC may be transported intact into the cytosol, and

points to the possibility of a similar model of uptake to the one described above. Once transported across the endosomal membrane by MirB, TAFC would be broken down by the esterase to release the iron.

Of course, it is also possible that transport in *A. fumigatus* occurs independently of endocytosis and involves simply transport of the ferrated siderophore across the plasma membrane. While this possibility cannot be ruled out, it is worthwhile to note that evidence gathered to date would point to endocytosis-mediated uptake being true for not only *S. cerevisiae*, but quite possibly also *Candida albicans* and *Ustilago maydis* (Ardon et al. 1998; Hu et al. 2002). Furthermore, preliminary data from the immunofluorescence experiments in our study would seem to indicate that localization of MirB in *S. cerevisiae* is quite similar to that of endogenous *S. cerevisiae* siderophore transporters; that is, that it localizes to punctuate structures, likely endosomal compartments. However, immunofluorescence studies in *A. fumigatus* would be required before it could be determined if this is the default pattern of MirB localization, or simply a consequence of expression in *S. cerevisiae*.

In yeast, internalization of membrane permeases is mediated by ubiquitination. Covalent attachment of one or a few small molecules of ubiquitin (Ub) to the permease is the only signal to date that has been found to promote endocytosis of these transporters (Lauwers et al. 2010). The adaptor protein Ede1p, containing a Ub binding domain, and the vesicle coat protein clathrin, which forms the characteristic polyhedral lattice around the vesicle, are the first proteins to arrive at the endocytic site (Toret & Drubin 2007). This is followed by recruitment of numerous proteins, including coat and adapter proteins, as well as Las17p (yeast orthologue of the human WASP, Wiskott- Aldrich

syndrome protein) which activates the Arp2/3 complex required for actin assembly at the endocytic site. Actin assembly recruits the myosin motor protein Myo5p, and its activity drives internalization of the coat module. The last step involves coat and WASP/myosin module disassembly, leading to docking and fusion of the vesicle with the early endosome. Clathrin-mediated endocysis is an evolutionarily conserved process and many features of this pathway are conserved from yeasts to mammalian cells (Engqvist-Goldstein & Drubin 2003). While comparatively little is know about endocytosis in filamentous fungi, numerous similarities have been found between the fungal and mammalian/yeast endocytic trafficking pathways (Peñalva 2010).

Once yeast membrane proteins reach the early endosome, they are sorted to their proper compartments. Proteins targeted for recycling to the plasma membrane appear to first transit from the early endosome to the *trans*-Golgi network (TGN), where they are eventually returned to the plasma membrane via the exocytic pathway, similar to newly synthesized membrane proteins (Shaw et al. 2001). With regards to the yeast siderophore-transporters, there is some evidence that cycling occurs directly from the plasma membrane to endosomes and back to the plasma membrane (Kim et al. 2002). Alternatively, membrane proteins may be targeted for degradation and in this case transit from the early endosome to the late endosome before being sorted to the multivesicular body (MVB), which will eventually fuse with the vacuole. While there is still much that is unknown with regards to the specific signals and proteins that direct sorting to either of these pathways, ubiquitination of membrane proteins in yeast has been shown to act as a MVB sorting signal and is required for sorting to the MVB and delivery to the vacuole

(Lauwers et al. 2010). In contrast, exit of vesicles from the TGN towards endosomes does not appear to require ubiquitination.

The lack of apparent secondary bands or smears on the westerns (Figure 3-15) would indicate that degradation of MirB-FLAG wildtype and mutant proteins is unlikely to be a major factor in these strains. This, in addition to evidence from preliminary MirBWT immunofluorescence data of localization primarily to small punctate endosomal-like compartments, as opposed to the much larger vacuole, or the cytosol, would seem to indicate that the MirBWT proteins are being sorted properly to the endosomal pathway and plasma membrane. While some of the MirBWT proteins may be targeted to the vacuole for degredation, and in fact likey are, it does not appear to be the primary site of localization. It will be interesting to compare these localization patterns to those of the MirB mutants, especially the tyrosine (577) and alanine (125) substitution mutants, and the second half of loop 7 and loop 3 deletion mutants, which show a complete lack of function.

An interesting question that is raised by the endocytosis-mediate model of uptake presented above is how these transporters can function as proton symporters, considering that, at least in the case Arn1p in *S. cerevisiae*, the transporter re-locates to the PM only in the presence of bound siderophore and that the entire siderophore-transporter complex is then endocytosed, not transported across the membrane. For Arn1p, it has been proposed that movement to the outward conformation, brought on as a result of binding of the siderophore to the first site, would expose both the second siderophore binding site and the proton binding site. This would allow the proton to bind either at the plasma membrane, or possibly before relocation, while still in the endosome (Kim et al. 2005).

Once binding of the second substrate molecule (ferrichrome) occurs and the complex is endocytosed, the change in conformation to the inward-open form would release both the siderophore and proton to the cytosol.

The results of this study have provided important insight into siderophore uptake in *A. fumigatus* and the structural requirements of siderophore-transporters in both *A. fumigatus* and *S. cerevisiae*, and likely fungal transporters in general. The seventh extracellular loop, perhaps especially the tyrosine residues, appears to play a very important role in uptake of siderophores in both *A. fumigatus* and *S. cerevisiae*. In Arn1p select mutations in the seventh loop of Arn1p lead to complete loss of binding at the first binding site, the receptor site (Kim et al. 2005). However, these mutants retained partial function of the second binding site, the transporter site. Mutations in yet another set of loop seven amino acids in yeast lead to defects in the transporter site, but the receptor site remained active. Additionally, all of these mutants were found not to relocalize to the plasma membrane from endosomes upon exposure to ferrichrome. Taken together, these results indicate that this loop, in addition to forming the receptor site and part of the transporter site, is also involved in plasma membrane relocalization and conformational changes in the transporter.

In this study, a single amino acid in the first loop, alanine 125, was found to be absolutely necessary for uptake of Fe-TAFC in MirB. While no such amino acid has been found in *S. cerevisiae,* evidence suggests that the first loop is still very important for uptake in this organism. Substitutions of residues in the first loop of Arn1p resulted in a partial loss of affinity for ferrichrome at the transporter site and significantly reduced ferrichrome uptake, although they did not prevent relocalization to the PM (Kim et al.

2005). The authors theorize that this loop, in addition to being involved in forming part of the second site, may also be involved in conformational changes required for movement to the inward-open conformation once the second ferrichrome molecule has bound the transporter site.

In addition to the first and seventh loop mutants of *Afu* MirB, deletion of the third loop resulted in complete loss-of-function. Two tryptophan residues near the C-terminal end of this loop were found to reduce uptake but their absence alone is not enough to explain the phenotype of the deletion mutant. Therefore, there must still be other important amino acids in this loop. Since no mutagenesis data is available on the third loop of Arn1p, the importance of this loop in *S. cerevisiae* ferrichrome uptake has yet to be determined.

Deletion of the sixth loop and mutation of arginine 570 of *Afu* MirB were also found to negatively impact uptake, thought these were not as pronounced as the previously described mutations in the first, third and seventh loops.

Further research is still necessary to elucidate how exactly siderophore-transporters recognize and transport ferrated siderophores. Protein structures and more extensive mutagenesis studies will be necessary before a complete model of recognition, binding, and transport in *A. fumigatus* and fungal siderophore-transporters in general can be established. This may prove to be difficult, since crystallization of membrane proteins remains problematic (Ubarretxena-Belandia & Stokes 2010). However, as methods for purification of membrane proteins and creation of stable diffraction-quality crystals continue to improve, and as new methods are developed, such as electron

crystallography, obtaining 3D structures of membrane proteins will become easier and more feasible in the future.

It is critical that we better understand the mechanism by which *A. fumigatus* obtains TAFC and consequently, iron, since this is the key to its survival in the human host. Moreover, the synthesis and transport of siderophores present possible target areas in the development of new drugs as these biochemical pathways do not exist in humans.

Appendices

Appendix 1: Troubleshooting

Immunoblotting

Optimization of conditions necessary for detection of MirB-FLAG on western blot proved to be long and complicated. As was mentioned briefly in Results, initially, subcellular fractionation by differential centrifugation was attempted to both confirm expression of MirB-FLAG and determine subcellular localization of the protein. This method, previously described by Sun-Wada et al. (1998), yielded either extremely faint or none existent bands in the isolated fractions. Various steps were taken to improve protein yield including increasing initial culture size (100ml to 300ml), varying induction times in galactose (O/N, 2hrs, 5hrs) and creating spheroplasts before fractionation. Urea was also added to the protein-loading buffer in various amounts (2-8M) to enhance denaturation. Finally, to increase sensitivity, the detection method was changed from colorimetric to chemiluminescent. However, none of these changes were successful in confirming expression of MirB-FLAG. As such, the method was forgone in favour of protein extraction by trichloroacetic acid precipitation.

In addition to using TCA precipitations, SDS-PAGE gels were modified to include 8M urea. This technique proved to be more successful as bands were detected for all MirBWT and mutant proteins. However, as discussed in the Results section, bands of the same size as expected for MirB-FLAG were also detected in PHY14-URA. TCA

preps of PHY14-URA were repeated several times to make sure this result was not an error. Additionally to make sure that this was not due to accidental contamination of PHY14-URA with a MirB containing strain, colony PCR was conducted on PHY14-URA cultures. As well, empty PHY14 cells were transformed a second time with pESC-URA, but bands were detected in this strain also. Westerns were attempted with a different primary anti-FLAG antibody, but an even greater amount of background was observed in these blots. Finally, it was discovered that pre-adsorption of the original anti-FLAG monoclonal antibody to PHY14-URA lysates present on dot blots (Figure 4-2) was able to remove the background band observed in this strain, and consequently pre-adsorbed antibody was used for all western blots.

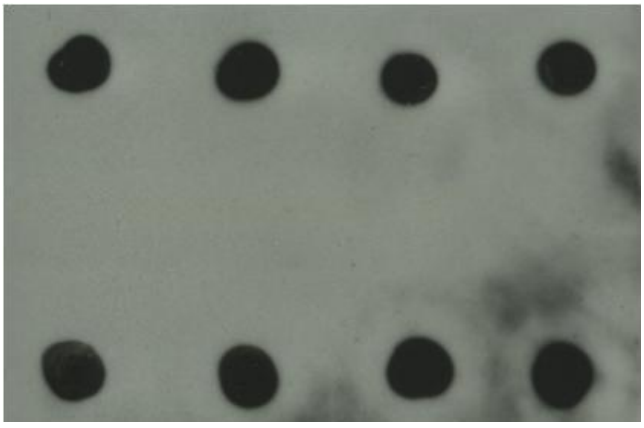

Figure 4-2. Dot blot assay of PHY14-URA whole cell lysates with monoclonal anti-FLAG antibody.

Growth assays

As mentioned in some detail above growth assays were initially performed using liquid cultures. These were originally done using cultures grown in flasks, but this was quickly replaced by growth on 96-well plates. However it proved to be extremely

difficult to obtain meaningful growth curves. The main problem encountered was the rather slow growth observed for MirBWT in raffinose and/or galactose media. As a result, growth of MirBWT and PHY14-URA was comparable in SR + gal media with the iron chelators BPS or dipyridyl plus Fe-TAFC. Attempts were made to optimize the experiment by varying a number of factors including the initial inoculum size (OD_{620} 0.1-0.35), the amount of galactose in the media (0.2-0.5 %), the amount of BPS used (250-1000 µM), the amount of Fe-TAFC added (10-50 µM), and by using a different iron chelator, 2,2'-dipyridyl (250 µM). These failed to enhance growth of MirBWT and the liquid assays were subsequently forgone in favor of growth assays on solid agar, which proved to be much more successful.

^{55}Fe-TAF uptake assays

A few issues were encountered with the ^{55}Fe uptake assays. The original intent was to do a time course assay, measuring uptake every ~ 5 min over a 20-30 min period of incubation of the cells with ^{55}Fe-TAFC. However, because little uptake was observed during this period, the incubation time was eventually increased to 60 min and radioactivity measured once at the end. In addition, a high degree of fluctuation in background radioactivity was observed using the original protocol. This was thought to potentially be due to 1) residual ^{55}Fe-TAFC bound to the glass filtration apparatus and 2) non-specific binding of ^{55}Fe-TAFC to the surface of the cells. In order to remove as much of the residual ^{55}Fe as possible, the glass filtration apparatus was soaked O/N in 5 % nitric acid before use in an experiment. Additionally, samples of extra yeast cells were passed through the column first, before the addition of the samples of interest, in an effort to bind off any residual ^{55}Fe-TAFC. In order to reduce non-specific binding of ^{55}Fe to the

surface of the cells, BSA and cold Fe-TAFC was added to the wash buffers. Together, these changes were effective in reducing the fluctuation in background radioactivity and allowed for accurate measurements of ^{55}Fe-TAF uptake in all strains.

Appendix 2: Purification of TAFC

While the TAFC utilized for the uptake and growth assays was acquired from Linda Pinto, I also attempted purification of desferri TAFC, the protocol for which is presented below.

Aspergillus fumigatus was grown in 2 L flasks in modified Grimm-Allen low iron media at 37°C. Mycelia were separated from culture supernatant using Miracloth, and discarded. Amberlite XAD16 (Supelco) resin, which binds to siderophores, was added to the supernatant and the mixture incubated ~ 1 hour at 37 °C with shaking. The Amberlite beads were added to a column and the siderophores eluted from the resin first with methanol:water:acetic acid (50:49.9:0.1) for fractions 1 & 2, and then by 100% methanol (fractions 3 & 4). Fractions were evaporated to remove liquid and subsequently freeze dried for two days. Purity of TAFC in the fractions was checked by thin layer chromatography (80% methanol solvent). While TAFC was successfully isolated, impurities were also found. These are most likely other siderophores or some derivative.

Appendix 3: Localization of a MirB-GFP construct in *A. fumigatus*

In the first year of research, the thesis project was focused on determining the subcellular localization of MirB in *Aspergillus fumigatus*. The strategy was to construct a *mirB-gfp* fusion vector, replace endogenous *mirB* via homologous recombination, and determine localization in both iron replete and iron limited conditions using immunofluorescence.

The technique of fusion PCR, according to the protocol outlined by Szewczyk et al. (2006), was used to create the *mirB-gfp* fusion construct (6 kb) (Figure 4-3). The ends of the construct contained homologous flanking regions, necessary for homologous recombination at the *mirB* locus. This PCR product was used for transformation of *A. fumigatus* pyrG^AF:: ΔKu80 (strain #1151) protoplasts, which are deficient in the Ku80 protein required for non-homologous end-joining, and therefore displaying an increased frequency of homologous recombination (Ferreira et al. 2006).

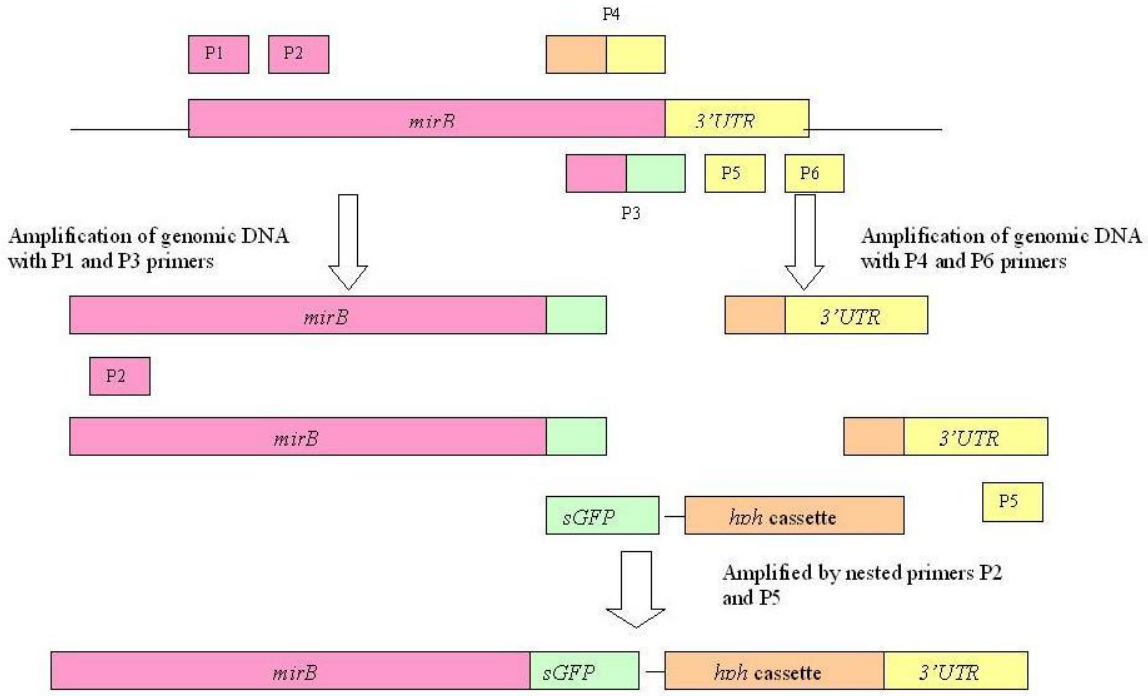

Figure 4-3. Schematic representation of *mirB-sgfp* fusion construct. Primers P1 and P3 were used to amplify upstream and *mirB* proper. The downstream portion of *mirB* (labelled 3'UTR) was amplified using P4 and P6. P3 and P4 contain regions that overlap in sequence with *sgfp* or the *hph* cassette, respectively. All three segments were fused together and amplified using P2 and P5.

Three separate fragments of DNA were amplified by PCR: the first contained the coding sequence of *mirB* (A.f. strain ATCC 13073) and upstream regulatory regions including putative SREA GATA sites; the second fragment contained the region immediately downstream of *mirB;* and the third contained *sgfp* and the hygromycin phospho-transferase (hph) cassette, a positive selectable marker for fungi. The three fragments were joined together using fusion PCR with the *sgfp* fragment flanked by the two *mirB* sequences Figure 4-3. This allowed for the creation of ~1 kb of homologous flanking regions at each side of the tagged *mirB* gene, necessary for homologous

recombination at the *mirB* locus. The fusion construct was successfully amplified and isolated (Figure 4-4).

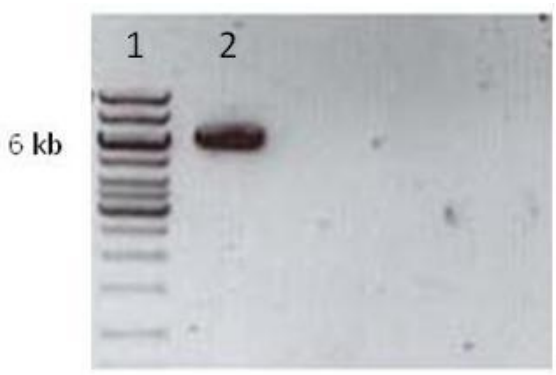

Figure 4-4. 7% gel electrophoresis of fusion PCR product. Lane 1: Ladder, Lane 2: fusion product (6 kb).

This PCR product was used for transformation of protoplasts of the *A. fumigatus* strain *pyrG^AF:: ΔKu80* (strain #1151). Two of the first transformants isolated, T1 and T2, were found to be hygromycin resistant and were selected for analysis. PCR analysis of T1 genomic DNA was performed using primers that bind from the start of *mirB* to the end of *sgfp* (Refer to Figure 4-3), resulting in amplification of a 3kb portion of the construct (Lane T1, Figure 4-5). For T2, a 2 kb portion of the construct was amplified, from the middle of *mirB* to the middle of the *hph* cassette (Lane T2, Figure 4-5). Controls using T1 and T2 genomic DNA and primers for the *nst1* gene (1.8 kb) of *A. fumigatus,* as well as a control with wildtype DNA, were also performed. Additionally, PCR amplification of the entire 6 kb construct, using primers P1 and P6 (Figure 4-3), was carried out (not shown). Result from this PCR suggested successful homologous recombination of *mirB-sgfp* at the locus replacing endogenous *mirB.*

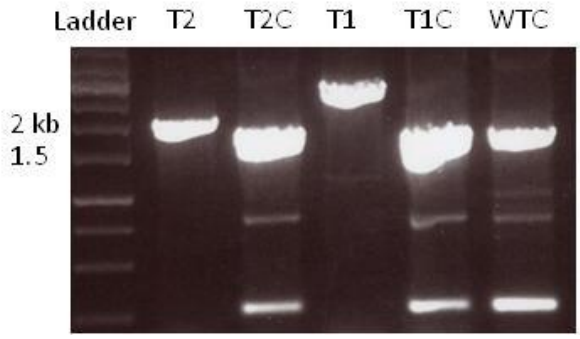

Figure 4-5. PCR of putative transformants T1 and T2. Each colony was tested for the presence of the fusion construct using primers designed to bind to a portion of the construct. A 2kb portion was amplified for T2 and a 3 kb portion for T1 (Lane T2 and T1). Controls for T1 and T2 were run using primers for the nst1 gene (1.8 kb) of *A. fumigatus* (Lane T2C and T1C). A control using wt DNA and nst1 was also carried out (Lane WTC).

The entire 6 kb fusion construct in both T1 and T2 was sequenced (Macrogen Korea). Sequencing of T1 revealed a single base insertion in the GA linker sequence between *mirB* and *gfp*, indicating that this construct may be non-functional. No major errors were found in the sequence of T2.

To check for expression of the fusion protein, numerous western blots were carried out on T1 and T2 grown in iron limited media using whole cell homogenate. Attempts were made to detect the chimeric protein using biotinylated anti-gfp antibodies (1:1,000) and an HRP-Streptavidin conjugate (1:15,000). The expected MW of MirB-GFP is 94 kDa. The blots did not reveal the presence of the chimeric protein in either T1 or T2 samples (Figure 4-6). Although a certain amount of background was observed, no significant bands at the 94 kDa mark were visible. Additional western blots were performed with various concentrations of both primary antibody and HRP-Streptavidin conjugate (not shown). None of the blots showed a band at 94 kDa. It is of interest to note that T1 and T2 show two stronger bands, when compared to the control, at around the 43

kDa mark. It is possible that this band may represent a truncated version of the chimeric protein. Successful immunoblotting may be hindered in part by the low concentration of protein isolated from *A. fumigatus* as well as a high degree of background on the blots. It is worthwhile to note that the immunoblotting was carried out using a colorimetric substrate. The use of a more sensitive chemiluminescent substrate may prove to be more successful.

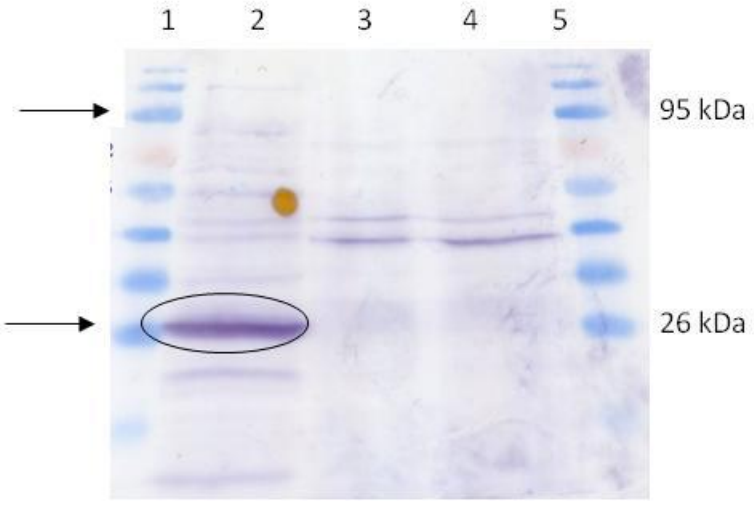

Figure 4-6. Western Blot of putative transformants T1 and T2. A GFP expressing strain was used as a positive control. Strains were grown in iron limited conditions. Expected molecular weight of the GFP (arrow, 27 kDa) and MirB (67 kDa) chimeric protein is 94 kDa (arrow). Lane 1 & 5: Stained protein ladder; Lane 2: GFP; Lane 3: T1; Lane 4: T2.

Although T1 and T2 were originally thought to have successfully undergone homologous recombination at the *mirB* locus, PCR amplification of the region around the loci has proven to be exceptionally difficult making it impossible to rule out the possibility that endogenous *mirB* is still present in these strains. Additionally, fluorescent microscopy using these strains has revealed significant background fluorescence making it very difficult to identify potential fluorescence from MirB-GFP.

In an attempt to isolate additional transformants, four more transformations were attempted. A total of 37 possible transformants from these transformations were analysed. Colonies resistant to hygromycin were isolated from these but were found to contain only the hygromycin resistance gene, not the complete fusion construct (data not shown). Protoplasts created for the fourth transformation were grown and digested in low iron media with the hope that in this way the *mirB* locus would be more easily accessible for homologous recombination. However, none of these transformants were found to carry the 6 kb fusion construct.

In summary, the *mirB-gfp* fusion construct (6 kb) was successfully created using fusion PCR. Only two transformants, T1 and T2, were found to possess the entire 6 kb construct and of these two only one, T2, was found not to contain any errors during sequencing. However, transformation of *Aspergillus fumigatus* protoplasts and identification of positive transformants proved to be difficult and problematic. As such, the decision was made to re-focus the project on site-directed mutagenesis of MirB.

Reference List

Abramson, J. et al., 2003. Structure and mechanism of the lactose permease of Escherichia coli. *Science (New York, N.Y.)*, 301(5633), pp.610-5. Available at: http://www.ncbi.nlm.nih.gov/pubmed/12893935 [Accessed July 21, 2010].

Adams, H. et al., 2006. Interaction of TonB with the outer membrane receptor FpvA of Pseudomonas aeruginosa. *Journal of bacteriology*, 188(16), pp.5752-61. Available at: http://www.ncbi.nlm.nih.gov/pubmed/16885443.

Adjimani, J. & Emery, T., 1988. Stereochemical aspects of iron transport in Mycelia sterilia EP-76. *Journal of bacteriology*, 170(3), p.1377. Available at: http://jb.asm.org/cgi/content/abstract/170/3/1377.

Agarwal, R., 2009. Allergic bronchopulmonary aspergillosis. *Chest*, 135(3), pp.805-26. Available at: http://www.ncbi.nlm.nih.gov/pubmed/19265090.

Agilent Technologies, QuikChange Primer Design. Available at: https://www.genomics.agilent.com/CollectionSubpage.aspx?PageType=Tool&SubPageType=ToolQCPD&PageID=15.

Aimanianda, V. et al., 2009. Surface hydrophobin prevents immune recognition of airborne fungal spores. *Nature*, 460(7259), pp.1117-21. Available at: http://www.ncbi.nlm.nih.gov/pubmed/19713928.

Anderson, M.T. & Armstrong, S.K., 2006. The Bordetella bfe system: growth and transcriptional response to siderophores, catechols, and neuroendocrine catecholamines. *Journal of bacteriology*, 188(16), pp.5731-40. Available at: http://www.ncbi.nlm.nih.gov/pubmed/16885441.

Ardon, O. et al., 1998. Iron uptake in Ustilago maydis: tracking the iron path. *Journal of bacteriology*, 180(8), p.2021. Available at: http://jb.asm.org/cgi/content/abstract/180/8/2021.

Arnold, K. et al., 2006. The SWISS-MODEL workspace: a web-based environment for protein structure homology modelling. *Bioinformatics (Oxford, England)*, 22(2), pp.195-201. Available at: http://www.ncbi.nlm.nih.gov/pubmed/16301204.

Askwith, C. et al., 1994. The FET3 gene of S. cerevisiae encodes a multicopper oxidase required for ferrous iron uptake. *Cell*, 76(2), pp.403-10. Available at: http://www.ncbi.nlm.nih.gov/pubmed/8293473.

Barry, S.M. & Challis, G.L., 2009. Recent advances in siderophore biosynthesis. *Current opinion in chemical biology*, 13(2), pp.205-15. Available at: http://www.ncbi.nlm.nih.gov/pubmed/19369113.

Beare, P.A. et al., 2003. Siderophore-mediated cell signalling in Pseudomonas aeruginosa: divergent pathways regulate virulence factor production and siderophore receptor synthesis. *Molecular Microbiology*, 47(1), pp.195-207.

Beasley, F.C. & Heinrichs, D.E., 2009. Siderophore-mediated iron acquisition in the staphylococci. *Journal of inorganic biochemistry*, pp.1-7. Available at: http://www.ncbi.nlm.nih.gov/pubmed/19850350.

Beasley, Federico C et al., 2009. Characterization of staphyloferrin A biosynthetic and transport mutants in Staphylococcus aureus. *Molecular microbiology*, 72(4), pp.947-63. Available at: http://www.ncbi.nlm.nih.gov/pubmed/19400778.

Bickel, H. et al., 1960. Stoffwechselprodukte von Actinomyceten. 26. Mitteilung. Über die Isolierung und Charakterisierung der Ferrioxamine A—F, neuer Wuchsstoffe der Sideramin-Gruppe. *Helvetica Chimica Acta*, 43, pp.2118-2128.

Birney, E., Clamp, M. & Durbin, R., 2004. GeneWise and Genomewise. *Genome research*, 14(5), pp.988-95. Available at: http://www.ncbi.nlm.nih.gov/pubmed/15123596.

Bowers, K. & Stevens, T.H., 2005. Protein transport from the late Golgi to the vacuole in the yeast Saccharomyces cerevisiae. *Biochimica et biophysica acta*, 1744(3), pp.438-54. Available at: http://www.ncbi.nlm.nih.gov/pubmed/15913810 [Accessed September 21, 2010].

Brakhage, A.A. & Langfelder, K., 2002. Menacing mold: the molecular biology of Aspergillus fumigatus. *Annual review of microbiology*, 56, pp.433-55. Available at: http://www.ncbi.nlm.nih.gov/pubmed/12142473.

Braun, V. & Endriss, F., 2007. Energy-coupled outer membrane transport proteins and regulatory proteins. *Biometals : an international journal on the role of metal ions in biology, biochemistry, and medicine*, 20(3-4), pp.219-31. Available at: http://www.ncbi.nlm.nih.gov/pubmed/17370038.

Braun, V., Mahren, S. & Ogierman, M., 2003. Regulation of the FecI-type ECF sigma factor by transmembrane signalling. *Current opinion in microbiology*, 6(2), p.173–180. Available at: http://linkinghub.elsevier.com/retrieve/pii/S1369527403000225.

Brickner, J.H. & Fuller, R.S., 1997. SOI1 encodes a novel, conserved protein that promotes TGN-endosomal cycling of Kex2p and other membrane proteins by modulating the function of two TGN localization signals. *The Journal of cell biology*, 139(1), pp.23-36. Available at: http://www.pubmedcentral.nih.gov/articlerender.fcgi?artid=2139830&tool=pmcentrez&rendertype=abstract.

Brookman, J.L. & Denning, D.W., 2000. Molecular genetics in Aspergillus fumigatus. *Current opinion in microbiology*, 3(5), p.468–474. Available at: http://linkinghub.elsevier.com/retrieve/pii/S1369527400001247.

Bryant, N.J. & Stevens, T.H., 1997. Two separate signals act independently to localize a yeast late Golgi membrane protein through a combination of retrieval and retention. *The Journal of cell biology*, 136(2), pp.287-97. Available at: http://www.pubmedcentral.nih.gov/articlerender.fcgi?artid=2134822&tool=pmcentrez&rendertype=abstract.

Buchanan, S.K. et al., 1999. Crystal structure of the outer membrane active transporter FepA from Escherichia coli. *Nature structural biology*, 6(1), pp.56-63.

Budde, A.D. & Leong, S.A., 1989. Characterization of siderophores from Ustilago maydis. *Mycopathologia*, 108(2), pp.125-33. Available at: http://www.ncbi.nlm.nih.gov/pubmed/2531844.

Bös, C., Lorenzen, D. & Braun, V., 1998. Specific in vivo labeling of cell surface-exposed protein loops: reactive cysteines in the predicted gating loop mark a ferrichrome binding site and a ligand-induced conformational change of the Escherichia coli FhuA protein. *Journal of bacteriology*, 180(3), pp.605-13. Available at: http://www.ncbi.nlm.nih.gov/pubmed/9457864.

Cao, Z. et al., 2002. Spectroscopic Observations of Ferric Enterobactin Transport. *Journal of Biological Chemistry*, 278(2), pp.1022-1028. Available at: http://www.jbc.org/cgi/doi/10.1074/jbc.M210360200.

Carrano, C.J. et al., 1996. Coordination Chemistry of the Carboxylate Type Siderophore Rhizoferrin: The Iron(III) Complex and Its Metal Analogs. *Inorganic chemistry*, 35(22), pp.6429-6436. Available at: http://www.ncbi.nlm.nih.gov/pubmed/11666790.

Carswell, C.L., Rigden, M.D. & Baenziger, J.E., 2008. Expression, purification, and structural characterization of CfrA, a putative iron transporter from Campylobacter jejuni. *Journal of bacteriology*, 190(16), pp.5650-62. Available at: http://www.ncbi.nlm.nih.gov/pubmed/18556796.

Chakraborty, R., Storey, E. & van der Helm, D., 2007. Molecular mechanism of ferricsiderophore passage through the outer membrane receptor proteins of Escherichia coli. *Biometals : an international journal on the role of metal ions in biology, biochemistry, and medicine*, 20(3-4), pp.263-74. Available at: http://www.ncbi.nlm.nih.gov/pubmed/17186377.

Charlang, G. et al., 1981. Cellular and extracellular siderophores of Aspergillus nidulans and Penicillium chrysogenum. *Molecular and cellular biology*, 1(2), pp.94-100. Available at: http://www.ncbi.nlm.nih.gov/pubmed/6242827.

Chenna, R., 2003. Multiple sequence alignment with the Clustal series of programs. *Nucleic Acids Research*, 31(13), pp.3497-3500. Available at: http://www.nar.oupjournals.org/cgi/doi/10.1093/nar/gkg500.

Clarke, T.E. et al., 2002. X-ray crystallographic structures of the Escherichia coli periplasmic protein FhuD bound to hydroxamate-type siderophores and the antibiotic albomycin. *The Journal of biological chemistry*, 277(16), pp.13966-72. Available at: http://www.ncbi.nlm.nih.gov/pubmed/11805094.

Clarke, T.E. et al., 2000. The structure of the ferric siderophore binding protein FhuD complexed with gallichrome. *Nature structural biology*, 7(4), pp.287-91. Available at: http://www.ncbi.nlm.nih.gov/pubmed/10742172.

Cobessi, D., Celia, H. & Pattus, F., 2005. Crystal structure at high resolution of ferric-pyochelin and its membrane receptor FptA from Pseudomonas aeruginosa. *Mol. Biol.*, 352, pp.893-904.

Cobessi, D. et al., 2005. The crystal structure of the pyoverdine outer membrane receptor FpvA from Pseudomonas aeruginosa at 3.6 angstroms resolution. *Journal of molecular biology*, 347(1), pp.121-34. Available at: http://www.ncbi.nlm.nih.gov/pubmed/15733922.

Cowart, R.E., Singleton, F.L. & Hind, J.S., 1993. A Comparison of Bathophenanthrolinedisulfonic Acid and Ferrozine as Chelators of Iron(II) in Reduction Reactions. *Analytical Biochemistry*, 211(1), pp.151-155.

Cox, C. & Adams, P., 1985. Siderophore activity of pyoverdin for Pseudomonas aeruginosa. *Infection and immunity*, 48(1), p.130. Available at: http://iai.asm.org/cgi/content/abstract/48/1/130.

Dagenais, T.R.T. & Keller, N.P., 2009. Pathogenesis of Aspergillus fumigatus in Invasive Aspergillosis. *Clinical microbiology reviews*, 22(3), pp.447-65. Available at: http://www.ncbi.nlm.nih.gov/pubmed/19597008.

Dale, S.E., Sebulsky, M.T. & Heinrichs, D.E., 2004. Involvement of SirABC in iron-siderophore import in Staphylococcus aureus. *Journal of bacteriology*, 186(24), p.8356. Available at: http://jb.asm.org/cgi/content/abstract/186/24/8356.

Dang, S. et al., 2010. Structure of a fucose transporter in an outward-open conformation. *Nature*, 467(7316), pp.734-738. Available at: http://www.ncbi.nlm.nih.gov/pubmed/20877283 [Accessed October 1, 2010].

Dix, D.R. et al., 1994. The FET4 gene encodes the low affinity Fe(II) transport protein of Saccharomyces cerevisiae. *The Journal of biological chemistry*, 269(42), pp.26092-26099.

Drechsel, H. et al., 1993. Purification and chemical characterization of staphyloferrin B, a hydrophilic siderophore from staphylococci. *Biometals : an international journal on the role of metal ions in biology, biochemistry, and medicine*, 6(3), pp.185-92. Available at: http://www.ncbi.nlm.nih.gov/pubmed/8400765.

Drechsel, H. & Jung, G., 1998. Peptide siderophores. *Journal of peptide science : an official publication of the European Peptide Society*, 4(3), pp.147-81. Available at: http://www.ncbi.nlm.nih.gov/pubmed/18832174.

Engqvist-Goldstein, A.E.Y. & Drubin, David G, 2003. Actin assembly and endocytosis: from yeast to mammals. *Annual review of cell and developmental biology*, 19, pp.287-332. Available at: http://www.ncbi.nlm.nih.gov/pubmed/14570572 [Accessed October 12, 2010].

Ferguson, A. D. et al., 1998. Siderophore-Mediated Iron Transport: Crystal Structure of FhuA with Bound Lipopolysaccharide. *Science*, 282(5397), pp.2215-2220. Available at: http://www.sciencemag.org/cgi/doi/10.1126/science.282.5397.2215.

Ferguson, A.D. et al., 2002. Structural basis of gating by the outer membrane transporter FecA. *Science (New York, N.Y.)*, 295(5560), pp.1715-9. Available at: http://www.ncbi.nlm.nih.gov/pubmed/11872840.

Ferreira, M.E.S. et al., 2006. The akuB KU80 Mutant Deficient for Nonhomologous End Joining Is a Powerful Tool for Analyzing Pathogenicity in Aspergillus fumigatus. *Eukaryotic Cell*, 5(1), pp.207-211.

Flückiger, U. et al., 2006. Treatment options of invasive fungal infections in adults. *Swiss medical weekly : official journal of the Swiss Society of Infectious Diseases, the Swiss Society of Internal Medicine, the Swiss Society of Pneumology*, 136(29-30), pp.447-63. Available at: http://www.ncbi.nlm.nih.gov/pubmed/16937323.

Frishman, D. & Argos, P., 1996. Incorporation of non-local interactions in protein secondary structure prediction from the amino acid sequence. *Protein engineering*, 9(2), pp.133-42. Available at: http://www.ncbi.nlm.nih.gov/pubmed/9005434.

Gasteiger, E. et al., 2005. Protein identification and analysis tools in the ExPASy server. In J. M. Walker, ed. *The Proteomics Protocols Handbook*. Humana Press, pp. 571-607. Available at: http://www.ncbi.nlm.nih.gov/pubmed/10027275.

Gifford, A.H.T., Klippenstein, J.R. & Moore, M.M., 2002. Serum Stimulates Growth of and Proteinase Secretion by Aspergillus fumigatus. *Infection and immunity*, 70(1), pp.19-26.

Grass, G., 2006. Iron transport in Escherichia coli: all has not been said and done. *Biometals : an international journal on the role of metal ions in biology, biochemistry, and medicine*, 19(2), pp.159-72. Available at: http://www.ncbi.nlm.nih.gov/pubmed/16718601.

Greenwald, J. et al., 2007. Real time fluorescent resonance energy transfer visualization of ferric pyoverdine uptake in Pseudomonas aeruginosa. A role for ferrous iron. *The Journal of biological chemistry*, 282(5), pp.2987-95. Available at: http://www.ncbi.nlm.nih.gov/pubmed/17148441.

Gruenheid, S. et al., 1999. The iron transport protein NRAMP2 is an integral membrane glycoprotein that colocalizes with transferrin in recycling endosomes. *The Journal of experimental medicine*, 189(5), pp.831-41. Available at: http://www.pubmedcentral.nih.gov/articlerender.fcgi?artid=2192949&tool=pmcentrez&rendertype=abstract.

Gupta, R. & Brunak, S., 2002. Prediction of glycosylation across the human proteome and the correlation to protein function. *Pacific Symposium on Biocomputing*, 7, pp.310-322.

Haag, H. et al., 1993. Purification of yersiniabactin: a siderophore of Yersinia enterocolitica. *Journal of General Microbiology*, 139, pp.2159-2165.

Haas, H., 2004. Molecular Genetics of Iron Uptake and Homeostasis in Fungi. In G. A. Marzluf & R. Brambl, eds. *The Mycota III: Biochemistry and Molecular Biology*. Berlin: Springer, pp. 1-31.

Haas, H., Eisendle, M. & Turgeon, B.G., 2008. Siderophores in fungal physiology and virulence. *Annual review of phytopathology*, 46, pp.149-87. Available at: http://www.ncbi.nlm.nih.gov/pubmed/18680426.

Haas, H. et al., 2003. Characterization of the Aspergillus nidulans transporters for the siderophores enterobactin and triacetylfusarinine C. *Biochemical Journal*, 371, pp.505-513.

Heymann, P., Ernst, J.F. & Winkelmann, G., 2000. Identification and substrate specificity of a ferrichrome-type siderophore transporter (Arn1p) in Saccharomyces cerevisiae. *FEMS microbiology letters*, 186(2), pp.221-7. Available at: http://www.ncbi.nlm.nih.gov/pubmed/10802175.

Heymann, P. et al., 2002. The Siderophore Iron Transporter of Candida albicans (Sit1p/Arn1p) Mediates Uptake of Ferrichrome-Type Siderophores and Is Required for Epithelial Invasion. *Infection and Immunity*, 70(9), pp.5246-5255.

Hirai, T. & Subramaniam, S., 2004. Structure and transport mechanism of the bacterial oxalate transporter OxlT. *Biophysical journal*, 87(5), pp.3600-7. Available at: http://www.pubmedcentral.nih.gov/articlerender.fcgi?artid=1304825&tool=pmcentrez&rendertype=abstract [Accessed August 23, 2010].

Hirokawa, T., Boon-Chieng, S. & Mitaku, S., 1998. SOSUI: classification and secondary structure prediction system for membrane proteins. *Bioinformatics (Oxford, England)*, 14(4), pp.378-9. Available at: http://www.ncbi.nlm.nih.gov/pubmed/9632836.

Hissen, A.H.T. et al., 2004. Survival of Aspergillus fumigatus in Serum Involves Removal or Iron from Transferrin: the Role of Siderophores. *Infection and Immunity*, 72(3), pp.1402-1408.

Hissen, A.H.T. et al., 2005. The Aspergillus fumigatus Siderophore Biosynthetic Gene sidA, Encoding L-Ornithine N5-Oxygenase, Is Required for Virulence. *Infection and Immunity*, 73(9), pp.5493-5503.

Horton, P. et al., 2007. WoLF PSORT: protein localization predictor. *Nucleic acids research*, 35(Web Server issue), pp.W585-7. Available at: http://www.ncbi.nlm.nih.gov/pubmed/17517783.

Hossain, M.B. et al., 1980. Circular Dichroism, Crystal Structure, and Absolute Configuration of the Siderophore Ferric N,N□ ,N‟-Triacetylfusarinine, FeC39H57N60. *Journal of the American Chemical Society*, 102, pp.5766-5773.

Hu, C.-J. et al., 2002. Characterization and functional analysis of the siderophore-iron transporter CaArn1p in Candida albicans. *The Journal of biological chemistry*, 277(34), pp.30598-605. Available at: http://www.ncbi.nlm.nih.gov/pubmed/12060662 [Accessed November 2, 2010].

Huang, Y. et al., 2003. Structure and mechanism of the glycerol-3-phosphate transporter from Escherichia coli. *Science (New York, N.Y.)*, 301(5633), pp.616-20. Available at: http://www.ncbi.nlm.nih.gov/pubmed/12893936.

Imbert, M., Bechet, M. & Blondeau, R., 1995. Comparison of the Main Siderophores Produced by Some Species of Streptomyces. *Current Microbiology*, 31, pp.129-133.

Imbert, M. & Blondeau, R., 1998. On the iron requirement of lactobacilli grown in chemically defined medium. *Current microbiology*, 37(1), pp.64-6. Available at: http://www.ncbi.nlm.nih.gov/pubmed/9625793.

Imperi, F., Tiburzi, F. & Visca, P., 2009. Molecular basis of pyoverdine siderophore recycling in Pseudomonas aeruginosa. *Proceedings of the National Academy of Sciences of the United States of America*, 106(48), pp.20440-5. Available at: http://www.ncbi.nlm.nih.gov/pubmed/19906986.

James, E.H. et al., 2005. Mutational Analysis of a Bifunctional Ferrisiderophore Receptor and Signal-Transducing Protein from Pseudomonas aeruginosa. *Journal of bacteriology*, 187(13), pp.4514-4520.

Jin, B. et al., 2006. Iron acquisition systems for ferric hydroxamates, haemin and haemoglobin in Listeria monocytogenes. *Molecular Microbiology*, 59(4), pp.1185-1198. Available at: http://www.blackwell-synergy.com/doi/abs/10.1111/j.1365-2958.2005.05015.x.

Johnson, L., 2008. Iron and siderophores in fungal-host interactions. *Mycological research*, 112(Pt 2), pp.170-83. Available at: http://www.ncbi.nlm.nih.gov/pubmed/18280720.

Julenius, K. et al., 2005. Prediction, conservation analysis, and structural characterization of mammalian mucin-type O-glycosylation sites. *Glycobiology*, 15(2), pp.153-64. Available at: http://www.ncbi.nlm.nih.gov/pubmed/15385431 [Accessed August 6, 2010].

Kaplan, J., 2002. Mechanisms of cellular iron acquisition: another iron in the fire. *Cell*, 111(5), pp.603-6. Available at: http://www.ncbi.nlm.nih.gov/pubmed/12464171.

Keogh, M.-C. et al., 2006. A phosphatase complex that dephosphorylates gammaH2AX regulates DNA damage checkpoint recovery. *Nature*, 439(7075), pp.497-501. Available at: http://www.ncbi.nlm.nih.gov/pubmed/16299494.

Kim, Y., Lampert, S.M. & Philpott, C.C., 2005. A receptor domain controls the intracellular sorting of the ferrichrome transporter, ARN1. *The EMBO journal*, 24(5), pp.952-62. Available at: http://www.ncbi.nlm.nih.gov/pubmed/15719020.

Kim, Y., Yun, C.-W. & Philpott, C.C., 2002. Ferrichrome induces endosome to plasma membrane cycling of the ferrichrome transporter, Arn1p, in Saccharomyces cerevisiae. *The EMBO journal*, 21(14), pp.3632-42. Available at: http://www.ncbi.nlm.nih.gov/pubmed/12110576.

Koebnik, R., 2005. TonB-dependent trans-envelope signalling: the exception or the rule? *Trends in microbiology*, 13(8), pp.343-7. Available at: http://www.ncbi.nlm.nih.gov/pubmed/15993072.

Kragl, C. et al., 2007. EstB-mediated hydrolysis of the siderophore triacetylfusarinine C optimizes iron uptake of Aspergillus fumigatus. *Eukaryotic cell*, 6(8), pp.1278-85. Available at: http://www.ncbi.nlm.nih.gov/pubmed/17586718.

Krewulak, K.D., Shepherd, C.M. & Vogel, H.J., 2005. Molecular dynamics simulations of the periplasmic ferric-hydroxamate binding protein FhuD. *Biometals : an international journal on the role of metal ions in biology, biochemistry, and medicine*, 18(4), pp.375-86. Available at: http://www.ncbi.nlm.nih.gov/pubmed/16158230.

Krewulak, K.D. & Vogel, H.J., 2008. Structural biology of bacterial iron uptake. *Biochimica et biophysica acta*, 1778(9), pp.1781-804. Available at: http://www.ncbi.nlm.nih.gov/pubmed/17916327.

Köster, W., 2001. ABC transporter-mediated uptake of iron, siderophores, heme and vitamin B12. *Research in microbiology*, 152(3-4), pp.291-301. Available at: http://www.ncbi.nlm.nih.gov/pubmed/11421276.

Larsen, R.A., Thomas, M.G. & Postle, K., 1999. Protonmotive force, ExbB and ligand-bound FepA drive conformational changes in TonB. *Molecular Microbiology*, 31(6), pp.1809-1824.

Latgé, J.P., 1999. Aspergillus fumigatus and aspergillosis. *Clinical Microbiology Reviews*, 12(2), p.310. Available at: http://cmr.asm.org/cgi/content/abstract/12/2/310.

Latgé, J.-P., 2001. The pathobiology of Aspergillus fumigatus. *Trends in Microbiology*, 9(8), pp.382-389. Available at: http://linkinghub.elsevier.com/retrieve/pii/S0966842X01021047.

Lauwers, E. et al., 2010. The ubiquitin code of yeast permease trafficking. *Trends in cell biology*, 20(4), pp.196-204. Available at: http://www.ncbi.nlm.nih.gov/pubmed/20138522.

Law, C.J., Maloney, P.C. & Wang, D., 2009. Ins and Outs of Major Facilitator Superfamily Antiporters. *Annual review of microbiology*, 62, pp.289-305.

Lesuisse, E., Simon-Casteras, M. & Labbe, P., 1998. Siderophore-mediated iron uptake in Saccharomyces cerevisiae: the SIT1 gene encodes a ferrioxamine B permease that belongs to the major facilitator superfamily. *Microbiology*, (144), pp.3455-3462.

Locher, K.P., Lee, A.T. & Rees, D.C., 2002. The E. coli BtuCD structure: a framework for ABC transporter architecture and mechanism. *Science (New York, N.Y.)*, 296(5570), pp.1091-8. Available at: http://www.ncbi.nlm.nih.gov/pubmed/12004122.

Locher, K.P. et al., 1998. Transmembrane signaling across the ligand-gated FhuA receptor: crystal structures of free and ferrichrome-bound states reveal allosteric changes. *Cell*, 95(6), pp.771-8. Available at: http://www.ncbi.nlm.nih.gov/pubmed/9865695.

Maglott, D. et al., 2005. Entrez Gene: gene-centered information at NCBI. *Nucleic acids research*, 33(Database issue), pp.D54-8. Available at: http://www.pubmedcentral.nih.gov/articlerender.fcgi?artid=539985&tool=pmcentrez&rendertype=abstract.

Marchler-Bauer, A. & Bryant, S.H., 2004. CD-Search: protein domain annotations on the fly. *Nucleic acids research*, 32(Web Server issue), pp.W327-31. Available at: http://www.pubmedcentral.nih.gov/articlerender.fcgi?artid=441592&tool=pmcentrez&rendertype=abstract [Accessed January 7, 2011].

Matzanke, B.F. et al., 1987. Role of siderophores in iron storage in spores of Neurospora crassa and Aspergillus ochraceus. *Journal of bacteriology*, 169(12), pp.5873-6. Available at: http://www.ncbi.nlm.nih.gov/pubmed/2960664.

Meiwes, J. et al., 1990. Isolation and characterization of staphyloferrin A, a compound with siderophore activity from Staphylococcus hyicus DSM 20459. *FEMS microbiology letters*, 67, pp.201-206.

Meyer, V., 2008. Genetic engineering of filamentous fungi--progress, obstacles and future trends. *Biotechnology advances*, 26(2), pp.177-85. Available at: http://www.ncbi.nlm.nih.gov/pubmed/18201856.

Miller, M.C. et al., 2006. Crystal structure of ferric-yersiniabactin, a virulence factor of Yersinia pestis. *Journal of inorganic biochemistry*, 100(9), pp.1495-500. Available at: http://www.ncbi.nlm.nih.gov/pubmed/16806483.

Mircescu, M.M. et al., 2009. Essential role for neutrophils but not alveolar macrophages at early time points following Aspergillus fumigatus infection. *The Journal of infectious diseases*, 200(4), pp.647-56. Available at: http://www.pubmedcentral.nih.gov/articlerender.fcgi?artid=2745295&tool=pmcentrez&rendertype=abstract [Accessed August 19, 2010].

Moore, R.E., Kim, Y. & Philpott, C.C., 2003. The mechanism of ferrichrome transport through Arn1p and its metabolism in Saccharomyces cerevisiae. *Proceedings of the National Academy of Sciences*, 100(10), p.5664. Available at: http://www.pnas.org/cgi/content/abstract/100/10/5664.

Morschhäuser, J., 2010. Regulation of multidrug resistance in pathogenic fungi. *Fungal genetics and biology : FG & B*, 47(2), pp.94-106. Available at: http://www.ncbi.nlm.nih.gov/pubmed/19665571.

Müller, A. et al., 2006. An [{Fe(mecam)}2]6- bridge in the crystal structure of a ferric enterobactin binding protein. *Angewandte Chemie (International ed. in English)*, 45(31), pp.5132-6. Available at: http://www.ncbi.nlm.nih.gov/pubmed/16927323.

Müller, S.I., Valdebenito, M. & Hantke, Klaus, 2009. Salmochelin, the long-overlooked catecholate siderophore of Salmonella. *Biometals : an international journal on the role of metal ions in biology, biochemistry, and medicine*, 22(4), pp.691-5. Available at: http://www.ncbi.nlm.nih.gov/pubmed/19214756.

Oberegger, H. et al., 2001. SREA is involved in regulation of siderophore biosynthesis, utilization and uptake in Aspergillus nidulans. *Molecular Microbiology*, 41(5), p.1077–1089. Available at: http://scholar.google.com/scholar?hl=en&btnG=Search&q=intitle:SREA+is+involved+in+regulation+of+siderophore+biosynthesis,+utilization+and+uptake+in+Aspergillus+nidulans#0.

Oide, S. et al., 2006. NPS6, encoding a nonribosomal peptide synthetase involved in siderophore-mediated iron metabolism, is a conserved virulence determinant of plant pathogenic ascomycetes. *The Plant cell*, 18(10), pp.2836-53. Available at: http://www.ncbi.nlm.nih.gov/pubmed/17056706.

O'Brien, I.G. & Gibson, F., 1970. The structure of enterochelin and related 2,3-dihydroxy-N-benzoylserine conjugates from Escherichia coli. *Biochimica et biophysica acta*, 215(2), pp.393-402. Available at: http://www.ncbi.nlm.nih.gov/pubmed/4926450.

O'Gorman, C.M., Fuller, H.T. & Dyer, P.S., 2009. Discovery of a sexual cycle in the opportunistic fungal pathogen Aspergillus fumigatus. *Nature*, 457(7228), pp.471-4. Available at: http://www.ncbi.nlm.nih.gov/pubmed/19043401 [Accessed July 16, 2010].

Pao, S.S., Paulsen, I.T. & Saier, M.H., 1998. Major Facilitator Superfamily. *Microbiology and molecular biology reviews*, 62(1), pp.1-34.

Payne, S.M., 1994. Detection, isolation, and characterization of siderophores. *Methods in enzymology*, 235, pp.329-44. Available at: http://www.ncbi.nlm.nih.gov/pubmed/8057905 [Accessed January 29, 2011].

Peñalva, M.Á., 2010. Endocytosis in filamentous fungi: Cinderella gets her reward. *Current opinion in microbiology*, 13(6), pp.684-92. Available at: http://www.ncbi.nlm.nih.gov/pubmed/20920884 [Accessed February 10, 2011].

Philpott, C.C., 2006. Iron uptake in fungi: a system for every source. *Biochimica et biophysica acta*, 1763(7), pp.636-45. Available at: http://www.ncbi.nlm.nih.gov/pubmed/16806534.

Posey, J.E. & Gherardini, F.C., 2000. Lack of a Role for Iron in the Lyme Disease Pathogen. *Science*, 288(5471), pp.1651-1653. Available at: http://www.sciencemag.org/cgi/doi/10.1126/science.288.5471.1651 [Accessed March 1, 2011].

Radestock, S. & Forrest, L.R., 2011. The alternating-access mechanism of MFS transporters arises from inverted-topology repeats. *Journal of Molecular Biology*. Available at: http://linkinghub.elsevier.com/retrieve/pii/S0022283611001410 [Accessed February 14, 2011].

Rementeria, A. et al., 2005. Genes and molecules involved in Aspergillus fumigatus virulence. *Rev Iberoam Micol*, 22, p.1–23. Available at: http://scholar.google.com/scholar?hl=en&btnG=Search&q=intitle:Genes+and+molecules+involved+in+Aspergillus+fumigatus+virulence#0.

Renshaw, J. et al., 2002. Fungal siderophores: structures, functions and applications. *Mycological Research*, 106(10), pp.1123-1142. Available at: http://linkinghub.elsevier.com/retrieve/pii/S0953756208601677.

Schaffner, A., Douglas, H. & Braude, A., 1982. Selective protection against conidia by mononuclear and against mycelia by polymorphonuclear phagocytes in resistance to Aspergillus. Observations on these two lines of defense in vivo and in vitro with human and mouse phagocytes. *The Journal of clinical investigation*, 69(3), pp.617-31. Available at: http://www.pubmedcentral.nih.gov/articlerender.fcgi?artid=371019&tool=pmcentrez&rendertype=abstract.

Schalk, I.J., Abdallah, M.A. & Pattus, F., 2002. Recycling of pyoverdin on the FpvA receptor after ferric pyoverdin uptake and dissociation in Pseudomonas aeruginosa. *Biochemistry*, 41(5), pp.1663-71. Available at: http://www.ncbi.nlm.nih.gov/pubmed/11814361.

Schalk, I.J., Lamont, I.L. & Cobessi, D., 2009. Structure–function relationships in the bifunctional ferrisiderophore FpvA receptor from Pseudomonas aeruginosa. *BioMetals*, 22(4), p.671–678. Available at: http://www.springerlink.com/index/H73678H81N0N5281.pdf.

Schrettl, M., Winkelmann, G. & Haas, H., 2004. Ferrichrome in Schizosaccharomyces pombe--an iron transport and iron storage compound. *Biometals : an international journal on the role of metal ions in biology, biochemistry, and medicine*, 17(6), pp.647-54. Available at: http://www.ncbi.nlm.nih.gov/pubmed/15689108.

Schrettl, Markus et al., 2004. Siderophore biosynthesis but not reductive iron assimilation is essential for Aspergillus fumigatus virulence. *The Journal of experimental medicine*, 200(9), pp.1213-9. Available at: http://www.ncbi.nlm.nih.gov/pubmed/15504822.

Schrettl, Markus et al., 2007. Distinct roles for intra- and extracellular siderophores during Aspergillus fumigatus infection. *PLoS pathogens*, 3(9), pp.1195-207. Available at: http://www.ncbi.nlm.nih.gov/pubmed/17845073.

Schrettl, Markus et al., 2008. SreA-mediated iron regulation in Aspergillus fumigatus. *Molecular microbiology*, 70(1), pp.27-43. Available at: http://www.pubmedcentral.nih.gov/articlerender.fcgi?artid=2610380&tool=pmcentrez&rendertype=abstract [Accessed February 21, 2011].

Scott, D.C., Newton, S. & Klebba, P.E., 2002. Surface loop motion in FepA. *Journal of bacteriology*, 184(17), p.4906. Available at: http://jb.asm.org/cgi/content/abstract/184/17/4906.

Sebulsky, M.T. et al., 2004. FhuD1, a Ferric Hydroxamate-binding Lipoprotein in Staphylococcus aureus. *Journal of Biological Chemistry*, 279(51), pp.53152-53159. Available at: http://www.jbc.org/cgi/doi/10.1074/jbc.M409793200.

Sebulsky, M.T. et al., 2003. The role of FhuD2 in iron(III)-hydroxamate transport in Staphylococcus aureus. Demonstration that FhuD2 binds iron(III)-hydroxamates but with minimal conformational change and implication of mutations on transport. *The Journal of biological chemistry*, 278(50), pp.49890-900. Available at: http://www.ncbi.nlm.nih.gov/pubmed/14514690.

Sebulsky, T. et al., 2000. Identification and Characterization of a Membrane Permease Involved in Iron-Hydroxamate Transport in Staphylococcus aureus. *Journal of bacteriology*, 182(16), pp.4394-4400.

Shaw, J.D. et al., 2001. Yeast as a model system for studying endocytosis. *Experimental cell research*, 271(1), pp.1-9. Available at: http://www.ncbi.nlm.nih.gov/pubmed/11697876.

Shen, J., Meldrum, A. & Poole, K., 2002. FpvA receptor involvement in pyoverdine biosynthesis in Pseudomonas aeruginosa. *Journal of bacteriology*, 184(12), p.3268. Available at: http://jb.asm.org/cgi/content/abstract/184/12/3268.

Siegrist, M.S. et al., 2009. Mycobacterial Esx-3 is required for mycobactin-mediated iron acquisition. *Proceedings of the National Academy of Sciences of the United States of America*, 106(44), pp.18792-7. Available at: http://www.ncbi.nlm.nih.gov/pubmed/19846780.

Silver, P., 2009. Indirect immunofluorescence labeling in the yeast Saccharomyces cerevisiae. *Cold Spring Harbor protocols*, 2009(11), p.pdb.prot5317. Available at: http://www.ncbi.nlm.nih.gov/pubmed/20150056 [Accessed February 3, 2011].

Soubani, A.O. & Chandrasekar, P.H., 2002. The Clinical Spectrum of Pulmonary Aspergillosis*. *Chest*, 121(6), pp.1988-1999. Available at: http://www.chestjournal.org/cgi/doi/10.1378/chest.121.6.1988 [Accessed January 20, 2011].

Sun-Wada, G.H. et al., 1998. Functional expression of the human UDP-galactose transporters in the yeast Saccharomyces cerevisiae. *Journal of biochemistry*, 123(5), pp.912-7. Available at: http://www.ncbi.nlm.nih.gov/pubmed/9562625.

Szewczyk, E. et al., 2006. Fusion PCR and gene targeting in Aspergillus nidulans. *Nature protocols*, 1(6), pp.3111-20. Available at: http://www.ncbi.nlm.nih.gov/pubmed/17406574.

Thau, N. et al., 1994. rodletless mutants of Aspergillus fumigatus. *Infection and immunity*, 62(10), p.4380. Available at: http://iai.asm.org/cgi/content/abstract/62/10/4380.

The Fungal Research Trust, Image Bank - Acute invasive pulmonary aspergillosis. *The Aspergillus Website*. Available at: http://www.aspergillus.org.uk/indexhome.htm?secure/image_library/./1ipa/index.html~main [Accessed February 7, 2011].

The Fungal Research Trust, 1998. Image Library - Aspergillus fumigatus. *The Aspergillus Website*. Available at: http://www.aspergillus.org.uk/indexhome.htm?secure/image_library/speciesindex.php~main [Accessed February 7, 2011].

The Gene Ontology Consortium, 2000. Gene Ontology : tool for the unification of biology. *Nature Genetics*, 25(may), pp.25-29.

Thornton, C.R., 2010. *Chapter 6 - Detection of Invasive Aspergillosis* 1st ed., Elsevier Inc. Available at: http://dx.doi.org/10.1016/S0065-2164(10)70006-X.

Toret, C.P. & Drubin, D. G., 2007. The budding yeast endocytic pathway. *Journal of Cell Science*, 120(8), pp.1501-1501. Available at: http://jcs.biologists.org/cgi/doi/10.1242/jcs.03446 [Accessed April 15, 2011].

Tusnády, G.E. & Simon, I., 1998. Principles governing amino acid composition of integral membrane proteins: application to topology prediction. *Journal of molecular biology*, 283(2), pp.489-506. Available at: http://www.ncbi.nlm.nih.gov/pubmed/9769220.

Ubarretxena-Belandia, I. & Stokes, D.L., 2010. *Present and future of membrane protein structure determination by electron crystallography.* 1st ed., Elsevier Inc. Available at: http://www.ncbi.nlm.nih.gov/pubmed/21115172 [Accessed March 14, 2011].

Van Der Helm, D. et al., 2002. Bipartite gating in the outer membrane protein FecA. *Biochemical Society transactions*, 30(4), pp.708-10. Available at: http://www.ncbi.nlm.nih.gov/pubmed/12196171.

Vincent, M.J., Martin, A.S. & Compans, R.W., 1998. Function of the KKXX motif in endoplasmic reticulum retrieval of a transmembrane protein depends on the length and structure of the cytoplasmic domain. *The Journal of biological chemistry*, 273(2), pp.950-6. Available at: http://www.ncbi.nlm.nih.gov/pubmed/9422755.

Waldorf, A.R., Levitz, S.M. & Diamond, R.D., 1984. In vivo bronchoalveolar macrophage defense against Rhizopus oryzae and Aspergillus fumigatus. *The Journal of infectious diseases*, 150(5), pp.752-60. Available at: http://www.ncbi.nlm.nih.gov/pubmed/6387001.

Walsh, T.J. et al., 2008. Treatment of aspergillosis: clinical practice guidelines of the Infectious Diseases Society of America. *Clinical infectious diseases : an official publication of the Infectious Diseases Society of America*, 46(3), pp.327-60. Available at: http://www.ncbi.nlm.nih.gov/pubmed/18177225.

Wandersman, C. & Delepelaire, P., 2004. Bacterial iron sources: from siderophores to hemophores. *Annual review of microbiology*, 58, pp.611-47. Available at: http://www.ncbi.nlm.nih.gov/pubmed/15487950.

Wheatley, M. & Hawtin, S.R., 1999. Glycosylation of G-protein-coupled receptors for hormones central to normal reproductive functioning: its occurrence and role. *Human reproduction update*, 5(4), pp.356-64. Available at: http://www.ncbi.nlm.nih.gov/pubmed/10465525.

Winkelmann, G., 2001. Siderophore transport in Fungi. In G. Winkelmann, ed. *Microbial Transport Systems*. Weinheim: Wiley-VCH, pp. 463-479.

Winkelmann, G. & Huschka, H., 1987. Molecular recognition and transport of siderophores in fungi. In G. Winkelmann, D. van Der Helm, & J. B. Neilands, eds. *Iron Transport in Microbes, Plants and Animals*. Weinheim: Wiley-VCH, pp. 317-336.

Wyckoff, E.E., Mey, A.R. & Payne, S.M., 2007. Iron acquisition in Vibrio cholerae. *Biometals : an international journal on the role of metal ions in biology, biochemistry, and medicine*, 20(3-4), pp.405-16. Available at: http://www.ncbi.nlm.nih.gov/pubmed/17216354.

Yin, Y. et al., 2006. Structure of the multidrug transporter EmrD from Escherichia coli. *Science (New York, N.Y.)*, 312(5774), pp.741-4. Available at: http://www.ncbi.nlm.nih.gov/pubmed/16675700 [Accessed August 23, 2010].

Yun, C.W. et al., 2001. The role of the FRE family of plasma membrane reductases in the uptake of siderophore-iron in Saccharomyces cerevisiae. *The Journal of biological chemistry*, 276(13), pp.10218-23. Available at: http://www.ncbi.nlm.nih.gov/pubmed/11120744.

Yun, C.W. et al., 2000. Desferrioxamine-mediated iron uptake in Saccharomyces cerevisiae. Evidence for two pathways of iron uptake. *Journal of Biological Chemistry*, 275(14), p.10709. Available at: http://www.jbc.org/cgi/content/abstract/275/14/10709.

Yun, C.W. et al., 2000. Siderophore-iron uptake in Saccharomyces cerevisiae. *Journal of Biological Chemistry*, 275(21), p.16354. Available at: http://www.jbc.org/content/275/21/16354.full.

Zawadzka, A.M. et al., 2009. Siderophore-Mediated Iron Acquisition Systems in Bacillus cereus: Identification of Receptors for Anthrax Virulence-Associated Petrobactin. *Biochemistry*, 48, pp.3645-3657.

Zawadzka, A.M. et al., 2009. Characterization of a Bacillus subtilis transporter for petrobactin, an anthrax stealth siderophore. *Proceedings of the National Academy of Sciences*, pp.1-6. Available at: www.pnas.org/cgi/doi/10.1073/pnas.0904793106.